Oil & Natural Gas Technology

DOE Award No.: DE-NT0005667

Final Report

October 2008 – September 2012

ASSESSING THE EFFICACY OF THE AEROBIC METHANOTROPHIC BIOFILTER IN METHANE HYDRATE ENVIRONMENTS

Submitted by:
University of California
Santa Barbara CA 93106

Principal Investigator: David L. Valentine

Prepared for:
United States Department of Energy
National Energy Technology Laboratory

September 14, 2012

Office of Fossil Energy

TABLE OF CONTENTS

Executive Summary	3
Publications Arising	4
Chapter 1: Methanotrophy in Microbial Mats	6
Chapter 2: Pelagic Methanotrophy: Studies from the Pacific Ocean	32
Chapter 3: Pelagic Methanotrophy: Studies from the Gulf of Mexico	72
Concluding Remarks	91
Acknowledgment	93
Disclaimer	93

LIST OF FIGURES

Figure 1:	Benthic mat surfaces	24
Figure 2:	Fatty acids in mats	25
Figure 3:	Gas headspace from mat incubations	26
Figure 4:	Hierarchical clustering of mat phylochip gradient fractions	27
Figure 5:	Phylochip hydridization intensities from mat incubations	28
Figure 6:	Recovered benthic mat plate	29
Figure 7:	Isotope incorporation from mat incubations	30
Figure 8:	Relative abundance of taxa occupying microbial mats	31
Figure 9:	Southern California Bight study area	57
Figure 10:	Santa Monica Basin reference hydrocasts from 2007	58
Figure 11:	Sampling over a pingo structure in the Santa Monica Basin	59
Figure 12:	Santa Monica Basin hydrocasts from 2009	60
Figure 13:	Hydrocasts from other borderland basins	61
Figure 14:	Methane oxidation rate profiles from several borderland basins	62
Figure 15:	Differences in methanotrophy between 2007 and 2009 expeditions	63
Figure 16:	Annotated temperature-salinity diagrams for the Santa Monica Basin	64
Figure 17:	Hydrographic comparison between years in the Santa Monica Basin	65
Figure 18:	Fractional abundance of isotopes in 13C/D incubations	66
Figure 19:	Isotope enrichments in lipids for stable isotope probing experiments	67
Figure 20:	Mass spectra for fatty acids from isotope probing experiments	68
Figure 21:	Bacterial community structure from isotope probing experiments	69
Figure 22:	Phylogenetic tree of 16SrRNA from isotope probing	70
Figure 23:	Phylogenetic tree of methane monooxygenase from isotope probing	71
Figure 24:	Gulf of Mexico sampling stations near spill site	81
Figure 25:	Chemical variations in dissolved gases during the gulf spill	82
Figure 26:	Microbial communities in the deep plumes from the gulf spill	83
Figure 27:	Oxidation potential for methane and propane from the gulf spill	84
Figure 28:	Gulf of Mexico sampling stations for September and October, 2010	85
Figure 29:	Gulf spill microbial communities before and after methane loss	86
Figure 30:	Model results interpolating methanotrophic rate for gulf spill	87

Figure 31: Model demonstration of autoinoculation in the gulf spill 88
Figure 32: Model results showing evolution of microbial community for gulf spill 89
Figure 33: Model results showing impacts of recirculation for gulf spill 90

LIST OF TABLES

Table 1: Summarized metadata for Shane Seep 19
Table 2: Fatty acid relative abundance from mats 20
Table 3: Fatty acid carbon isotopes from mats 21
Table 4: Elemental abundance of mats 22
Table 5: Phylochip rank scores for mats 23
Table 6: Incubation protocols for 13C/D isotope probing 54
Table 7: Fatty acid isotopes from 13C/D isotope probing 55
Table 8: Water column properties from Santa Barbara and Santa Monica Basins 56
Table 9: Hydrocarbon discharge and respiration potential for the gulf spill 80

EXECUTIVE SUMMARY

In October 2008 the University of California at Santa Barbara (UCSB) initiated investigations of water column methane oxidation in methane hydrate environments, through a project funded by the National Energy Technology Laboratory (NETL) entitled: assessing the efficacy of the aerobic methanotrophic biofilter in methane hydrate environments. This Final Report describes the scientific advances and discoveries made under this award as well as the importance of these discoveries in the broader context of the research area.

Benthic microbial mats inhabit the sea floor in areas where reduced chemicals such as sulfide reach the more oxidizing water that overlies the sediment. We set out to investigate the role that methanotrophs play in such mats at locations where methane reaches the sea floor along with sulfide. Mats were sampled from several seep environments and multiple sets were grown in-situ at a hydrocarbon seep in the Santa Barbara Basin. Mats grown in-situ were returned to the laboratory and used to perform stable isotope probing experiments in which they were treated with 13C-enriched methane. The microbial community was analyzed, demonstrating that three or more microbial groups became enriched in methane's carbon: methanotrophs that presumably utilize methane directly, methylotrophs that presumably consume methanol excreted by the methanotrophs, and sulfide oxidizers that presumably consume carbon dioxide released by the methanotrophs and methylotrophs. Methanotrophs reached high relative abundance in mats grown on methane, but other bacterial processes include sulfide oxidation appeared to dominate mats, indicating that methanotrophy is not a dominant process in sustaining these benthic mats, but rather a secondary function modulated by methane availability.

Methane that escapes the sediment in the deep ocean typically dissolved into the overlying water where it is available to methanotrophic bacteria. We set out to better understand the efficacy of this process as a biofilter by studying the distribution of methane oxidation and disposition of methanotrophic populations in the Pacific Ocean. We investigated several environments including the basins offshore California, the continental margin off Central America, and the shallow waters around gas seeps. We succeeded in identifying the distributions of activity in these environments, identified potential physical and chemical controls on methanotrophic activity, we further revealed details about the methanotrophic communities active in these settings, and we developed new approaches to study methanotrophic communities. These findings should improve our capacity to predict the methanotrophic response in ocean waters, and further our ability to generate specific hypotheses as to the ecology and efficacy of pelagic methanotrophic communites.

The discharge of methane and other hydrocarbons to Gulf of Mexico that followed the sinking of the Deepwater Horizon provided a unique opportunity to study the methanotorphic biofilter in the deep ocean environment. We set out to understand the consumption of methane and the bloom of methanotrophs resulting from this event, as a window into the regional scale release of gas hydrate under rapid warming scenarios. We found that other hydrocarbon gases, notably propane and ethane, were preferred

for consumption over methane, but that methane consumption accelerated rapidly and drove the depletion of methane within a matter of months after initial release. These results revealed the identity of the responsible community, and point to the importance of the seed population in determining the rate at which a methanotrophic community is able to respond to an input of methane.

Collectively, these results provide a significant advance in our understanding of the marine methanotrohic biofilter, and further provide direction and context for future investigations of this important phenomenon. This project has resulted in fourteen publications to date, with five more circulating in draft form, and several others planned.

PUBLICATIONS ARRISING FROM THIS AWARD:

1. Mau S, Heintz MB, Kinnaman FS, Valentine DL (2010) Compositional variability and air-sea flux of ethane and propane in the plume of a large, marine seep field near Coal Oil Point, CA. **Geo-Marine Letters** 30: 367-378.
2. Redmond MC, Valentine DL, Sessions AL (2010) Identification of Novel Methane-, Ethane-, and Propane-Oxidizing Bacteria at Marine Hydrocarbon Seeps by Stable Isotope Probing. **Applied and Environmental Microbiology** 76: 6412-6422.
3. Valentine DL (2010) Measure methane to quantify the oil spill. **Nature** 465: 421-421.
4. Valentine DL, Kessler JD, Redmond MC, Mendes SD, Heintz MB, et al. (2010) Propane Respiration Jump-Starts Microbial Response to a Deep Oil Spill. **Science** 330: 208-211.
5. Valentine DL, Reddy CM, Farwell C, Hill TM, Pizarro O, et al. (2010) Asphalt volcanoes as a potential source of methane to late Pleistocene coastal waters. **Nature Geoscience** 3: 345-348.
6. Valentine, DL. (2010) An opportunity to assess the behavior of methane released in the deep ocean. **Fire in the Ice** 10 (2)5.
7. Valentine DL (2011) Emerging Topics in Marine Methane Biogeochemistry. **Annual Review of Marine Science**, Vol 3 3: 147-171
8. *Kessler JD, *Valentine DL, Redmond MC, Du MR, Chan EW, et al. (2011) A Persistent Oxygen Anomaly Reveals the Fate of Spilled Methane in the Deep Gulf of Mexico. **Science** 331: 312-315. *Kessler and Valentine are co-first authors
9. Pack MA, Heintz MB, Reeburgh WS, Trumbore SE, Valentine DL, et al. (2011) A method for measuring methane oxidation rates using low-levels of (14)C-labeled methane and accelerator mass spectrometry. **Limnology and Oceanography-Methods** 9: 245-260.
10. Redmond MC, Valentine DL (2011) Natural gas and temperature structured a microbial community response to the Deepwater Horizon oil spill. **Proceedings of the National Academy of Sciences of the United States of America**. Doi:10.1073/pnas.1108756108
11. Mau S, Heintz MB, Valentine DL (2011) Quantification of CH4 loss and transport in dissolved plumes of the Santa Barbara Channel, California. **Continental Shelf Research** 32, 110-120. doi:10.1016/j.csr.2011.10.016
12. Ryerson T, Camilli R, Kessler J, Kujawinski EB, Reddy CM, et al. (2012) Chemical composition measurements quantify Deepwater Horizon hydrocarbon emissions and distribution in the marine environment. **Proceedings of the National Academy of Sciences**, USA. doi/10.1073/pnas.1110564109

13. Heintz MB, Mau S, Valentine DL (2012) Physical Control on Methanotrophic Potential in Waters of the Santa Monica Basin, Southern California. **Limnology and Oceanography** 57(2) 420-432. doi:10.4319/lo.2012.57.2.0420
14. Valentine DL, Mezić I, Maćešić S, Črnjarić-Žic N, Ivić S, et al. (2012) Dynamic autoinoculation and the microbial ecology of a deep water hydrocarbon irruption. **Proceedings of the National Academy of Sciences of the United States of America**. doi/10.1073/pnas.1108820109

Manuscripts Submitted or in Draft Form:

Farwell CA, MB Heintz, AL Sessions and DL Valentine (in preparation for Geochimica et Cosmochimica Acta) Stable isotope probing for lipids of marine methanotrophs using deuterium and carbon-13.

Heintz MB, JW Pohlman, SC Bagby, M Elvert, MJ Wooler, C Ruppel and DL Valentine (in preparation for PLoS ONE) Enhanced Methane Consumption in Ice Covered Arctic Lakes.

Pack MA, MB Heintz, WS Reeburgh, SE Trumbore, DL Valentine, X Xu and ERM Druffel (submitted in revised form) Methane oxidation in the eastern tropical north Pacific water column. Limnology and Oceanography.

Paul BG, H Ding, SC Bagby, MC Redmond, GL Anderson and DL Valentine (in preparation for Applied and Environmental Microbiology) Methane-oxidizing bacteria shunt carbon to microbial mats at a marine hydrocarbon seep

Redmond MC, PA Tavormina, VJ Orphan and DL Valentine (in preparation for Applied and Environmental Microbiology) Dynamics of Hydrocarbon Monooxygenase Genes in the Deep Ocean Following the Deepwater Horizon Spill.

Chapter 1. Methanotrophy in Microbial Mats

Preface: In this section we describe results relating to our studies on methanotrophic microbial mats. The most informative experiments are presented, and we provide some context in the form of comparison to environmental samples. This work relates to Tasks 2-5 in our original proposal and is currently being prepared for submission to the peer reviewed literature with a working title and author list as follows:

Working Title: Methane-oxidizing bacteria shunt carbon to microbial mats at a marine hydrocarbon seep

Author List: Blair G. Paul, Dr. Haibing Ding, Dr. Sarah C. Bagby, Dr. Molly C. Redmond, Dr. Gary L. Andersen, and Dr. David L. Valentine

Summary: Methane can support marine bacterial productivity via direct coupling to oxygen, or by oxidation of methane-converted products. Still, few studies have identified a network of viable bacteria associated with carbon produced from methane oxidation. We analyzed the abundance and natural isotope composition of fatty acids and used DNA stable isotope probing (DNA-SIP) to assess the incorporation of methane-derived carbon by microbial mats grown from an active gas vent at Shane Seep, in the shallow Coal Oil Point seep field off Santa Barbara, CA. Monounsaturated hexadecanoic (16:1) fatty acids were shown to be abundant and ^{13}C-depleted in the environmental samples, suggesting that methane carbon contributes to a large fraction of mat biomass. Members of the methanotrophic family *Methylococcaceae* were indicated by SIP as major $^{13}CH_4$ consumers, with additional ^{13}C incorporation by relatives of *Methylophaga* and *Sulfurovumaceae*, likely as secondary consumers of methane-derived organic matter and CO_2, respectively. PhyloChip assays showed that sulfide-oxidizing ε-proteobacteria and methylotrophic γ-proteobacteria were the most abundant mat residents. This study demonstrates the rapid percolation of methane's carbon through trophic interactions among aerobic bacteria at hydrocarbon seeps.

INTRODUCTION

Benthic microbial mats often exist near sources of reduced chemicals along the sea floor. These mats are typically filamentous and composed of sulfide oxidizing bacteria, including *Beggiatoa*, *Thioploca*, *Sulfuovum,* and *Sulfurimonas* (12, 25, 26, 39). Lipid biomarker evidence has previously been used to imply that bacteria actively consume methane in microbial mats from Shane Seep at Coal Oil Point, offshore Goleta, CA (10). This shallow hydrocarbon seep emits 1900-3300 m^3 of gas per day (7, 38). Previous studies have shown changes in bacterial communities with increasing concentrations of dissolved hydrocarbons within Shane Seep sediments (21, 31). Ding and Valentine (2008) found $\delta^{13}C$ depleted 16:1 fatty acids measured close to the $\delta^{13}C$ signature of methane gas at Shane Seep, suggesting that mats from a shallow hydrocarbon seep harbor aerobic methanotrophs. Microbial mats have been shown to harbor both anaerobic methanotrophs in the Black Sea (2, 20, 36), and aerobic methanotrophs in hydrothermal vent and cave systems (8, 16). Aerobic methanotrophs may support a

diverse bacterial community in microbial mats, while consuming significant amounts of methane.

Aerobic methanotrophs are a key control in the flux of methane from the ocean to the atmosphere (32). Aerobic bacteria that metabolize methane directly or utilize methyl biproducts of methane oxidation (e.g. methanol) are known as methanotrophs and methylotrophs, respectively (13, 23). Methanotrophs and methylotrophs are of ecological significance, contributing to primary production from methane and its derivatives, and in turn, supporting heterotrophic bacteria and eukaryotes in a range of marine communities (4, 6, 13). Although benthic microbial mats are often located at hydrocarbon seeps, aerobic methanotrophs have not been shown to actively metabolize methane in microbial mats at marine hydrocarbon seeps.

Bacterial populations supported in microbial mats at Shane Seep remain unidentified. We first sought to examine the variation in mats growing at Shane Seep, including lipid compositions and stable carbon isotope ratios compared with isotope signatures of seep gases, CO_2 and CH_4. We employed PhyloChip 16S rRNA gene microarrays to characterize the taxonomic composition of environmental mat samples from Shane Seep. Stable isotope probing (SIP) can be employed to track the incorporation of isotope-labeled substrates, such as ^{13}C-methane into biomass (27, 29). Organisms consuming $^{13}CH_4$ incorporate heavy carbon into their DNA to become enriched with the isotopic label and separable from the DNA of other organisms. This method assumes that an optimal time point, at which substrate metabolism is incorporated into the nucleic acid of an organism of interest, can be reached during incubation. To target the direct and indirect consumers of methane in these mats, we tracked variation in taxonomic structure during $^{13}CH_4$-ammended incubations. These approaches were collectively aimed at identifying both organisms responsible for direct oxidation of methane and organisms utilizing methane-derived carbon, while residing in the seep mats.

MATERIALS AND METHODS

Study Site

Our study site, known as Shane Seep, is located in the Coal Oil Point (C.O.P.) Seep Field offshore Goleta, CA (Table 1). Shane Seep exhibits a continuous flux of hydrocarbon gases, which have been the subject of several geochemical studies (7, 19, 38). Naturally occurring microbial mats were grown during in situ incubations at Shane Seep (referred to as “Environmental/Seep”), while some mats were subsequently used for ex situ SIP incubations with ^{13}C-methane (referred to as “Experimental/SIP”) (Table 2).

Environmental - Sampling.

In order to study microbial mats under natural seep conditions, we deployed an in situ benthic growth device that allowed mat growth and removal for geochemical analyses or ex situ incubations. Growth surface modules with one rough side (10cm × 10cm) were affixed to a larger mounting plate (60cm x 60cm) and positioned over an active gas vent at Shane Seep (Figure 1A). Additionally, a duplicate growth device was positioned 30m from the seep field. Any biomass recovered from the device outside the seep field served as a control to compare with Shane Seep mat biomass. The benthic growth device was deployed for a 14-week in situ growth experiment. Mats developed

without sampling for two weeks, after which SCUBA divers retrieved samples weekly (Figure 1B). Samples were transported to the laboratory in sealed containers with seawater collected at the in situ growing location. Mats were stored at in situ temperature(12 °C) until processed (same day;as below). After 14 weeks of sample retrievals, a large offshore storm occurred and resulting wave action mangled the benthic growing deployment (Figure 6). This event marked the endpoint for in situ/environmental sampling in 2007.

Environmental - Elemental and Fatty Acid Analyses.

Elemental analysis (C, %H, %N, and %S, by weight) was conducted on Seep Mat samples using a CEC 440HA automated organic elemental analyzer (Exeter Analytical). Fatty acids were extracted from microbial mat samples obtained from the in situ growth experiments. Fatty acid extraction procedures were conducted according to Ding and Sun (9). Briefly, microbial mat was scraped from individual growth plate modules, before extraction with methanol and methylene chloride - methanol (2:1 v/v). Fatty acids were processed using an HP-5890 series II GC and concentrations were determined with an HP-3396 series III integrator, as previously published (10). Fatty acids were heated them with BF_3/Methanol to form fatty acid methyl-esters (FAMEs) for GC analysis. The isotope ratios of fatty acids were calculated based on isotope ratio of FAMEs and methanol.

Stable isotope ratios (δ13C, δ15N, δ34S) were measured by GC-IRMS at the UC Santa Barbara Marine Science Institute Analytical Laborartory (Thermo Finnigan), as previously published (10). The system was run with helium carrier gas, at a flow rate of 1.0 mL/min. FAME compounds were oxidized with Cu/Ni/Pt wire at 950°C via GC combustion. The oxidized compounds were converted to CO_2 and measured by IRMS relative to a CO_2 standard (Air Liquid).

Environmental - DNA Extraction and PCR.

Microbial DNA was extracted from a SIP-dedicated microbial mat using a bead beating and spin column protocol (Fast DNA SPIN for Soil, MP Biomedicals). PCR was conducted with universal bacterial primers: 27F (5'- AGAGTTTGATCCTGGCTCAG -3') and1492R (5'- GGTTACCTTGTTACGACTT -3')**.** PCR product was cleaned using the SV Wizard PCR Cleanup Kit (Promega) and quantified using a BioAnalyzer 2100, with high sensitivity dsDNA reagent kits (Agilent Biosciences).

Environmental - PhyloChip Assays.

High-density 16S rRNA gene G2 custom microarrays (3) were used to examine the microbial community structure of seep mat samples. The G2 PhyloChip targets ~300,000 sequence probes to assay microbial diversity at the sub-family and OTU level. PhyloChip processing was conducted at Lawrence Berkeley National Laboratory (LBNL) as previously described (3). Briefly, the 16S rRNA gene was PCR amplified from template mat DNA and quantified by gel electrophoresis. Sample PCR product (500 ng) was spiked with an internal amplicon mixture of known concentrations (standard). The pooled product and standard was fragmented using DNAse, and the fragments were biotinylated and hybridized °(48 C) to array probes overnight. The chips were washed, stained, and scanned, and CEL files were used for analysis.

Hybridization scores for each chip were scaled to the standard, then $\log_2$-transformed. The detailed criteria for scoring the probe hybridization scores were described elsewhere (3, 14). OTU and higher level taxa selection for G2 data analysis followed Hazen *et al*. (2010), though for G2 arrays, PhyCA parameters (Stage1 and Stage2) were selected to give results similar to the previously used CEL analysis pf>=0.9 parameter for scoring an OTU present. To be scored 'present', an OTU had to meet the following thresholds: Stage 1 $rQ_1 \geq 0.379$, $rQ_2 \geq 0.565$, $rQ_3 \geq 0.82$, and pf>=0.93. Passing OTU were then evaluated for cross-hybridization potential (Stage 2 analysis). In Stage 2, a cutoff point of r_xQ_3 values>=0.515 was employed, and those subfamilies that passed this criteria were designated 'present' and used for relative richness comparisons. OTU within the passing subfamilies were used for relative abundance comparisons. The hybridization scores for OTU not called present in a sample were reassigned a zero value.

Experimental - CH_4 SIP Incubations.

Stable isotope DNA-probing (DNA-SIP) enrichments were conducted with microbial mat samples recovered from a benthic growth deployment at Shane Seep, on September 3, 2008. SIP-dedicated mats were grown in situ for 11 weeks, prior to retrieval for laboratory incubations. Samples were collected in sealable containers, with seawater from Shane Seep, and immediately stored near in situ temperature (12°C) before incubations began (same day). During incubation, mats were enriched with ^{13}C-labeled methane as a metabolic substrate, while parallel controls were incubated with $^{12}CH_4$. Incubations lasted up to 142 hours, and were conducted in the dark, at in situ temperature, in re-sealable tedlar septum bags. Mat samples were kept under 250ml of seawater from Shane Seep, and an initial 170ml headspace gas mixture was provided, including methane (3.9-4.9%), oxygen (18.8-19.5%), nitrogen (74.6-77.2%), and carbon dioxide (0.1-1%), at atmospheric pressure (1atm). Methane consumption and carbon dioxide production were monitored throughout the incubations by thermal conductivity detector gas chromatography (GC-TCD), using a 3000A MicroGC (Agilent). Conversion of ^{13}C into microbial biomass was measured using a Thermo-Finnigan gas chromatography Isotope Ratio Mass Spectrometer(Marine Science Analytical Lab, UC Santa Barbara).

Experimental - DNA Extraction and Density Separation.

Nucleic acids were purified (as above) from $^{13}CH_4$ SIP, $^{12}CH_4$ control, and time=0("t=0") samples harvested after 111 hours. We separated DNA by density via ultracentrifugation of SIP and t=0 samples in a solution of cesium chloride (27). The $^{12}CH_4$ incubation DNA was not fractionated, to compare SIP and t=0 density fractions with non-fractioned DNA. We recovered twelve fractions from each sample's density gradient. DNA was quantified from the fractions using the Bioanalyzer High-Sensitivity dsDNA kit (Agilent Biosciences).

Experimental - Clone Sequencing and PhyloChip Assays.

SIP fractionated DNA and non-SIP unfractionated DNA was subjected to 16S rRNA gene amplification, followed by sequencing of cloned amplicons or use of amplicons for PhyloChip analysis. Cloning was performed using a PCR Cloning Kit (Qiagen).

Plasmid purification and sequencing was done at the U.C. Berkeley DNA Sequencing Facility. Clone library sequences were assessed for quality and assembled using Geneious (v.5.5.6;Biomatters Ltd.). Sequences were screened for putative chimeras first using the Mothur tool, Chimera Slayer (33). We additionally looked for chimeras with Mallard (1) and manually scanned BLAST alignments of all sequences with suspected chimeras. Putatively chimeric sequences were discarded before further clone library analysis. 16S rRNA taxonomy was assigned to clone library sequences at the family level and representative sequences were obtained using the RDP SeqMatch tool (37). Clone library sequences were compared via ClustalW global alignment (22) with representative sequences of methanotrophs for PhyloChip OTUs that were indicated as ^{13}C-enriched by SIP.

Terminal restriction fragment length polymorphism (T-RFLP) profiling was conducted from amplified 16S rDNA, however these data did not offer additional information about taxonomic composition beyond what was ascertained from clone sequences and PhyloChip analysis.

Whereas only two SIP fractions (1.707g/ml and 1.731g/ml) were analyzed through clone library sequencing, seven fractions (1.697g/ml-1.763g/ml) were assessed using PhyloChip. Additionally, we employed PhyloChip to assess one t=0 fraction (1.753g/ml) and the unfractioned $^{12}CH_4$ incubation DNA.

To determine the grouping of PhyloChip OTU scores from SIP fractions (seven incubation fractions and one t=0 fraction), hybridization scores were subjected to hierarchical clustering by average-linkage with the R package, Vegan (28). Clustering was performed on euclidean distances among SIP fractions, derived from hybridization values of OTUs that met detection criteria in all SIP fractions and all SEEP samples. We also assessed the structuring of SIP fractions clustering from OTUs that were most abundant (top 10) in at least one of the three SEEP samples. To infer the significance of each cluster, we assessed approximately unbiased bootstrap resampling p-values, using the R package, pvclust (34). This approach helped to indicate the following groups: high-density ^{13}C-enriched fractions; high-density non-enriched fractions; and low-density non-enriched fractions. A taxon was assigned membership as “13C-enriched” if it passed the following PhyloChip criteria: i) the OTU ranked among the top 10 OTUs in one of the putatively ^{13}C-enriched fractions; ii) the OTU hybridization score was higher for the enriched fractions than all non-enriched fractions. Conversely, a taxon was considered “non-enriched” if: i) it exhibited high abundance (ranked top 10) in one of the low-density, non-enriched fractions; ii) the OTU hybridization score exceeded the values from all ^{13}C-enriched fractions.

Nucleotide sequence accession numbers.

Sequences from the SIP 16S rDNA clone libraries were submitted to the GenBank database, under the accession numbers JX567952 to JX568074.

RESULTS

Environmental - Fatty Acids, Elemental Compositions, Stable Isotopes.

Whereas microbial mats were visible on each plate recovered from within the seep field, none of the control plates, deployed 30m outside of the seep, exhibited any mat growth. We extracted lipids from all 14 SEEP samples and detected 25 unique fat-

ty acids; 12 of 25 fatty acids exceeded 5% abundance in at least one SEEP sample (Tables 2 & 3). The saturated and unsaturated forms of hexadecanoic acid comprised the most abundant fatty acids in environmental samples (Figure 2A). The 16:1 fatty acids were the single most abundant in 7 of 14 samples, and exhibited depleted $\delta^{13}C$ values (< -35‰) in 4 SEEP samples (Figure 2B). The lowest $\delta^{13}C$ measurements in lipids were from SEEP samples 3, 6, and 13, while the greatest depletion was measured from 16:1 ω5 lipids (-49.4‰). While ^{13}C-depleted 16:0 lipids were found in only one sample, putatively identified 9-methoxy 16:0 fatty acids were depleted to $\delta^{13}C$ < -30‰ in five samples, constituting fully 27% of fatty acids in SEEP 10. Our $\delta^{13}C$ measurements from total mat biomass indicated SEEP samples 3 and 6 as the most enriched and most depleted, respectively (Table 4). We chose SEEP samples 3, 6, and 7 for PhyloChip analysis (below), based upon high, low, and intermediate $\delta^{13}C$ values, respectively.

Environmental - Taxonomic Composition.

Three SEEP samples(SEEP 3, 6, and 7) were assayed via PhyloChip (G2) to profile the 16S rDNA-based taxonomy and corresponding relative abundances of organisms in the mats. For this study, we only addressed OTUs that were considered present in at least one density gradient fraction (SIP or t=0 non-SIP) *and* one of the three Seep Mat samples. A total of 838 OTUs, corresponding to the subfamily taxonomic level, met the detection criteria. The PhyloChip's hybridization intensities for each OTU probe set were used to infer relative abundances of each taxon detected in the mats (summarized in Table 5).

The abundant taxa in each of the Seep Mat samples were predominantly comprised of sulfide-oxidizing bacteria, methylotrophs, and methanotrophs. The most abundant representatives of these metabolic niches belong to the taxonomic groups *Sulfuricurvaceae*, *Methylophaga*, and *Methylococcaceae*, respectively. OTUs representing the *Pseudomonadaceae* family contributed to 41% of all 838 OTUs detected (data not shown) from the SIP and Seep Mat assays, including some representatives at high abundance in Seep Mat 6 and Seep Mat 7.

Experimental - CH_4-SIP Enrichments.

After growing at Shane Seep for 11 weeks, microbial mats were retrieved and subjected to laboratory methane enrichment incubations. Stable isotope-probing incubations were administered $^{13}CH_4$, while control incubations were run with $^{12}CH_4$ (e.g., natural abundance) to compare the relative incorporation of isotopically enriched methane into biomass and DNA. We tracked headspace gases CH_4, CO_2, and O_2 during our 111-hour stable isotope-probing incubations (Figure 3), finding similar patterns in ^{13}C-CH_4 experimental incubations and ^{12}C-CH_4 controls. Pseudoreplicate experimental incubations harvested at 4, 98, and 142 hours showed a time-dependent increase in biomass ^{13}C content, while ^{13}C content in pseudoreplicate controls was unchanged (Figure 7).

Experimental - Taxonomic Composition.

We examined the association of seep mat residents with methane-derived carbon by profiling the stable isotope-probed 16S rDNA from mat samples, using clone sequence analysis and PhyloChip assays. We analyzed clone libraries from SIP fractions,

SIP-2 (1.707g/mL) and SIP-4 (1.731g/mL), finding evidence suggestive of density-driven taxon abundance shifts (Figure 8). The greatest difference marked by abundance in fraction SIP-2 over SIP-4, was attributed to the family *Rhodobacteraceae*. Sequences with nearest similarity to the family *Methylococcaceae* accounted for the most pronounced abundance difference, dominating fraction SIP-4 over SIP-2. Using PhyloChip analysis of the SIP gradient, we sought to confirm the density-based abundance shifts for these taxa and determine which differences were driven by ^{13}C-enrichment.

Among 12 fractions from the ^{13}C-SIP gradient, seven fractions (from 1.697g/mL to 1.763g/mL;SIP-1 – SIP-7) were selected for PhyloChip analysis, based on the ability to amplify appreciable PCR product from the 16S rRNA gene. Additionally, one t=0 fraction (non-enriched;1.753g/mL) was compared with the seven SIP fractions using PhyloChip. We used hierarchical clustering analysis of each fraction's OTU hybridization scores to interpret PhyloChip patterns between SIP-DNA fractions and identify taxa involved in ^{13}C enrichment (Figure 4). The first grouping that emerged from clustering included fractions SIP-4 (1.731g/mL) and SIP-5 (1.741g/mL; highest density). Grouping apart from SIP-4 and SIP-5, were the fractions of lowest density (SIP-1, SIP-2, and SIP-3;1.697-1.719g/mL) and a separate group of fractions marked by higher density (SIP-6, SIP-7, and t=0;1.753-1.763g/mL). The same clustering structure was maintained for a subset of taxa that included the dominant OTUs, based on top-10 abundance in the environmental SEEP samples.

OTUs driving similarity between fractions SIP-1 and SIP-2 (low density) and dissimilarity to denser fractions were characterized as "non-enriched". The separation of fractions, SIP-6, SIP-7, and t=0, from lighter fractions suggested a density-driven pattern was exhibited by some taxa, which could naturally consist of heavier DNA or may have been enriched with ^{13}C label. Fraction SIP-5 appeared more similar to SIP-1, SIP-2, and SIP-3 than to denser fractions. OTUs driving similarity between SIP-4, SIP-5 and lighter fractions could include taxa that were partially ^{13}C-enriched, which naturally contain lighter DNA. Association with ^{13}C-enrichment was therefore not attributable to the highest-density SIP fractions. We characterized OTUs as "putatively ^{13}C-enriched" if they were dominant in fractions SIP-4 and SIP-5 and by contrast, showed low abundance in fractions SIP-1, SIP-2, and t=0. However, OTUs that showed abundance in fractions SIP-3, SIP-6 and SIP-7 could not be positively attributed to ^{13}C-enrichment.

A group of PhyloChip taxa were characterized by greater abundance in the two lightest SIP fractions (1.697g/mL and 1.707g/mL) compared with the putatively ^{13}C-enriched fractions (Figure 5B). This group included OTU representatives of the family *Pseudomonadaceae*, the genus *Marinobacter* and the genus *Rhodobacter*. Conversely, a group of PhyloChip taxa was identified by peak abundance in the putatively ^{13}C-enriched fractions, SIP-4 and SIP-5, which included members of the methanotrophic family *Methylococcaceae* and the methylotrophic genus *Methylophaga*. Representative OTUs of these two taxa exhibited the greatest shift from low abundance in non-enriched SIP fractions to the highest abundance in the putatively enriched fractions (Figure 5A). A similar, but weaker abundance shift was observed for *Cytophaga* (OTU 8205), *Methylococcaceae (OTU 1355)*, *Saprospiraceae (OTU 8048)*, and *Sulfurovumaceae* (OTU 5283); we classified these three taxa as "partially enriched". The two *Methylococcaceae* OTUs representing known methanotrophs that were putatively ^{13}C-enriched were compared with SIP clone library sequences. The PhyloChip representative sequences

for these two *Methylococcaceae* subfamily OTUs shared >95% similarity with 24 sequences from the SIP clone library. Whereas the dominant *Methylococcaceae* subfamily among SIP PhyloChips (OTU 1537) and its closest clone library match were 95.2% identical, OTU 1355 showed >96% identical sites aligned with each of the 24 related clone sequences(>98% identity shared with 19 of 24 sequences).

DISCUSSION:

Factors driving variability in seep mats.

The spatial variation of mat composition is quite apparent from visual inspection of samples alone. Mats range from thin, sheet-like biofilms to filamentous structures. Mats also exhibit variation in color, including green, brown, and white. These differences are observed across individual mats and between different mat samples, and are likely influenced by the proximity and path of venting gas. Some temporal variation in mat composition is apparent from both visual observation and fatty acid profiles; environmental/SEEP samples retrieved during the last three weeks of in situ growth were predominantly composed of white filamentous mats and exhibited high concentrations of ^{13}C-depleted (< -30‰) 16:1 lipids. The abrupt disruption of mat growth by an offshore storm illustrates how these communities are subject to dynamic physical factors expected to influence any shallow benthic community. The morphological variations are accompanied by variations in taxonomic composition. Whereas some taxa, including sulfide-oxidizing bacteria (Sulfurovumaceae; Sulfuricurvaceae) and methanotrophs (Methylococcaceae), are evidently dominant across all PhyloChip assays of environmental samples, others show greater fluctuation—namely the genus *Methylophaga*, and the family *Pseudomonadaceae*. Populations represented by these taxa may account for the variability among lipid profiles found in the seep mat samples.

Constraints of the SIP approach.

Stable isotope probing of a complex microbial community aims to target ^{13}C-substrate assimilation by a subset of organisms that become enriched in “heavy” DNA fractions compared to “light” DNA fractions (27, 29). Clustering of PhyloChip abundance differences across a SIP gradient helped to clearly identify heavy fractions, grouping separately from light and heavy-control fractions, and indicate the association with ^{13}C uptake. However, it is more difficult to infer $^{13}CH_4$ utilization from taxa that are enriched in both the heavier SIP fractions and the control “heavy” fraction. It is therefore possible that some organisms, with high genomic or 16S rDNA G+C% (or both), do not meet our criteria to be considered $^{13}CH_4$ labeled.

Direct assimilation of methane carbon.

Methanotrophic bacteria that belong to the family, *Methylococcaceae*, are present in microbial mats at Shane Seep. Using SIP, we identified two metabolically active taxa among the 12 *Methylococcaceae* subfamilies found in our mat samples (including SIP fractions). The SIP experiment indicates that members of the *Methylococcaceae* subfamily are responsible for assimilation of methane to biomass in the microbial mats. Though PhyloChip OTU 1537 appears to represent to the more abundant methanotrophic population by PhyloChip assay alone, OTU 1355 was shared greater similarity with all *Methylococcaceae*-related SIP clone library sequences. This PhyloChip vs.

clone sequence discrepancy might result from hybridization by the two closely related probe sets with DNA from one bacterial population. Cross-hybridization of DNA to the OTU probe sets can be evidenced by similar PhyloChip abundance trends across samples, as detected from these two *Methylococcaceae*-related OTUs from our SIP fractions. Still, PhyloChip succeeds at elucidating a ^{13}C-enrichment pattern that can be generally assigned to the *Methylococcaceae* family, while comparison with clone library sequences provides better identification of the specific OTU responsible for $^{13}CH_4$ uptake. Detection of ^{13}C-depleted 16:1 fatty acids ($\delta < -35‰$) in 5 samples from Shane Seep supports the claim that *Gammaproteobacteria*-classified methanotrophs actively convert methane-derived carbon to biomass.

Indirect utilization of methane-derived carbon.

Mat samples collected during the 14-week growth experiment exhibit fluctuations in abundant fatty acids with more depleted δ^{13}C values than those detected by Ding and Valentine (10). Fatty acids 16:1 and 16:0 in particular showed greater ^{13}C-depletion compared with previously published results from Shane Seep mats. Lipids found in marine methanotrophs tend to include a combination of 16:1 and 16:0 fatty acids, whereas our findings of abundant 18-carbon fatty acids (18:0 and 18:1) found in addition to 16:1 and 16:0 might be indicative of sulfide-oxidizing *Epsilonproteobacteria* (17, 18, 35). The association of abundant methylotrophs and autotrophic sulfide-oxidizers with $^{13}CH_4$ in our SIP study informs our interpretation of the ^{13}C depleted 16:0 and methoxylated 18:0 lipids found in natural seep mat samples. It appears that methane-derived carbon is available to C1 and autotrophic bacteria including methylotrophs and sulfide-oxidizers, in the form of methanol and CO_2. Whereas the concentrations in closed-system SIP incubations are negligible before production from methane, CO_2 constitutes up to 17% of dissolved gases at Shane Seep. Autotrophic bacteria can therefore obtain carbon from either the surrounding seawater or neighboring methanotrophic bacteria.

Our results describe non-methanotrophic bacteria as residents of Shane Seep mat communities, which may benefit from oxidized methane. Methylotrophic bacteria from the genus *Methylophaga* are prominent in Shane Seep mats. PhyloChip evidence suggests that methylotrophic *Gammaproteobacteria* are not only abundant in Shane Seep mats, but they are also able to use carbon that is made available via methane oxidation. A methane-SIP experiment with oxic-layer sediments from Shane Seep previously found that methylotrophic bacteria, including *Methylophilaceae and Methylophaga*, were primarily involved in $^{13}CH_4$ utilization, while known methanotrophs were less abundant (31). By contrast, our SIP DNA-labeling experiment shows that methylotrophs coexist with abundant methanotrophic residents of the mat communities. Methylotrophic taxa described in these mats have not been previously shown to oxidize methane and instead, use methanol as a carbon source (23). However, the close association with ^{13}C-carbon in our SIP study suggests that *Methylophaga* are an important group of organisms to the processing of methane-derived carbon within these mats.

This study supports our hypothesis that sulfide oxidizing bacteria and methanotrophs co-inhabit the microbial mats of Shane Seep (10). Sulfide oxidizing autotrophs belonging to the *Epsilonproteobacteria* were consistently the most abundant taxa detected by PhyloChip analysis of all mat samples. Sulfurospirillaceae, Sulfuricurvaceae, or Sulfurovumaceae are represented among the top 10 abundant taxa in each of the

environmental mat samples. Sulfide oxidizing bacteria are often the most abundant organisms found in benthic mats in both methane seep and non-seep environments, where reduced sulfur diffuses upwards from underlying sediments (12, 25, 26, 39). However, autotrophic sulfide oxidizers had not been previously found to coexist with aerobic methanotrophs within a microbial mat at a marine seep.

Unknown role of *Pseudomonadaceae* in seep mats.

Although Shane Seep mats appear to be predominantly composed of sulfide-oxidizing bacteria, the *Pseudomonadaceae* family comprises the major fraction of OTUs represented by a single family on the PhyloChip assays of these mats. This may however, reflect an overrepresentation of these taxa from ribosomal RNA sequences that contribute to curated databases. Though *Pseudomonadaceae* OTUs did not represent the most abundant taxa in the enriched, heavy SIP fractions, some *Pseudomonadaceae* representatives were slightly enriched in the presence of methane. It is difficult to attribute a specific metabolism to the actively labeled *Pseudomonadaceae* taxa in our SIP experiments. Cross feeding by secondary consumers is a common observation of other methane SIP studies (16, 29, 31). The association of *Pseudomonadaceae* with methane is likely explained by secondary consumption of either methanotroph biomass or metabolic biproducts. The ability for *Pseudomonas* strains to fix carbon dioxide was previously demonstrated by $^{13}CO_2$ labeling experiments (11). Several species belonging to the *Pseudomonadaceae* family have been shown to degrade aromatic hydrocarbons, including phenol, benzene, naphthalene, and other polycyclic aromatic hydrocarbons (5, 15, 24, 40). It is plausible that *Pseudomonas* inhabitants of the Shane Seep mats might derive carbon from abundant aromatic hydrocarbons, CO_2, or from cellular biomass (30).

REFERENCES:

1. Ashelford K. E., Chuzhanova N. A., Fry J. C., Jones A. J., and Weightman A. J. 2006. New screening software shows that most recent large 16S rRNA gene clone libraries contain chimeras. Applied and Environmental Microbiology 72:5734-5741.
2. Blumenberg M., Seifert R., Nauhaus K., Pape T., and Michaelis W. 2005. In vitro study of lipid biosynthesis in an anaerobically methane-oxidizing microbial mat. Appl Environ Microbiol 71:4345-51.
3. Brodie E. L., DeSantis T. Z., Parker J. P. M., Zubietta I. X., Piceno Y. M., and Andersen G. L. 2007. Urban aerosols harbor diverse and dynamic bacterial populations. Proceedings of the National Academy of Sciences 104:299.
4. Cavanaugh C. M., Levering P. R., Maki J. S., Mitchell R., and Lidstrom M. E. 1987. Symbiosis of methylotrophic bacteria and deep-sea mussels.
5. Charng M. K., Voice T. C., and Criddle C. S. 1993. Kinetics of competitive inhibition and cometabolism in the biodegradation of benzene, toluene, and p-xylene by two Pseudomonas isolates. Biotechnol Bioeng 41:1057-65.
6. Childress J. J., Fisher C. R., Brooks J. M., Kennicutt M. C., Bidigare R., and Anderson A. E. 1986. A methanotrophic marine molluscan (Bivalvia, Mytilidae) symbiosis: mussels fueled by gas. Science 233:1306.

7. Clark J. F., Leifer I., Washburn L., and Luyendyk B. P. 2003. Compositional changes in natural gas bubble plumes: observations from the Coal Oil Point marine hydrocarbon seep field. Geo-Marine Letters 23:187-193.
8. Crépeau V., Cambon Bonavita M. A., Lesongeur F., Randrianalivelo H., Sarradin P. M., Sarrazin J., and Godfroy A. 2011. Diversity and function in microbial mats from the Lucky Strike hydrothermal vent field. FEMS Microbiol Ecol 76:524-40.
9. Ding H., and Sun M. -Y. 2005. Biochemical degradation of algal fatty acids in oxic and anoxic sediment–seawater interface systems: effects of structural association and relative roles of aerobic and anaerobic bacteria. Marine Chemistry 93:1-19.
10. Ding H., and Valentine D. L. 2008. Methanotrophic bacteria occupy benthic microbial mats in shallow marine hydrocarbon seeps, Coal Oil Point, California. Journal of Geophysical Research 113:G01015.
11. Feisthauer S., Wick L. Y., Kästner M., Kaschabek S. R., Schlömann M., and Richnow H. H. 2008. Differences of heterotrophic 13CO2 assimilation by Pseudomonas knackmussii strain B13 and Rhodococcus opacus 1CP and potential impact on biomarker stable isotope probing. Environ Microbiol 10:1641-51.
12. Gilhooly W. P., Carney R. S., and Macko S. A. 2007. Relationships between sulfide-oxidizing bacterial mats and their carbon sources in northern Gulf of Mexico cold seeps. Organic Geochemistry 38:380-393.
13. Hanson R. S., and Hanson T. E. 1996. Methanotrophic bacteria. Microbiol Rev 60:439-71.
14. Hazen T. C., Dubinsky E. A., DeSantis T. Z., Andersen G. L., Piceno Y. M., Singh N., Jansson J. K., Probst A., Borglin S. E., Fortney J. L., Stringfellow W. T., Bill M., Conrad M. E., Tom L. M., Chavarria K. L., Alusi T. R., Lamendella R., Joyner D. C., Spier C., Baelum J., Auer M., Zemla M. L., Chakraborty R., Sonnenthal E. L., D'haeseleer P., Holman H. Y., Osman S., Lu Z., Van Nostrand J. D., Deng Y., Zhou J., and Mason O. U. 2010. Deep-sea oil plume enriches indigenous oil-degrading bacteria. Science 330:204-8.
15. Hill G. A., and Robinson C. W. 1975. Substrate inhibition kinetics: phenol degradation by Pseudomonas putida. Biotechnology and Bioengineering 17:1599-1615.
16. Hutchens E., Radajewski S., Dumont M. G., McDonald I. R., and Murrell J. C. 2003. Analysis of methanotrophic bacteria in Movile Cave by stable isotope probing. Environmental Microbiology 6:111-120.
17. Inagaki F. 2003. Sulfurimonas autotrophica gen. nov., sp. nov., a novel sulfur-oxidizing -proteobacterium isolated from hydrothermal sediments in the Mid-Okinawa Trough. INTERNATIONAL JOURNAL OF SYSTEMATIC AND EVOLUTIONARY MICROBIOLOGY 53:1801-1805.
18. Inagaki F. 2004. Sulfurovum lithotrophicum gen. nov., sp. nov., a novel sulfur-oxidizing chemolithoautotroph within the -Proteobacteria isolated from Okinawa Trough hydrothermal sediments. INTERNATIONAL JOURNAL OF SYSTEMATIC AND EVOLUTIONARY MICROBIOLOGY 54:1477-1482.
19. Kinnaman F. S. 2008. Microbial consumption of natural gas in marine sediments: Rates, distributions and isotope effects. PhD Dissertation. University of California, Santa Barbara. . Microbial consumption of natural gas in marine sediments: Rates, distributions and isotope effects. PhD Dissertation. University of California, Santa Barbara. .

20. Knittel K., Lösekann T., Boetius A., Kort R., and Amann R. 2005. Diversity and distribution of methanotrophic archaea at cold seeps. Appl Environ Microbiol 71:467-79.
21. LaMontagne M. G., Leifer I., Bergmann S., Van De Werfhorst L. C., and Holden P. A. 2004. Bacterial diversity in marine hydrocarbon seep sediments. Environ Microbiol 6:799-808.
22. Larkin M. A., Blackshields G., Brown N. P., Chenna R., McGettigan P. A., McWilliam H., Valentin F., Wallace I. M., Wilm A., Lopez R., Thompson J. D., Gibson T. J., and Higgins D. G. 2007. Clustal W and Clustal X version 2.0. Bioinformatics 23:2947-8.
23. Lidstrom M. E. 2001. Aerobic methylotrophic prokaryotes. The prokaryotes, 3rd edition, release 3.
24. Lu X., Zhang T., Han-Ping Fang H., Leung K. M. Y., and Zhang G. 2011. Biodegradation of naphthalene by enriched marine denitrifying bacteria. International Biodeterioration & Biodegradation 65:204-211.
25. Moussard H., Corre E., Cambon-Bonavita M. A., Fouquet Y., and Jeanthon C. 2006. Novel uncultured Epsilonproteobacteria dominate a filamentous sulphur mat from the 13 degrees N hydrothermal vent field, East Pacific Rise. FEMS Microbiol Ecol 58:449-63.
26. Nelson D. C., Wirsen C. O., and Jannasch H. W. 1989. Characterization of Large, Autotrophic Beggiatoa spp. Abundant at Hydrothermal Vents of the Guaymas Basin. Appl Environ Microbiol 55:2909-17.
27. Neufeld J. D., Vohra J., Dumont M. G., Lueders T., Manefield M., Friedrich M. W., and Murrell J. C. 2007. DNA stable-isotope probing. Nat Protoc 2:860-6.
28. Oksanen J., Kindt R., Legendre P., O'hara B., Simpson G. L., Stevens M. H. H., and Wagner H. H. 2008. vegan: Community Ecology Package. R package version 1.13-1. hhttp. vegan. r-forge. r-project. org/i.
29. Radajewski S., Webster G., Reay D. S., Morris S. A., Ineson P., Nedwell D. B., Prosser J. I., and Murrell J. C. 2002. Identification of active methylotroph populations in an acidic forest soil by stable-isotope probing. Microbiology 148:2331-42.
30. Redmond M. C. 2010. Hydrocarbon oxidizing bacteria at marine oil and gas seeps. . Hydrocarbon oxidizing bacteria at marine oil and gas seeps. PhD Dissertation. University of California, Santa Barbara. .
31. Redmond M. C., Valentine D. L., and Sessions A. L. 2010. Identification of novel methane-, ethane-, and propane-oxidizing bacteria at marine hydrocarbon seeps by stable isotope probing. Appl Environ Microbiol 76:6412-22.
32. Reeburgh W. S. 2007. Oceanic methane biogeochemistry. Chem Rev 107:486-513.
33. Schloss P. D., Westcott S. L., Ryabin T., Hall J. R., Hartmann M., Hollister E. B., Lesniewski R. A., Oakley B. B., Parks D. H., and Robinson C. J. 2009. Introducing mothur: open-source, platform-independent, community-supported software for describing and comparing microbial communities. Applied and environmental microbiology 75:7537-7541.
34. Suzuki R., and Shimodaira H. 2006. Pvclust: an R package for assessing the uncertainty in hierarchical clustering. Bioinformatics 22:1540-1542.
35. Takai K., Suzuki M., Nakagawa S., Miyazaki M., Suzuki Y., Inagaki F., and Horikoshi K. 2006. Sulfurimonas paralvinellae sp. nov., a novel mesophilic, hydrogen- and sulfur-oxidizing chemolithoautotroph within the Epsilonproteobacteria isolated from a deep-sea hydrothermal vent polychaete nest, reclassification of Thiomicrospira deni-

trificans as Sulfurimonas denitrificans comb. nov. and emended description of the genus Sulfurimonas. Int J Syst Evol Microbiol 56:1725-33.
36. Treude T., Knittel K., Blumenberg M., Seifert R., and Boetius A. 2005. Subsurface microbial methanotrophic mats in the Black Sea. Appl Environ Microbiol 71:6375-8.
37. Wang Q., Garrity G. M., Tiedje J. M., and Cole J. R. 2007. Naive Bayesian classifier for rapid assignment of rRNA sequences into the new bacterial taxonomy. Appl Environ Microbiol 73:5261-7.
38. Washburn L., Clark J. F., and Kyriakidis P. 2005. The spatial scales, distribution, and intensity of natural marine hydrocarbon seeps near Coal Oil Point, California. Marine and Petroleum Geology 22:569-578.
39. Zhang C. L., Huang Z., Cantu J., Pancost R. D., Brigmon R. L., Lyons T. W., and Sassen R. 2005. Lipid biomarkers and carbon isotope signatures of a microbial (Beggiatoa) mat associated with gas hydrates in the gulf of Mexico. Appl Environ Microbiol 71:2106-12.
40. Zhang Z., Hou Z., Yang C., Ma C., Tao F., and Xu P. 2011. Degradation of n-alkanes and polycyclic aromatic hydrocarbons in petroleum by a newly isolated Pseudomonas aeruginosa DQ8. Bioresour Technol 102:4111-6.

Table 1. Summarized metadata for Shane Seep.

Seep Parameters							
Location	Depth (m)	Mean Temperature (°C)	Gas Flux ($m^3 day^{-1}$)*	$\%CH_4$**	$\%CO_2$**	$\delta^{13}C\text{-}CH_4$ (‰)**	$\delta^{13}C\text{-}CO_2$ (‰)**
34°, 24.370'N; 119°, 53.428'W	22	12.6	3300	81 - 85.7	12 - 16.7	−50.5 - −53.9	15.8 - 18.4

* Reported by Washburn et al. 2005
**Percent of total hydrocarbon and CO_2 gas, measured by Kinnaman 2008 in samples collected from 21m-depth.

Table 2. Relative abundances of the 12 major FA types within the 14 seep samples. 'Other' includes the minor FAs, i.e. those that never exceeded 5% abundance in any sample. Percentages are calculated from relative FA concentrations by mass.

	Fatty Acids (% Abundance)												
Sample	12:0	14:1	14:0	15:0	16:1	16:1(5)	16:0	16:0 9-methoxy	18:1(9)	18:1(7)	18:0	18:0 methoxy	Other FAs
Seep Mat 1	2.0	3.2	11.8	4.1	23.9	0.9	23.7	1.2	4.7	4.5	4.5	0.2	15.4
Seep Mat 2	2.9	1.3	17.6	6.5	8.2	0.6	31.0	4.5	2.5	1.1	7.1	2.1	14.6
Seep Mat 3	2.9	2.9	16.6	4.8	18.1	0.7	27.4	0.3	5.6	3.3	3.9	1.2	12.2
Seep Mat 4	1.3	n.m.	15.0	6.0	2.5	n.d.	33.8	11.0	0.1	1.0	9.0	7.5	12.8
Seep Mat 5	3.7	4.6	15.1	4.3	15.9	n.d.	21.9	8.0	1.8	2.4	5.9	1.0	15.5
Seep Mat 6	2.0	4.4	11.4	3.7	32.9	n.m.	21.1	1.1	1.0	2.8	3.6	0.8	15.2
Seep Mat 7	10.9	7.2	16.1	0.6	15.6	n.d.	4.1	9.7	3.2	12.6	9.8	3.2	7.2
Seep Mat 8	9.4	8.1	17.3	1.3	22.2	n.m.	6.9	8.8	4.2	4.8	5.3	7.0	4.6
Seep Mat 9	1.9	4.2	7.0	1.5	46.7	2.8	12.7	1.5	2.1	11.9	1.3	0.4	6.1
Seep Mat 10	9.0	4.7	7.3	0.6	14.8	n.d.	6.5	27.5	2.1	9.8	2.7	5.9	9.1
Seep Mat 11	1.0	3.7	4.6	0.5	14.3	1.0	58.4	2.2	1.0	9.5	0.9	0.9	1.9
Seep Mat 12	1.2	2.1	5.3	1.7	44.3	6.2	14.1	3.1	1.2	11.8	1.5	1.4	5.9
Seep Mat 13	4.4	10.7	11.4	1.2	42.9	4.4	10.7	0.6	0.8	6.6	0.6	0.9	5.0
Seep Mat 14	7.4	15.1	14.1	1.2	37.2	n.d.	12.0	2.8	0.3	3.5	0.6	1.0	4.8

n.m. – concentration was not measured
n.d. – fatty acid was not detected

Table 3. δ13C values for the 12 major FA types within 14 seep samples. The 12 FA types exceeded 5% abundance in at least one of the 14 samples.

	δ¹³C (‰)											
Sample	12:0	14:1	14:0	15:0	16:1	16:1(5)	16:0	16:0 9-methoxy	18:1(9)	18:1(7)	18:0	18:0 methoxy
Seep Mat 1	-28.6	-10.8	-22.1	-27.5	-9.1	n.m.	-19	-21	-11.5	-7.8	-22.6	-17.8
Seep Mat 2	-32.3	-24.5	-27.6	-27.5	-26.2	n.m.	-25.1	-21.3	-27.1	-20.1	-25	-21.9
Seep Mat 3	-30.2	-29.4	-29.4	-28.8	-37.7	-49.4	-28.5	n.m.	-26.6	-35.1	-26.8	-26.1
Seep Mat 4	-30.6	-37.3	-26.2	-29.1	-18.6	n.d.	-24.1	-18.4	-31.9	-22.2	-22.7	-22.8
Seep Mat 5	-26.1	-19.8	-21.7	-27.1	-25.6	n.d.	-23.4	-21.8	-25.2	-5.9	-27.4	-16.7
Seep Mat 6	-24.6	-8.8	-21.1	-28.3	-27.9	-39.7	-26.6	-48.1	-27.2	-12.6	-26.8	-29
Seep Mat 7	-27.7	-7.6	-20	-30.2	-31.1	n.d.	-24	-31.6	-20	-11.8	-21.4	-28.8
Seep Mat 8	-27	-3.8	-19.3	-27.8	-25.2	-34.3	-25	-21.5	-35.6	-23.3	-21.0	-21
Seep Mat 9	-27.7	-0.9	-15.7	-31.3	-34.6	n.m.	-29.3	-31.1	-24.1	-25.7	-24.6	-30.3
Seep Mat 10	-25.3	-5.4	-17.5	-29.5	-35.9	n.d.	-27.5	-31.8	-22.7	-19.8	-23.4	-18.9
Seep Mat 11	-29.8	-2.2	-10	-29.6	-8.7	n.m.	-18.3	-11.5	-3.6	-7.5	-21.1	-7.7
Seep Mat 12	-28	-2.4	-13.5	-32	-35.4	n.m.	-19.9	-26.7	-18.4	-19	-22	-26.6
Seep Mat 13	-28.7	-12.5	-28.9	-31.5	-47.7	n.m.	-35.3	-41.3	-30.1	-34.3	-20.5	-44.1
Seep Mat 14	-28	-2.5	-13.9	-31	-31.3	n.d.	-25.7	-24.3	-20.4	-21.7	-18.6	-29.6

n.m. – fractionation was not measured
n.d. – fatty acid was not detected

Table 4. Elemental composition (relative abundance (as a weight %) of total C, S, N, H) and $\delta^{13}C$ values measured from total dry biomass in each of the environmental seep samples.

Sample	$\delta^{13}C$	%Carbon	%Sulfur	%Nitrogen	%Hydrogen
SEEP 1	-11.7	66.3	14.3	12.1	7.3
SEEP 2	-20.6	63.8	14.7	12.3	9.2
SEEP 3	-37.5	69.3	9.3	11.5	9.9
SEEP 4	-27.9	72.4	4.4	12.6	10.6
SEEP 5	-16.7	72.3	5.4	13.9	8.4
SEEP 6	-11.3	62.6	17.9	11.3	8.2
SEEP 7	-20.4	72.1	4.4	14.7	8.8
SEEP 8	-23.8	68.3	9.9	11.4	10.4
SEEP 9	-31.1	70.5	5.1	13.9	10.6
SEEP 10	-33.2	71.3	3.5	14.9	10.4
SEEP 11	-17.1	65.9	11.7	13.9	8.4
SEEP 12	-24.7	69.7	6.8	13.8	9.8
SEEP 13	-34.3	65.7	11.2	13.7	9.4
SEEP 14	-19.9	64.5	13.1	14.1	8.2

Table 5. Rank scores of the taxa dominating environmental SEEP samples 3, 6, and 7. Ranks are given for PhyloChip OTUs that were in the top 15 by hybridization intensity for SEEP 3, SEEP 6, or SEEP 7.

PhyloChip ID	Ranked Abundance		
Taxon/OTU#	SEEP 3	SEEP 6	SEEP 7
Sulfuricurvaceae 4650	n.d.	1	1
Sulfurovumaceae 4502	1	3	6
Sulfurovumaceae 5291	n.d.	n.d.	2
Sulfuricurvaceae 5120	2	4	4
Cytophaga 8205	3	5	5
Sulfurovumaceae 5283	n.d.	n.d.	3
Sulfurovumaceae 4400	4	n.d.	18
Sulfurovumaceae 5466	n.d.	2	7
Methylophaga 1419	5	60	n.d.
Helicobacteraceae 4353	6	n.d.	13
Sulfurovumaceae 4927	7	n.d.	n.d.
Methylococcaceae 1537	8	7	9
Sulfurovumaceae 4412	9	14	20
Sulfuricurvaceae 4473	10	9	8
Unclassified 1155	11	47	10
Sulfurovumaceae 4370	12	n.d.	27
Sulfuricurvaceae 5461	13	8	12
Sulfurovumaceae 4935	n.d.	6	n.d.
Pseudomonadaceae 1769	n.d.	12	11
Polaribacter 8414	14	15	25

n.d. Hybridization did not meet detection cutoff.

A.

B.

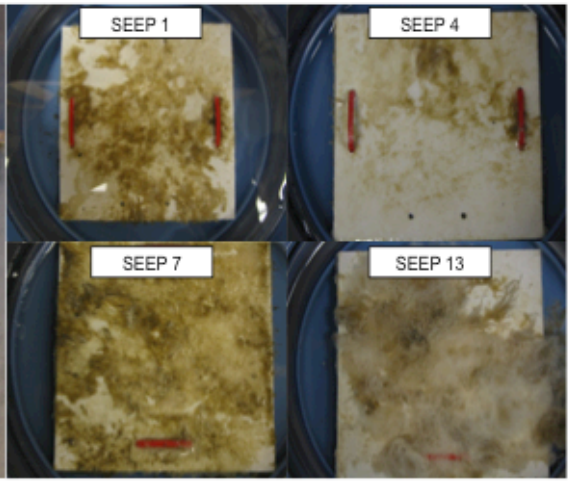

C.

	Mat Samples:	Environmental/SEEP	Experimental/SIP
Sampling	Location	Shane Seep	Shane Seep + Laboratory
	Dates	Dec. 20 '06 - Apr. 6 '07	June 25 '08 - Sept. 3 '08
	Growing time (in situ)	2-15 weeks	11 weeks
	Growing time (ex situ)	N.A.	4-6 days (98-142 hours)
	Controls	mats grown outside seep bed*	time=0; ^{12}C-CH_4 (non-SIP)
	Sample Names	"SEEP 1" – "SEEP 14"	"t=0"; "^{12}C t=F"; "SIP#" (1-7)
Analyses	Fatty Acid Profiles (Amounts + $\delta^{13}C$)	yes	no
	^{13}C-CH_4 Enrichment	no	100% ^{13}C
	PhyloChip Assays	yes	yes
	16S rDNA Cloning	no	yes

Figure 1. A. Benthic growing surfaces (white modules) affixed on a large pvc plate that was positioned at Shane Seep for in situ mat growth and subsequent sampling. B. SEEP samples displayed as individual growth modules (showing SEEP samples 1, 4, 7, and 13) collected weekly, during the environmental growth experiment at Shane Seep. C. Overview of mat growth, sample retrieval at Shane Seep, sample naming, and analyses performed on environmental (SEEP) and experimental (SIP) mats.

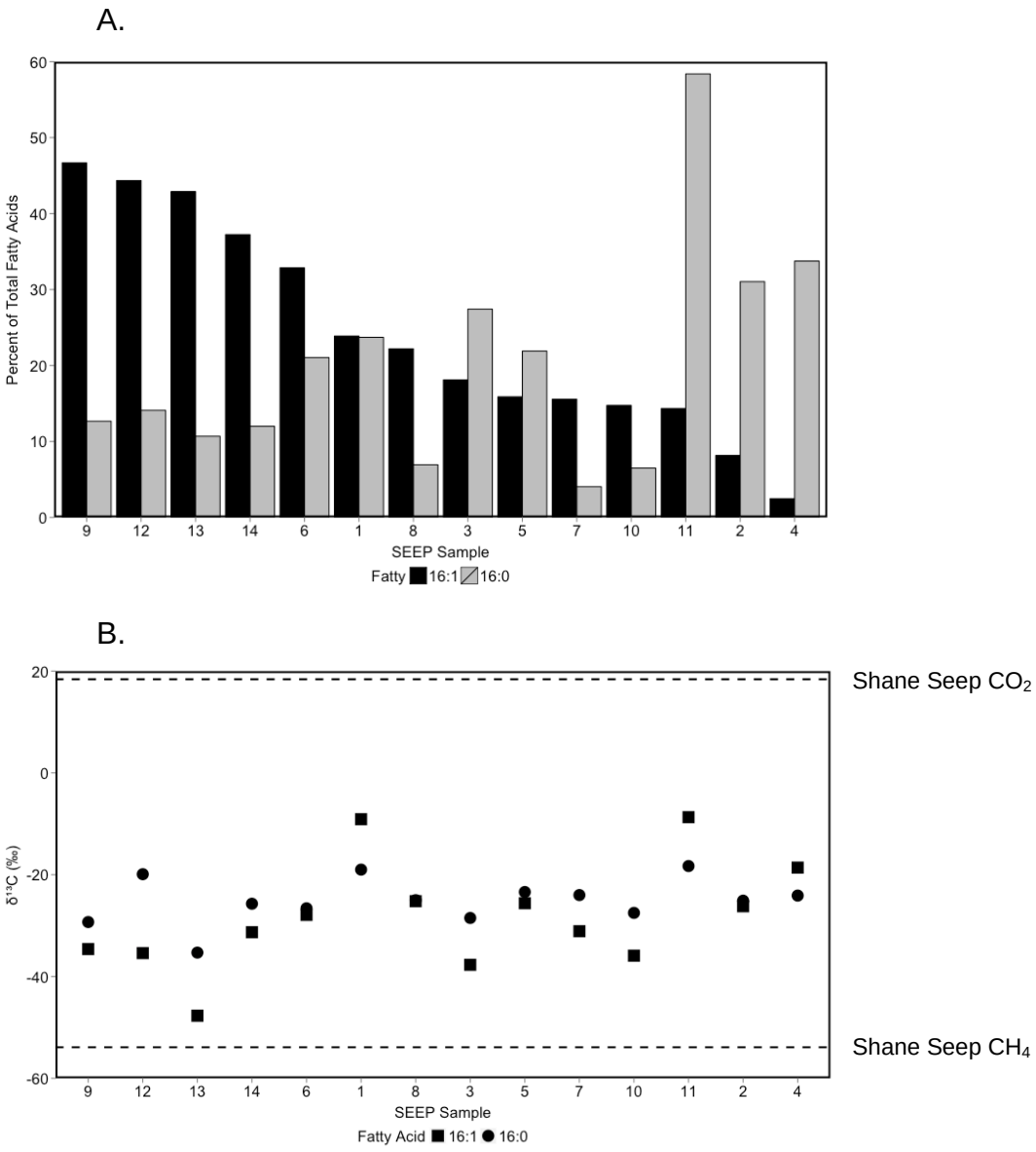

Figure 2. A) Relative abundance (with respect to all fatty acids detected) and B) δ13C values of major fatty acids 16:1 and 16:0 from each of the 14 seep samples grown at Shane Seep. Samples were ordered by 16:1 fatty acid abundance, in A and B.

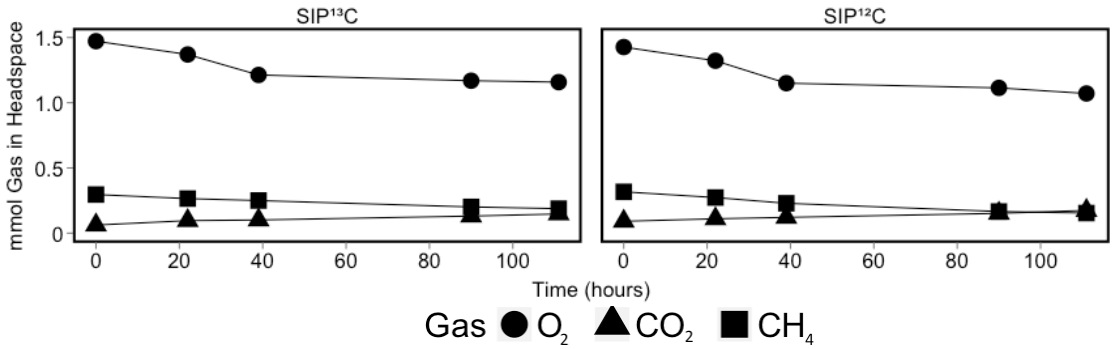

Figure 3. SIP enrichment ($^{13}CH_4$) and control ($^{12}CH_4$) headspace gas consumption of CH_4 and O_2 and production of CO_2 over 111-hour incubations with mats harvested from Shane Seep. Values reported in mmol were calculated from molar concentrations measured at multiple time-points.

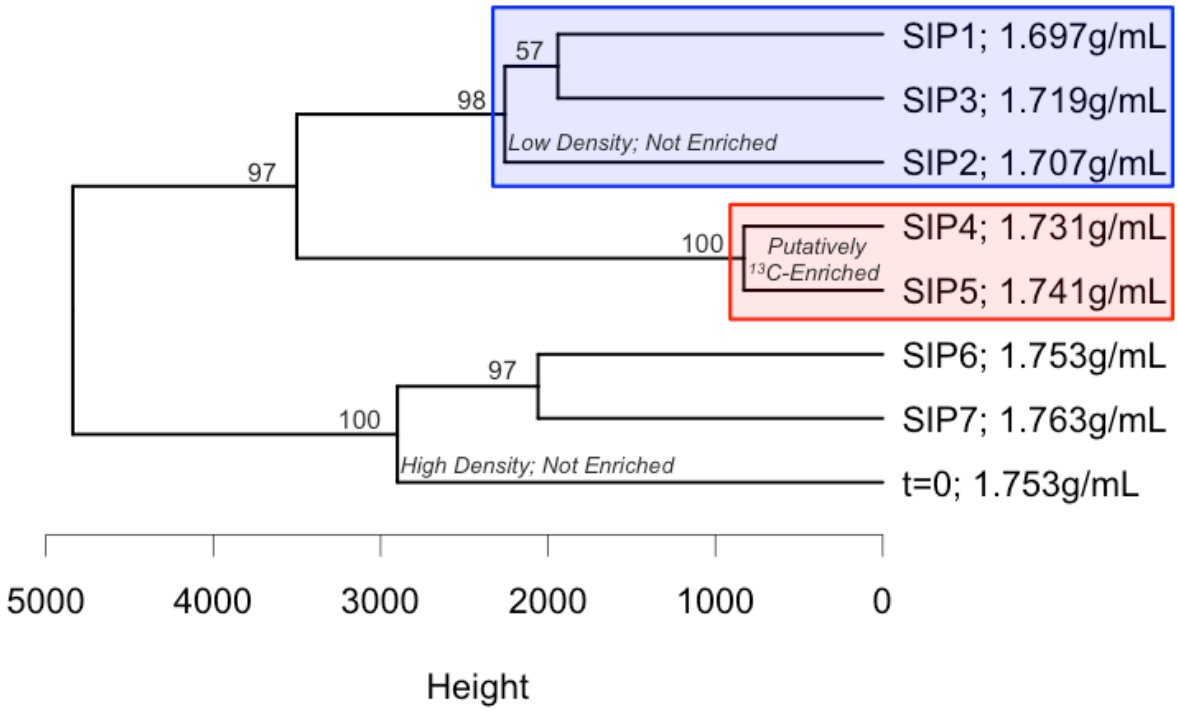

Figure 4. A hierarchical clustering dendogram, displaying the grouping of SIP density fractions and "t=0" fraction (1.753g/ml). Bootstrap resampling-derrived p-values are shown on each node as percentages (such that $p<0.05$ is >95). Average-linkage clustering was performed with Euclidean distances. The distance matrix was constructed from hybridization intensities of PhyloChip OTUs detected in all experimental/SIP samples and all environmental/SEEP samples. The same structure results from clustering with only OTUs derived from the top 10 abundant taxa in each SEEP sample.

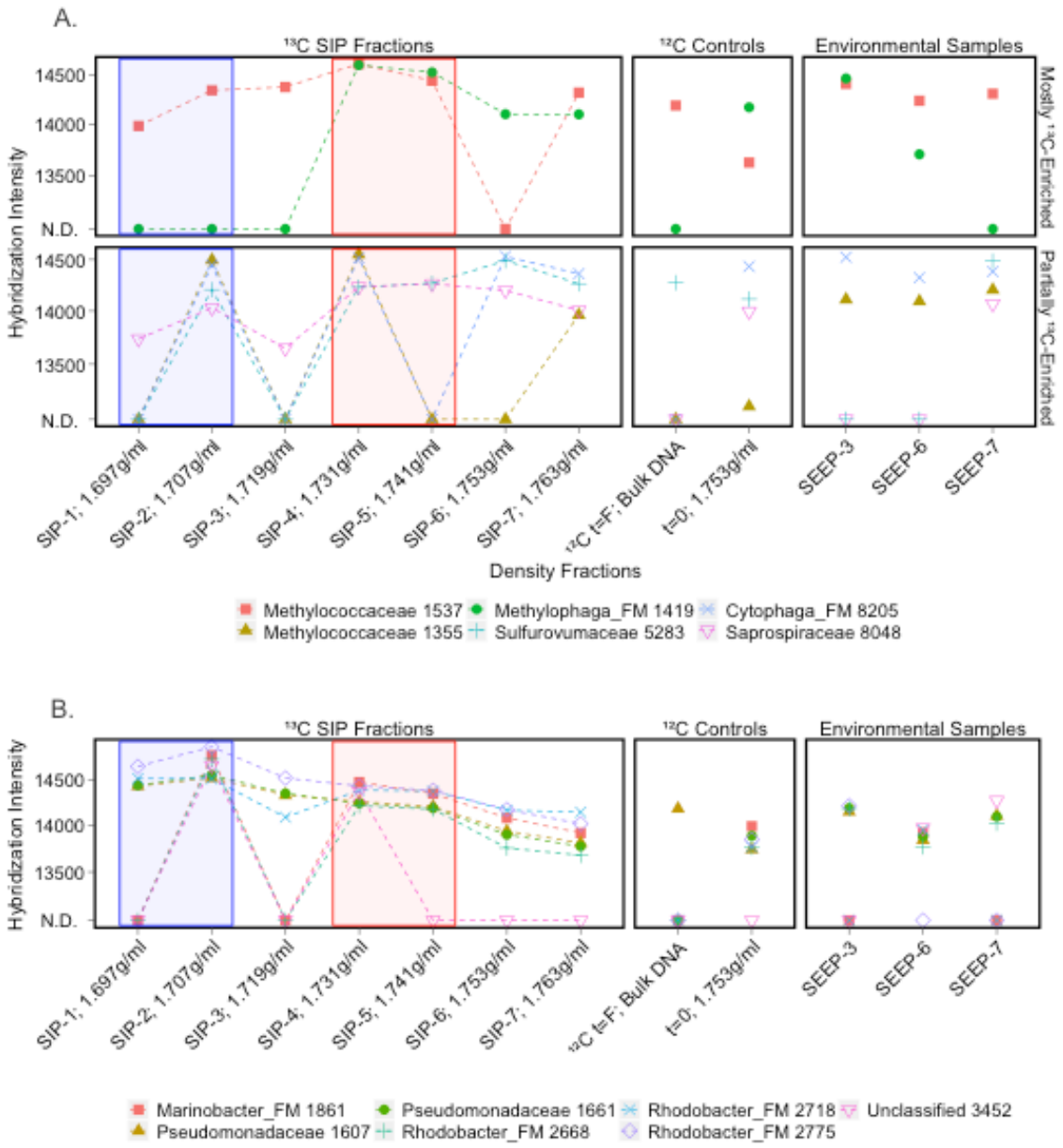

Figure 5. PhyloChip hybridization intensities are shown across experimental/SIP density fractions, experimental/SIP control samples, and environmental/SEEP samples. A) Taxa that are distinctly abundant in ^{13}C-associated fractions ("SIP-4; 1.731g/ml" or"SIP-5; 1.741g/ml") compared with lower abundancesin *all* non-enriched fractions ("SIP-1; 1.697g/ml", "SIP-2; 1.707g/ml", and "t=0; 1.753g/ml"). Strongly enriched taxa are shown in the top panel; partially enriched taxa are shown in the bottom panel. B)Taxa that are distinctly abundant in either of the light fractions (SIP-1; 1.697g/ml or SIP-2; 1.707g/ml) compared with lower abundance in *both* enriched fractions ("SIP-4; 1.731g/ml" and "SIP-5; 1.741g/ml"). Taxa that were undetected by PhyloChip in a given fraction are plotted as N.D.

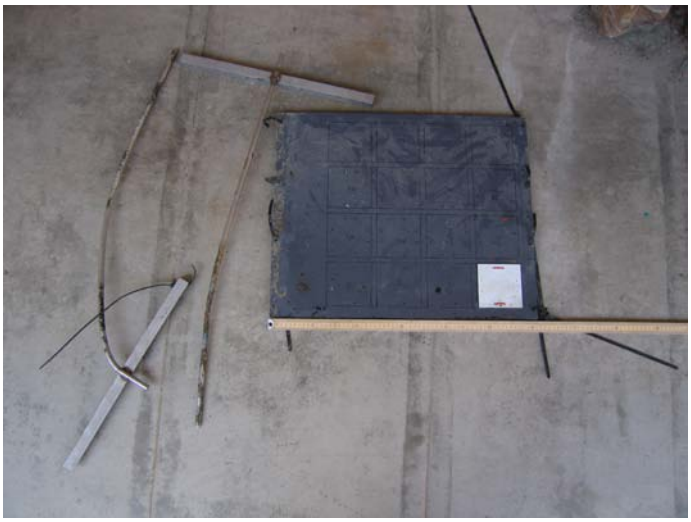

Figure 6. The dislodged benthic growing surface retrieved after a large offshore storm. The post-storm recovery of this device marked the end of the 14-week sampling period, associated with environmental “SEEP” samples. Mangled rebar pieces (right) were used to secure the device, positioned over venting Shane Seep gas.

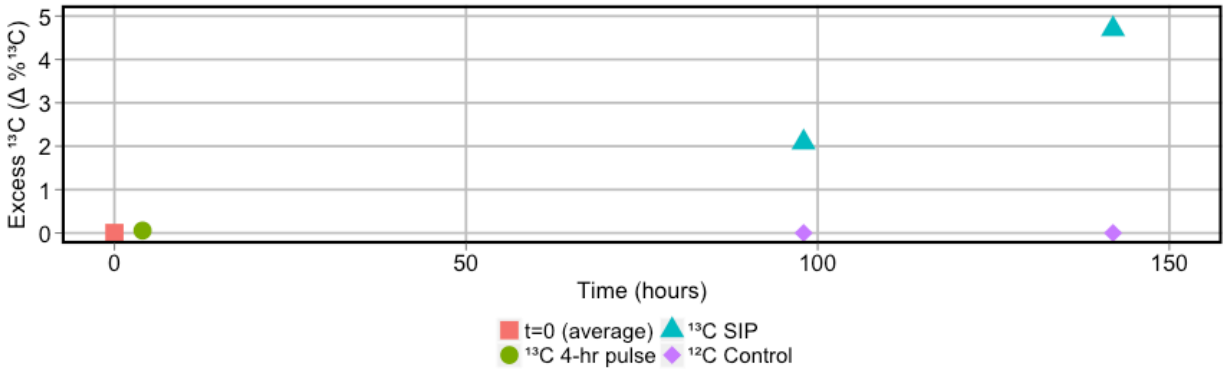

Figure 7. The isotope incorporation to biomass during SIP incubation is shown as a change in $\%^{13}C$ above background (t=0 $\%^{13}C$ subtracted from all values), from samples incubated with $^{13}CH_4$ and $^{12}CH_4$. The $^{13}CH_4$ incubations shown served as pseudoreplicates to the SIP incubation dedicated to DNA isolation ($^{13}CH_4$ incorporation not analyzed), as each was conducted with a separate mat sample.

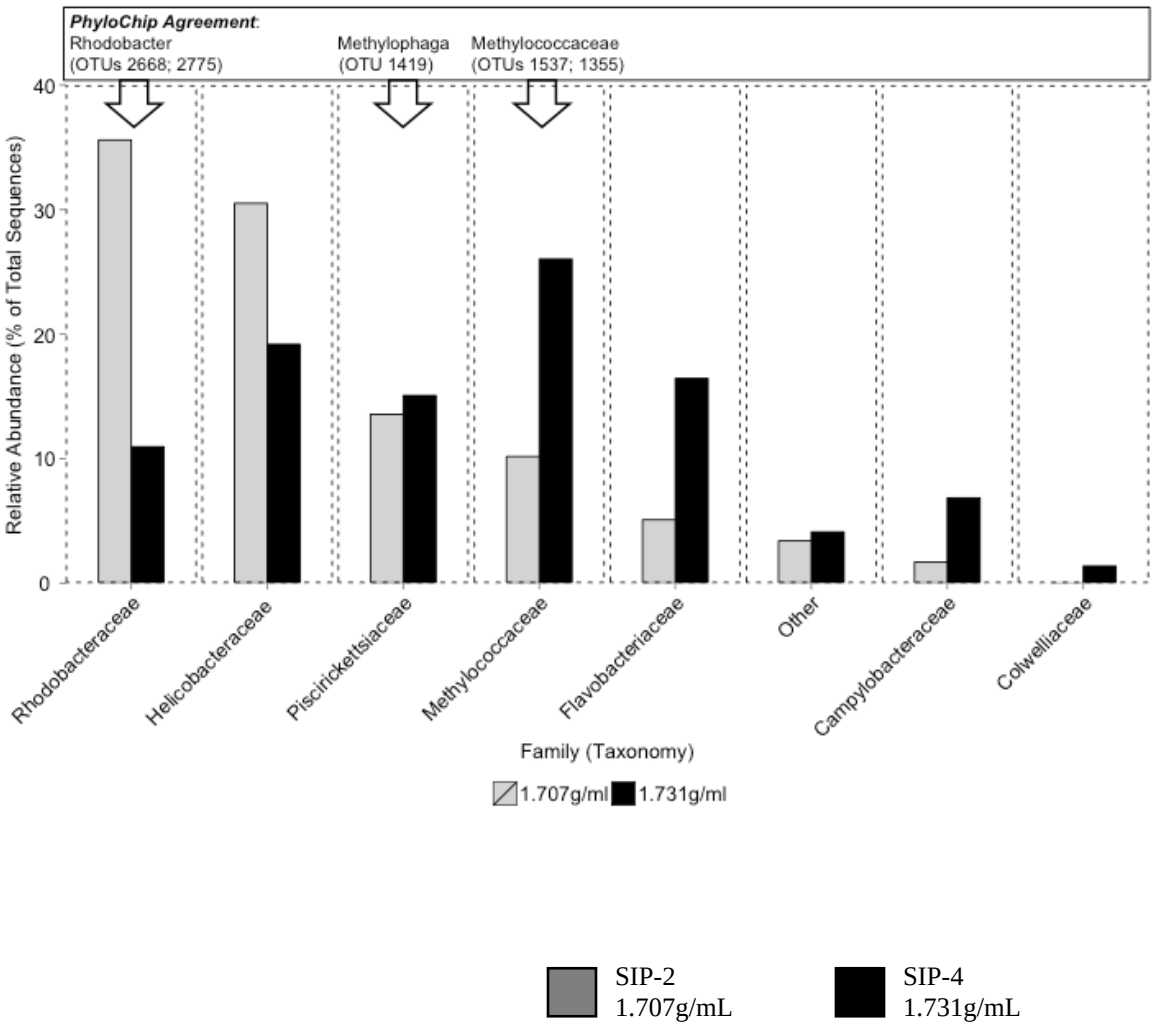

Figure 8. Relative abundances of taxa at the family level, shown as a percent of total clone library sequences. 16S rDNA clone libraries were constructed from two ^{13}C-SIP fractions ("SIP-4; 1.731g/ml" and "SIP-2; 1.707g/ml"). Family-level taxonomic annotations were obtained from sequence classi.Abundance differences consistent with PhyloChip results are indicated at the top of the graph. For reference: PhyloChip OTUs belonging to *Sulfurovumaceae* and *Sulfuricurvaceae* are closest related to the families *Campylobacteraceae* and *Helicobacteriaceae*; OTUs belonging to the genus *Methylophaga* are closest related to the family *Piscirickettsiaceae*.

Chapter 2. Pelagic Methanotrophy: Studies from the Pacific Ocean

Preface: In this section we describe results relating to our studies on methanotrophy in the waters of the Pacific Ocean. This work relates to Tasks 4-11 in our original proposal and includes studies from Basin settings and from the open ocean. The most informative results are presented, related to both published works and additional works in preparation as follows:

- → Mau S, Heintz MB, Kinnaman FS, Valentine DL (2010) Compositional variability and air-sea flux of ethane and propane in the plume of a large, marine seep field near Coal Oil Point, CA. **Geo-Marine Letters** 30: 367-378.
- → Redmond MC, Valentine DL, Sessions AL (2010) Identification of Novel Methane-, Ethane-, and Propane-Oxidizing Bacteria at Marine Hydrocarbon Seeps by Stable Isotope Probing. **Applied and Environmental Microbiology** 76: 6412-6422.
- → Valentine DL, Reddy CM, Farwell C, Hill TM, Pizarro O, et al. (2010) Asphalt volcanoes as a potential source of methane to late Pleistocene coastal waters. **Nature Geoscience** 3: 345-348.
- → Pack MA, Heintz MB, Reeburgh WS, Trumbore SE, Valentine DL, et al. (2011) A method for measuring methane oxidation rates using low-levels of (14)C-labeled methane and accelerator mass spectrometry. **Limnology and Oceanography-Methods** 9: 245-260.
- → Mau S, Heintz MB, Valentine DL (2011) Quantification of CH4 loss and transport in dissolved plumes of the Santa Barbara Channel, California. **Continental Shelf Research** 32, 110-120. doi:10.1016/j.csr.2011.10.016
- → Heintz MB, Mau S, Valentine DL (2012) Physical Control on Methanotrophic Potential in Waters of the Santa Monica Basin, Southern California. **Limnology and Oceanography** 57(2) 420-432. doi:10.4319/lo.2012.57.2.0420
- → Pack MA, MB Heintz, WS Reeburgh, SE Trumbore, DL Valentine, X Xu and ERM Druffel (submitted in revised form) Methane oxidation in the eastern tropical north Pacific water column. Limnology and Oceanography.
- → Farwell CA, MB Heintz, AL Sessions and DL Valentine (in preparation) Stable isotope probing for lipids of marine methanotrophs using deuterium and carbon-13.

Summary: Methane released from deep marine sediments may escape to the atmosphere or dissolve in the overlying water where its typical nanomolar concentrations feed pelagic methanotrophic bacteria. We investigated the consumption of dissolved methane along the North and Central American continental margins. Our approaches included methane oxidation rate measurements using tritium or low levels of carbon-14, stable isotope probing with carbon-13 and deuterium, concentration distributions using in-situ mass spectrometry and gas chromatography, and included the development of several new analytical approaches. Our results reveal patterns of methanotrophy among oceanic regimes to be primarily driven by methane availability and water mass history, and implicate bacterial type 1 methanotrophs as being important consumers of methane in the deep ocean environment.

INTRODUCTION

Methane is a radiatively active greenhouse gas, with approximately 23 times the warming potential of CO_2 (Lelieveld et al., 1993). Ocean sediments constitute a significant global reservoir of methane, and catastrophic releases have been associated with major climatic events (Hinrichs et al., 2003; Kennett et al., 2000; Zachos et al., 2008). Methane diffuses and advects from sediments to the overlying water column along continental margins (Judd, 2003; Klemme, 1987; Kvenvolden, 2002), but only a fraction of this methane is emitted to the atmosphere. The majority is consumed by microbes in the water column (Reeburgh, 2007) through the aerobic process of methane oxidation.

Aerobic methane oxidation has been observed in a number of pelagic marine environments (Rehder et al., 1999; Valentine et al., 2001; Ward and Kilpatrick, 1993; Ward et al., 1989) and is generally credited with sustaining ocean methane concentrations in the nanomolar range (Reeburgh, 2007). The existence of bacteria capable of using methane as a sole carbon source is well established, and these bacteria are recognized as either type I or type II methanotrophs based on internal membrane structure and carbon assimilation pathways (Hanson and Hanson, 1996). Distributions of type I and type II methanotrophs are known to be influenced by dissolved methane, oxygen and nitrate concentrations. Type I methanotrophs have been observed to dominate in marine and other saline environments (Bourne et al., 2000; Carini et al., 2005; Holmes et al., 1996), and several marine type I methanotrophs have been isolated in pure culture (Fuse et al., 1998; Lidstrom, 1988; Sieburth et al., 1987). However, the factors influencing diversity and activity of marine aerobic methanotrophs are still not well understood. Several recent studies targeting aerobic methanotroph genetic diversity in marine sediment (Losekann et al., 2007; Wasmund et al., 2009) and water column (Tavormina et al., 2011; Tavormina et al., 2008) environments are consistent with the action of primarily type I methanotrophs. Still, little is known about the distribution, diversity or metabolism of bacteria responsible for attenuation of methane in marine systems, particularly for ambient concentrations in the nanomolar range. These uncertainties represent fundamental gaps in our understanding of methane biogeochemistry.

Our primary study area was in the California current, an eastern boundary current system. The Southern California Bight is a distinctive region of this current system (Figure 9) , with water properties and circulation patterns influenced by both the variable poleward and equatorward transport of surface waters, and the poleward transport of deeper waters (Hickey 1998).

The California current travels along the eastern Pacific margin from Vancouver Island to Baja, California. At Point Conception, a bend in the coastline causes the California Current (CC) to flow further offshore, along the Santa Rosa – Cortes Ridge. As the current flows past the Southern California Bight, the southward flow bifurcates and, turning south-eastward, shoreward and then poleward, enters the borderland region (Jackson 1986). When poleward flow continues northward around Point Conception this flow is referred to as the California Countercurrent (CCC), and when waters re-circulate within the bight the flow is termed the Southern California Eddy (SCE) (Hickey 1998). Waters carried by the CC, CCC, and re-circulated in the upper water column in the SCE are collectively referred to as northern waters, and typically extend through the upper 250-300 m of the water column. The composition of northern Bight waters is spatially and seasonally variable (Lynn and Simpson 1987). During summer months, when the

off-shore CC is strongest, upwelling occurs along the northern coast (Emery 1960). A seasonally variable mixture of this upwelled water and off-shore northern water is carried into the Bight by the CCC. The composition of these waters evolves as they mix with upwelled southern waters from within Bight basins, and as the mixed waters are re-circulated through the borderland region by the SCE. During fall months, the CC slows and a greater proportion of off-shore northern water is carried into the Bight by the CCC. Also at this time the SCE weakens and CCC flow is predominantly poleward. Since these waters are not re-circulated within the borderland, there is less mixing and compositional change in the northern Bight waters, and they retain a T-S signature closer to that of off-shore northern waters carried by the CC (Hickey 1998).

The California Undercurrent (CUC) flows poleward along the continental margin below the CC, CCC, SCE current system. Deep southern waters, sourced from the Eastern Tropical Pacific, are carried poleward by the CUC, and mix with northern Bight waters in the 250-500 m depth range (Hickey 1998). Sverdrup and Fleming (1941) and Emery (1960) documented the mixing zone of northern and southern waters in the mid-water column and developed an empirical relationship for determining the proportions of northern and southern water in this region, based on T-S characteristics.

Here we describe the results of studies designed to better understand the controls on marine methanotrophy through better understanding of the distribution of metabolic rates as a function of environmental setting, the identities and interactions of the responsible microbes, and the time course changes in methanotrophic activity in nature. The SCE serves as a backdrop for most of these studies.

METHODS

Details of most our methods are available in the peer reviewed literature (see preface), except for the lipid stable isotope probing experiments as follows.

Trilaminate bag incubations

Incubation bags were constructed of a gas-impermeable and non-reactive trilaminate material with polyethylene, aluminum foil, and polypropylene layers (LPS Industries Inc., Newark, NJ, USA). The bags were sealed after construction using an Impulse heat sealer (TEW Electric Heating Company). The bags included two ports, one for filling with seawater and one that permitted both the bleeding of residual nitrogen gas during filling and the injection of gaseous incubation substrate. The ports were constructed by punching two 3/8” holes in one side of each bag. Each hole was sealed with a gas- and water-tight assembly consisting of a threaded nylon-barbed fitting that was inserted through (in this order) a Teflon washer, a Teflon-coated silicone septum, the trilaminate material, another Teflon-coated silicone septum, and finally a Teflon screw nut. With these ports open, each bag was soaked for several hours in 5% HCl, thoroughly rinsed with at least 2 L Nanopure water, and flushed with ultra-high purity N_2 gas for at least one hour prior to use.

To decrease pressure on the bags' seams during filling, each bag was filled while submerged in a water bath, keeping both ports above the surrounding water level. Care was taken to not introduce any water from the bath into the bags. Once filled, the bags were moved to a storage room kept at a constant 5.5°C, approximating the *in situ* tem-

perature. Incubations were conducted for a maximum of 5 days, chosen to allow sufficient label incorporation while limiting cross-feeding.

SIP incubations were carried out using [^{13}C]-methane (+99%, Isotec), [^{13}C]-CO_2 (+99%, Isotec), and deuterated methane (CH_3D, 98 atom % D, Sigma Aldrich). Details of the incubation protocol for each site are given in Table 1. Each sample bag was allowed to incubate at 5.5°C for 3 to 5 days. At the end of each incubation, water was filtered through a 1.2-µm glass fiber prefilter (Whatman GF/C) and a 0.7-µm (Whatman GF/F) glass fiber filter using stainless steel filter holders (Sartorius). The filtered water was discarded and the prefilter and filter stored in separate plastic Petri dishes at -80°C until return to shore.

Fatty acid extraction and isotope analysis

Biomass-laden GF/F and GF/C filters were lyophilized for 24 hours (K-series Lyophilizer, VirTis, Gardiner, NY). The dried filters were weighed, cut into small pieces, and transferred to a Teflon extraction vessel. The GF/F and GF/C filters for each site were extracted together in dichloromethane (DCM)/methanol (9:1) solution using a microwave extraction system (CEM Mars 5) at 100 °C for 20 minutes with stirring. The total lipid extract was transferred into 40-ml volatile organic acid vials and evaporated to dryness at 40°C under N_2. It was then saponified with 0.5M NaOH in 5% NaCl/H_2O, acidified to pH ~1 with HCl, and extracted 3x with methyl t-butyl ether (MTBE). Fatty acids were further purified from the collected extract by solid-phase extraction (PhenomenexSepra NH2, 0.5 g) with elution using 8 ml of 2% formic acid in DCM. Fatty acids were converted to their methyl esters by reacting with 10% BF_3 in methanol at 70°C for 20 minutes, and extracted three times with 10 ml hexane. The collected extract was dried over anhydrous Na_2SO_4 and concentrated under N_2 to a volume of <0.5 ml.

Fatty acid methyl ester (FAME) structure and relative abundance were quantified by GC-MS using a Thermo Finnigan Trace/DSQ instrument at the California Institute of Technology. GC separation employed a ZB-5ms column (Phenomenex; 30 m × 0.25 mm × 0.25 µm) with a programmable-temperature vaporization (PTV) injector. Column effluent was split (~80/20) between the MS and a flame ionization detector (FID) for simultaneous measurements. FAME abundance was calculated using FID response relative to a single internal standard, palmitic acid isobutyl ester, assuming identical response factors.

Stable carbon isotope ratios (δ^{13}C values) were measured using a Thermo Finnigan GC-IRMS at the Marine Science Institute Analytical Lab, University of California, Santa Barbara. This system used a Trace GC with an Omegawax 250 capillary column (Supelco; 30m × 0.25 mm x 0.25 µm) and split/splitless injector, GC combustion III interface, and Delta PlusXP mass spectrometer. The GC combustion III unit catalyzes the oxidation of organic analytes to CO_2 over Cu/Ni/Pt wire heated to 950°C, and water is removed through a selectively permeable Nafionmembrane. The carrier gas was helium with a flow rate of 1.2 ml min^{-1}. Carbon isotope ratios are reported in the conventional δ^{13}C notation as part-per-thousand (‰) variations from the Pee Dee Belemnite (VPDB) standard. Values of δ^{13}C for each compound were calibrated using a CO_2 working standard with a nominal δ^{13}C value of -32.6‰. All δ^{13}C values were normalized to a decanoic acid methyl ester isotope standard obtained from Arndt Schimmelmann at Indiana

University and then corrected for the addition of the methyl group from methanol, assuming $\delta^{13}C_{methanol}$ = -25‰.

Lipid extract were also used for compound-specific D/H analysis, performed at Caltech on a ThermoFinnigan Trace GC coupled to a Delta PlusXP IRMS via a ThermoFinnigan GC/TC pyrolysis interface operated at 1440°C. Three *n*-alkanes of known isotopic composition were co-injected with each sample. Two of these compounds (C_{17} and C_{22}) were used as reference peaks for the calibration of isotopic analyses, while the third (C_{23}) was treated as an unknown to assess accuracy. Hydrogen isotope ratios are presented in the conventionalδDnotation as part-per-thousand (‰) deviations from Standard Mean Ocean Water (VSMOW).Data were normalized to the SMOW/SLAP isotopic scale by comparison to an external standard mixture containing 15 *n*-alkanes with δD values from -41‰ to -256‰ (Sessions et al., 2001). FAME δD values were corrected for added methyl hydrogen by isotopic mass balance, with the δD value of methyl H derived from analyses of methylated phthalic acid of known isotopic composition (Sessions, 2006).

RESULTS AND DISCUSSION

Methanotrophic Potential

Methanotrophic potential was studied in sites throughout the Southern California Borderland at sites described in Redmond et al., 2010, Mau et al., 2011, Pack et al., 2011 and Heintz et al., 2012. The relationship between oxidation rate and environmental conditions was investigated to understand controls on methanotrophy and to develop methane budgets valid at local and basin scale. Here we present results from throughout the SCB, including a comparison of our results from this work with results from a previous cruise – provided for reference.

Depth profiles of methane concentrations for each of the 7 reference hydrocasts from 2010 are shown in Fig. 10a. Throughout the water column methane concentrations are above the saturation value expected for waters at atmospheric equilibrium. Concentrations in the upper 400 m range between 3-5 nmol L-1, with a subsurface methane maximum (7-15 nmol L-1) between 25-100 m. Elevated concentrations (10-100 nmol L-1) in mid-waters (550-600 m) observed on casts 3b and 3c suggest that low-resolution sampling in this zone on other casts may have precluded the detection of a mid-water maxima. Below 700 m, methane concentrations range from 5-242 nmol L-1, and maximum concentrations occur at ~ 800 m, near the depth of the crest of the pingo (Fig. 11). Concentrations decrease between the pingo crest and the seafloor. Cast 5, located 18 km away from the identified venting feature, shows elevated concentrations at both 750 m (37.6 nmol L-1) and in the deepest sample collected (895 m, 18.0 nmol L-1). These observations indicate that methane maxima below sill depth are not limited to the immediate vicinity of the identified venting feature.

Depth profiles of methane concentrations for each of the 5 hydrocasts from 2009 in the SMB are shown in Fig. 12a, and show similar trends to one another. Throughout the upper 700 m concentrations of methane are greater than the value expected for waters at atmospheric equilibrium. Concentrations are elevated in the upper 100 m, ranging from 4.0-9.3 nmol L-1, but without the distinct spike in concentration observed between 25-100 m in 2007. At all stations, concentrations increase between 300-500 m to maxima of 7.5-8.8 nmol L-1 at Sta. 6, 7, and 10, and to 75 nmol L-1 at Sta. 9. Concen-

trations gradually decrease between 500 and 700-800 m, and below 700 m concentrations reach the background level of 3-5 nmol L-1 at most sampling locations. At southern basin Sta. 6 and 7 a methane minimum occurs at 700 m, 50-100 m shallower than at the northern stations, and an increase in methane concentration (up to 33 and 5.3 nmol L-1) is observed below this depth. Methane concentrations at SPB and SCtB stations (Fig. 13a) show similar trends to those in the SMB above their respective sill depths (737 and 600 m), although concentrations are generally lower. Elevated methane concentrations are also observed in the mid-water column (350-600 m) in each of these basins. Below the SMB sill depth in the SCtB concentrations are at or below background (3-5 nmol L-1) levels.

Methane turnover times – July 2007– Depth profiles of turnover times for each of the 7 hydrocasts are shown in Fig. 10b. As a result of differences in sampling resolution, casts 3b, 3c, and 5 define the profile of turnover time through the upper and mid-water column, but limited data from casts 1, 2, 3a, and 4 match patterns observed in the higher-resolution casts (Fig. 10b). Relatively slow turnover times (0.5-3.5 years) are observed at 25-50 m, in the same depth range as the subsurface methane maxima. Turnover times become more rapid between 50-100 m, and show a gradual slowing from around 100 days to 1.6 years between 100-500 m. Mid-water turnover times are longest at 500 m, just above the small mid-water (550-600 m) methane maxima observed on casts 3b and 3c. At 500 m, turnover times range from 0.76 years to 3 years, but with most (4 out of 6) samples showing a tighter range (1.5-1.7 years). Below 700 m (Fig. 11) all samples show relatively rapid turnover times (17-65 days), and these are some of the most rapid turnover times yet reported in the marine water column. There is not a consistent relationship between methane concentration and turnover time in deep waters although, at Sta. 3a and 4, both concentration and turnover time decrease in the depth horizon at or above the venting feature (Fig. 11). This suggests a microbial response to methane input and an effective drawdown of methane. Longer turnover times generally correspond with lower methane concentrations in waters deeper than the venting feature (Fig. 11).

September 2009- Depth profiles of turnover times for each of the 5 hydrocasts in the SMB are shown in Fig. 12b. Depth profiles from the SPB and SCtB are shown in Fig. 13b. In all three basins, in the upper 100 m where concentrations are elevated and stable, turnover times slow from 0.1-0.2 years at 10 m to 1.5-2.2 years at 100 m. At 250-300 m, where methane concentrations shift from a decreasing to an increasing trend, turnover times become more rapid (0.3-0.5 years at Sta. 6,7, and 9), but generally are either stable or continue to grow longer below this narrow excursion. At depths greater than 400 m, turnover time begins to gradually speed up towards the bottom of each profile, where the fastest times are observed (15-219 days). In the SCtB, turnover times in the upper 600 m are comparable to those in the SMB and SPB. Below 600 m the waters of SMB and SCtB are no longer connected, and SCtB turnover times continue to slow to a maximum of 3.3 years at 750 m and then increase to 1.7 years in bottom waters. The shape of the SCtB turnover time profile below 600 m is similar to that observed in SMB and SPB deep waters, suggesting that this pattern is related to basin topography.

Methane oxidation rates – Depth profiles of methane oxidation rates from 2007 casts and 2009 casts are presented in Fig. 14a,b. Results from both expeditions show

that methane oxidation rates in the SMB and SPB range over about an order of magnitude through the water column. In 2007, 90% of samples collected between 25-700 m in the SMB (n=36) have oxidation rates in the range 2-22 nmol L-1 yr-1. Below 700 m (n=21), rates range from 44-491 nmol L-1 yr-1. In 2009, samples collected between 10-12 m (n=5) show elevated rates, between 23-101 nmol L-1 yr-1. Measurements made between 25-850 m in the SMB (n=80) fall into the range 1-12 nmol L-1 yr-1, with the exception of two deep water samples collected at Sta. 6 (850 and 890 m) with rates of 353 and 366 nmol L-1 yr-1. Above the 600 m sill depth, oxidation rates in the SCtB are on the low end of the range observed in the SMB and SPB, and are significantly slower below sill depth – ranging from ~ 0.6-2 nmol L-1 yr-1.

Fig. 15a shows the difference between 2007 and 2009 oxidation rates in the SMB. For comparison, the difference between the yearly averages from all samples at each depth, and the difference between 2007 and 2009 at the single station occupied both years (casts 5 and 6) are shown. There is a linear relationship (Fig. 15b) between the difference in the average methane oxidation rate and the difference in salinity between 50-250 m in 2007 and 2009 (y=0.052x-0.091, R2=0.99; n=5). The difference in both parameters decreases logarithmically with depth (Fig. 15c) (rox: y=248e-0.048x R2=0.95; S: y=230e-0.924x R2=0.99; n=5). This relationship is not explained by differences in methane solubility, (due to differences in temperature and salinity) between these two years.

Potential temperature, salinity, and oxygen - Fig. 16 shows annotated T-S diagrams with data from casts 5 and 6. Between 10–250 m there is a mixing zone of northern waters, between 250-500 m there is a mixing zone of northern and southern water, between 500-750 m there is a zone of southern water, and below 750 m deep basin waters are relatively uniform and trapped by northern and southern sills. Oxygen concentrations observed in 2007 and 2009 generally match well (Fig. 17a), save for divergence of 0.2-0.4 mL L-1 between 100-200 m. In both casts water is suboxic at about 250 m. Comparative profiles (casts 5 and 6) of temperature and salinity in the upper water column are shown in Fig. 17 b,c. These profiles indicate that in both cases, the thermocline and pycnocline were present at 11-12 m, and that salinity was significantly lower above ~150 m in 2009 (cast 6). T-S data from Sta. 5 and 6 are representative of what was observed for all casts on each trip (hydrocast data not shown for all stations; available upon request).

Depth profiles of methane concentration and turnover time are remarkably similar between stations on each trip, and show both common and distinctive features between trips. For the purposes of this discussion the water column is divided into 4 horizons; upper waters (10-250 m), mid-waters (250-500 m), lower waters (500-700 m), and bottom waters (>700 m). Each horizon corresponds to distinct T-S characteristics (Fig. 16).

Shallow regime (10-250 m)- The upper bound of this horizon is set by the shallowest samples collected. The lower bound is defined by the 250 m transition point between northern waters of the upper water column and the mixing zone between northern and southern waters in the mid-water column (Fig. 16). This transition occurs near the 26.6 $\sigma\theta$ isopycnal, where the core of the CUC is often observed during summer months (Lynn and Simpson 1987).

In 2009 (cast 6), lower salinities were observed at depths shallower than 250 m (i.e., at densities less than 26.5 kg m-3), and slightly (0.01-0.6°C) higher temperatures

were observed between 44-250 m (Figs. 16, 17 b,c). The difference in salinity above 250 m, between sampling periods, indicates that in September 2009 there was a higher proportion of water sourced from the offshore CC (Fig. 16). The slightly higher temperatures in 2009 initially appear contradictory to this interpretation, since the CC carries relatively cold waters, however these higher temperatures may be attributed to greater surface warming later in the season (September 2009 vs. July 2007), or may only appear relatively high as a result of an anomalously high proportion of relatively cold upwelled waters in 2007. In fact, in 2007 upwelling was reported to be unseasonably strong throughout the spring (McClatchie et al. 2008).

In July 2007 the upper waters are a mixture of CC water, saltier, colder, upwelled-waters, and southern waters, circulated within the borderland by the CCC and SCE (Fig. 9a, Fig. 16). Dynamic height maps show that the SCE was present in the borderland during sampling in 2007 (McClatchie et al. 2008). The mixing of these waters in the borderland resulted in the observed difference in T-S characteristics between trips, shifting the 2007 curve toward higher salinities and lower temperatures.

While methane concentrations in the upper 250 m are nearly the same in 2007 and 2009, turnover times, and thus oxidation rates, are different. In 2007, between 50-250 m, turnover times are faster (Figs. 10b, 12b) and oxidation rates higher (Figs. 14, 15). The difference in average oxidation rate (Fig. 15b) decreases as T-S characteristics converge at about 250 m. These patterns reinforce the observation that different water masses were present in 2007 and 2009, and suggest that higher methanotrophic potential observed in 2007 is related to water mass character.

We hypothesize that the difference in methanotrophic potential between the two distinct northern water mixtures observed in 2007 and 2009 is a result of their different histories and patterns of circulation within the borderland. The higher methanotrophic potential of 2007 may be due to the introduction of an active methanotrophic community from deep waters upwelled along the coast, or may be due to an increased residence time of northern waters in the methane-rich borderland region as they are re-circulated within the SCE. Lower methanotrophic potential in 2009 may be the result of low methanotroph abundance in waters carried by the CC in the absence of seasonal upwelling, or by the shorter residence time of waters in the borderland region, as they are transported through the area by the CCC rather than circulated within the area by the SCE. Competition with heterotrophic populations for nutrients, as suggested by greater O2 drawdown just below the depth of light penetration in cast 6 (Fig. 17a), is another potential contributing factor to diminished methanotrophic activity in 2009. These explanations remain speculative.

Although the physical processes discussed here, with regard to the CC system, operate on longer time scales and larger spatial scales than differences observed over periods of hours to days at a single station in Ward's 1992 study, these results reinforce the conclusion that physical processes are an important control on methane dynamics in the upper water column of the SMB, and provide a broader seasonal and spatial perspective.

While methane concentrations are similar between the current study and Ward's 1992 study, turnover times measured in the previous study were longer, ranging from non-detectable to a minimum turnover time of one year. A previous study where both 14C and 3H tracers were used to measure oxidation rates in the Black Sea water col-

umn showed substantial variability between these methods, especially in shallow waters (Reeburgh et al. 1991). However, in this study the two methods were not directly compared on water collected at the same time. These authors (Reeburgh et al. 1991) conclude that the observed variability may be attributed to changes in the water mass sampled as gyres drive lateral mixing over short time scales. The difference between the rates observed in Ward's study and in the current study may also be due to natural variability in the upper water column of the SMB, but the discrepancy highlights the need for additional intercomparison of available techniques, as conducted by Pack et al. (2011) for the low-level 14C, accelerator mass spectrometry based technique. The combined observations of long turnover times in Ward's study and long turnover times associated with the 2007 sub-surface methane maxima (25-50 m) in this study (Fig. 10) suggest that there may be unidentified physical or biological inhibitory factors capable of limiting methane oxidation in the upper water column.

Mid-water regime (250-600 m) - This horizon is characterized by the mixing zone between northern and southern waters, an increase in turnover time with depth, and a mid-water methane maximum. In 2007 methane concentrations are consistently in the 3-5 nmol L-1 range between 250-400 m with an increase in methane, variable between casts, between 450-600 m. In 2009 a more uniform increase in methane was detected below 250 m, with a maximum at 500 m (Fig. 12b). In 2007 and 2009 turnover times slowed between 250-500 m, and grew more rapid below the mid-water maximum. The maxima observed in both years are in the depth range over which maxima with similar magnitude were detected by (Ward and Kilpatrick 1993). Turnover times detected at the mid-water maximum in Ward and Kilpatrick's (1993) earlier study fall into the range of those measured in this study.

The detection of the mid-water methane maxima at stations throughout the SMB during three expeditions by Ward and Kilpatrick, and during both of our expeditions, leads to the conclusion that this feature is fed by persistent methane sources within the basin. Ward and Kilpatrick (1993) suggest that the source of the mid-water maximum is methane advected from the continental shelf through the suboxic water column. While there is no evidence contrary to this suggestion, at the time of their study the pingo had not yet been identified as a deepwater methane source.

Based on the observations of (Paull et al. 2008) gas from the pingo or other such structures is another likely contributor to the mid-water methane maxima. These authors observed an acoustic disturbance at 550 m using 330 kHz scanning sonar on an ROV and confirmed, with video observations, that this disturbance was associated with a rising stream of bubbles from the pingo. The pingo is located in the hydrate stability zone, at 800 m water depth and temperatures less than 5°C (Sloan et al. 1998; Paull et al. 2008). Thus, as bubbles emanate from the feature, they are able to develop hydrate skins that slow dissolution as they rise buoyantly through the water column (Brewer et al. 2002; Rehder et al. 2002; Rehder et al. 2009).

Since only dissolved methane is available for methanotrophic consumption, rising bubbles with hydrate skins allow gaseous methane to escape microbial consumption within the effective biological filter developed in the lower water column of this basin. Hydrate-skinned bubbles from this, and potentially other sites, effectively bypass the depths of most effective methanotrophic consumption (Figs. 10b, 5b) and may contribute to the basin-wide methane maxima at 500 m, in a zone with a less well-established

methane biofilter (Figs. 10b, 12b). However, the pingo is the largest, and one of the only, venting features yet observed in the SMB, so hydrate coated bubbles originating in deep waters likely are not the only source of methane to the 500-550 m maximum. Another potential source of methane is persistent seepage from basin walls at this depth, where sediment-hosted methane hydrate is also unstable.

Although there is a persistent methane maxima near 500 m throughout the SMB (Figs. 10a, 12a), and also in the SPB and SCtB (Fig. 13a), turnover times are longer at this depth than at depths both above and below (Figs 10a, 12b, 6b). Oxygen limitation cannot explain the relatively slow turnover times observed in mid-waters, since more rapid turnover times are observed in bottom waters with less oxygen. We suggest that this depth zone may represent the transition point between top-down and bottom-up controls on methane dynamics.

Above 500 m, as basin connections become increasingly constricted with depth, and the residence time of mixed layer waters grows longer, turnover times grow slower. In this depth zone the proportion of southern water increases with depth as northern and southern waters mix. However, an increasing proportion of southern water and the presence of a mixing zone above 500 m do not appear to be viable explanations for longer turnover times with increasing depth. Similar turnover times were observed in 2007 and 2009 (Figs. 10b, 12b), despite a larger proportion of northern water mixing throughout the 250-500 m depth zone in 2007 (Fig. 16).

Below 500 m, as basin connections continue shrink, and the residence time of southern waters grows longer, turnover times grow faster. Turnover times may be shorter in deeper waters as a result of increased residence time. Between 500-700 m, the size of the connections between the SMB and surrounding basins decreases (66.5 km at 500 m, 37.5 km at 600 m, 9.5 km at 700 m), allowing less water to flow through the basin, and for less lateral mixing between basins. A longer residence time for waters in the lower water column may mean a longer residence time for methanotrophic populations in an area with consistent methane replenishment from methane sources at the seafloor. Sources of the basin-scale mid-water maximum and controls on methanotrophic efficacy in the mid-water column remain to be fully elucidated.

Deep water regimes – The lower water column of the SMB can be divided into two zones; southern waters between 600-737 m and bottom waters below sill depth (737 m). Waters below sill depth are also southern in origin, but their long residence time in the restricted basin bottom changes their character, especially in terms of oxygen and nutrient renewal and methane concentration. In the zone between 600-737 m turnover times decrease with depth in both 2007 and 2009. This pattern may be caused by a growing or more active methanotrophic population with decreasing distance from methane sources at the seafloor. As mentioned above, the shorter residence time of southern waters with decreasing depth may also play a role, continually diluting and transporting the population away from methane source areas, and out of the basin. Turnover times grow faster with increasing depth in both 2007 and 2009, but at different rates. In 2007 turnover times are on the order of weeks by 700 m, while turnover times in 2009 do not fall into this range until 850 m. Broadly, this pattern reflects sampling of stations directly over the venting feature in 2007 and in other areas of the basin in 2009. However, turnover times in this depth zone are faster in 2007 (cast 5) than in 2009 (cast

6) at the station sampled during both expeditions, suggesting that there may be more to this trend than sampling bias.

Below 750 m, flow is restricted by sills on the northwestern and southeastern ends of the basin. However, it has been shown that waters below sill depth in this basin are not stagnant (Hickey 1991; Hickey 1992), and that deep-basin anoxia is avoided as a result of slow, continuous, mixing with southern deep waters moving through the basin, and also as a result of periodic flushing of basin bottom waters (Bograd et al. 2002).

Continuous influx of methane, and the long residence time of waters below sill depth enables development of an effective methanotrophic biofilter for dissolved methane. In 2007, at stations near the venting feature, concentrations as high as 242 nmol L-1 were measured, along with background level concentrations. In 2009, at stations at a distance from the venting feature, background concentrations (3-5 nmol L-1) and concentrations below saturation were measured. Turnover times are rapid in both cases. These results suggest that a methanotrophic community is stimulated by restricted plumes of methane, and is able to retain a high level of activity throughout basin bottom waters.

Physical controls – This study is the first to propose a direct link between microbial methane consumption and specific physical environmental features in the marine environment. In the SMB methanotrophic activity appears to be strongly influenced not only by substrate availability but also by topography, and the history and circulation patterns of the waters that host methanotrophic communities. Similar factors are likely structure methanotrophic communities in other methane-replete settings.

Microbial Communities and Stable Isotope Probing

Stable isotope probing was used to investigate the methanotrophic community in both the deep waters of the Santa Barbara and Santa Monica Basins, as well as in shallow hydrocarbon seeps. We use stable isotope probing (SIP) in two different ways. First was to identify the lipids of active methanotrophs in marine waters using methane concentrations near their ambient levels. This work also enabled the comparison of carbon and hydrogen assimilation into the lipids of naturally occurring deep-water methanotrophic communities. A second way we used stable isotope probing was to identify the DNA of bacteria actively consuming methane, ethane and propane in a shallow water hydracarbon seep at Coal Oil Point.

For the large volume (35L) SIP-lipid incubations, the lipids were extracted from filtered biomass that had been incubated for 3–5 days with 13C- and/or D-labeled methane. The five surviving incubations, identified in Table 6, were extracted to yield FAME fractions that were analyzed using GC-MS and GC-IRMS. The most abundant lipids in all samples were 16- and 18-carbon monounsaturated (16:1, 18:1) and saturated (16:0, 18:0) FA, accounting for >70% of the total FA (TFA) in all samples. The 16:1 FA were the most abundant, ranging from 40-45%TFA between samples. The 14:0 FA was also relatively abundant, accounting for 10-20% of TFA. Samples also contained small amounts of 14:1 and 12:0 FA. Values of δ13C for individual FA in the five samples are presented in Table 7. The control incubations (samples SB\13CO2\12CH4 and SM\13CO2\12CH4) displayed little or no 13C enrichment in any FA analyzed, with δ13C values ranging from -24.4 ‰ to -30.7 ‰ in the Santa Barbara Basin, and -19.0 ‰ to -27.5 ‰ for the Santa Monica Basin (Table 7). These values are more depleted than

those previously reported for bulk organic matter in this region and are interpreted as background levels for the specific FA analyzed here.

Substantial 13C enrichment was observed for individual FA in [13C]-CH4 incubations from both basins, compared to the control incubations. For the Santa Barbara Basin, the 16:1 FA for samples SB\13CH4\CH3D and SB\13CH4 showed the greatest level of 13C enrichment, with δ13C values exceeding 700‰ for each sample. 16:0 and 18:1 FA were the next most enriched in both SBB [13C]-CH4 incubations, though notably the relative enrichment of these FA differs between the two samples (Table 7). Slight 13C enrichments were observed in 14:0 FA in both SB\13CH4\CH3D and SB\13CH4; 14:1 was only enriched in sample SB\13CH4\CH3D, not SB\13CH4. The sole [13C]-CH4 incubation from the Santa Monica Basin (sample SM\13CH4\CH3D) exhibited 13C enrichment in 14:0, 16:0, 16:1, and 18:1 FA, but not in 18:0 FA (Table 7). As with samples from the Santa Barbara Basin, the most-enriched FA in sample SM\13CH4\CH3D was 16:1 FA (δ13C = 82 ‰).

Values of δD for individual fatty acids are also reported in Table 7. FA from the SB\13CO2\12CH4 and SB\13CH4 incubations were not enriched in D beyond previously reported background levels(Jones et al., 2008). Similar to the trend observed in 13C enrichments, 16:1 FA from SB\13CH4\CH3D had the largest D enrichment of any FA analyzed, while 16:0 FA displayed slight enrichment (Table 7). 14:0 and 18:0 fatty acids for this sample reflect background values for δD (Jones et al., 2008), whereas 18:1 FA displayed a slight enrichment of D. The SM\13CH4\CH3D incubation from the Santa Monica Basin showed a similar relative distribution of D label as for SB\13CH4\CH3D from the Santa Barbara Basin, with 16:1 FA being the most D-enriched. 16:0 and 18:1 FAMEs in this sample were more D-enriched than previously reported background values. δD values obtained for all FA analyzed in the SM\13CO2\12CH4 incubation sample reflect expected background values.

The uptake of isotope labels into fatty acids indicative of methanotrophs suggests that bacteria actively and vigorously consume methane in these deep ocean environments. While the 13C-based technique used here has previously been employed to probe methanotroph DNA and lipids from terrestrial and marine sediments (Holmes et al., 1996; Hutchens et al., 2004; Redmond et al., 2010), DNA of methylotrophs in marine surface waters (Neufeld et al., 2008a; Neufeld et al., 2008b), and DNA of methanotrophs from the Deepwater Horizon's contaminated plumes (Redmond and Valentine, 2011), we are aware of no published studies using SIP to probe lipids of natural methanotroph communities active at nanomolar methane concentration in deep oceanic waters. Our results indicate that (aerobic) methanotrophy in the deep ocean is mediated at least in part by bacteria. Although our samples contained too little material for analysis of archaeal lipids our data for bacterial lipids are consistent with Bacteria as major consumers of nanomolar-level methane in oxic marine systems.

This study further provides a comparison of methanotrophic activity between two deep, silled basins along the southern California Bight. The SBB and the SMB are 588 and 905 m deep, respectively. Bottom waters are dysoxic (0.1 to 0.2 ml O2 L-1) with stable temperatures (SMB, 5.1°C; SBB, 6.5°C). Methane in both basins is thought to be primarily of biogenic origin, with methanogenesis observed at >2 m sediment depth. Thermogenic gas vents through faults and anticlines of the inshore shelf system in both basins but no venting of this nature has been observed below sill depth. Exposed me-

thane hydrates and at least two distinct authigenic carbonate structures venting biogenic gas have been observed in the SMB (Paull et al., 2008), with one biogenic methane seep thus-far identified below sill depth in the Santa Barbara Basin (Hinrichs et al., 1999). High organic production and particulate flux (Crisp et al., 1979) in the Santa Barbara Basin may contribute to greater biogenic methane production in sediments there. Methane is likely to accumulate in restricted bottom waters of both basins primarily via diffusive flux through sediments (Martens et al., 1998), in addition to advective transport. Based on the relatively rapid metabolism of methane observed at both locations, we hypothesize that the flux of methane into the restricted waters of the deep basins sustains growth of vigorous methanotrophic communities, with oxidation rates (Table 8) indicating a more voracious community in the Santa Barbara Basin compared to the Santa Monica Basin.

The distribution of 13C-enriched FA holds clues to the identity of the active methanotrophs in these waters. The largest 13C enrichments were observed in the 16:1 FA in both the SBB and SMB with 16:0 and 18:1 FA also significantly enriched. Figure 18 shows the fractional abundance of 13C in individual FA as a percent of the total carbon or hydrogen in the major FAMEs analyzed. In general, these lipid classes have been observed in both type I and type II methanotrophic bacteria as well as in non-methane oxidizing methylotrophs (Guckert et al., 1991). The FA isomers 16:1(ω8c) and 18:1(ω8c) are known biomarkers of type I and type II methanotrophs, respectively, and have been used to detect and quantify these groups in environmental samples (Boon et al., 1996; Guezennec and Fiala-Medioni, 1996; Nichols et al., 1987). However, the 16:1(ω7c) and 18:1(ω7c) FA isomers have been observed in both type I and type II methanotrophs, though type II methanotrophs typically synthesize a greater proportion of the 18:1 isomer (Bodelier et al., 2009) with the converse true for type I methanotrophs (Guckert et al., 1991; Nichols et al., 1985). The greater 13C and D enrichment observed in 16:1 FA compared to 18:1 FA is consistent with proportions of these lipid classes observed in type I methanotrophs (Guckert et al., 1991; Holmes et al., 1999; Knief et al., 2003). 16:0 lipids have been observed in all strains of methanotrophs and methylotrophs, though in type I methanotrophs, they are less abundant than 16:1 lipids. The transformation of isotopically-labeled methane into primarily 16:1 FA suggests that new lipids are formed by type I methanotrophs, though the action of novel type II methanotrophs cannot be ruled out based on the data presented here.

A primary concern in SIP studies is that cross-feeding of the isotope label confuses primary consumers with secondary consumers, predators and autotrophs. Our results show a clear signal for D incorporationin lipids that mimics the pattern for 13C incorporation (Figure 18), possibly avoiding cross-feeding because the amendments were only 60 nM in methane. Our results also show no notable autotrophy from CO2. The clear signal for deuterium is largely attributable to its lower natural abundance compared to13C, but is tempered by several factors including the use of only a 25% label (e.g., CH3D), water as a source of lipid hydrogen (Sessions and Hayes, 2005; Sessions et al., 2002), and a greater variability in ambient lipid D content relative to 13C (Table 7). Nonetheless, the continued attenuation of excess D relative to excess13C provides a potential means to identify lipids or other metabolites produced by organisms cross feeding on methane-derived carbon. Methylotrophs are typically recipients of methane's carbon by cross-feeding (Hutchens et al., 2004; Kessler et al., 2011; Redmond

et al., 2010) as methanol is excreted in abundance by methanotrophs (Harwood 1972). We are unaware of any studies of hydrogen isotopes in lipids of methylotrophs, though water was identified as an important precursor for individual amino acids (Mosin et al., 1996) and for RNA (Batey et al. 1996) in methylotrophs. Attenuation of deuterium in the metabolic products of methylotrophs may potentially distinguish methanotrophs from methylotrophs. Alternatively, both groups may retain similar proportions of excess deuterium, in which case, deuterium attenuation could serve to distinguish methanotrophs/methylotrophs from other cross-feeding heterotrophs for which a majority of lipid hydrogen seemingly derives from water (Wegener et al., 2012; Zhang et al., 2009). While the results presented here do not address this point directly, our observation that only 17-26% of lipid-bound hydrogen originated from methane supports the concept that a D label is likely to be strongly attenuated at each trophic level, and could be used to identify cases where 13C label uptake results from cross-feeding or carbon reincorporation by autotrophy.

Our Stable isotope probing studies in hydrocarbon seeps were published in 2010 (Redmond et al., 2010) and identify methanotrophs active in hydrocarbon seep environments by linking methane-derived, isotopically enriched DNA to the sequence of the 16SrRNA gene of the responsible bacteria.

We were successful in identifying aerobic bacteria oxidizing gaseous hydrocarbons in surface sediment from the Coal Oil Point seep field, offshore Santa Barbara, California. After incubating sediment with 13C-labeled methane, ethane, or propane, we confirmed the incorporation of 13C into fatty acids (Figure 19 and Figure 20) and DNA (Figure 21). Terminal restriction fragment length polymorphism (T-RFLP) analysis and sequencing of the 16S rRNA and particulate methane monooxygenase (pmoA) genes in 13C-DNA revealed groups of microbes not previously thought to contribute to methane, ethane, or propane oxidation. First, 13C methane was primarily assimilated by Gammaproteobacteria from the family Methylococcaceae, Gammaproteobacteria related to Methylophaga, and Betaproteobacteria from the family Methylophilaceae (Figure 22). The latter two have not been previously shown to oxidize methane and may have been cross-feeding on methanol, but both were heavily labeled after just three days. pmoA sequences were affiliated with the Methylococcaceae, but most were not closely related to cultured methanotrophs (Figure 23). Second, 13C ethane was consumed by a novel group of Methylococcaceae. Growth with ethane as the major carbon source has not previously been observed in the Methylococcaceae; a highly divergent pmoA-like gene detected in the 13C-labeled DNA may encode an ethane monooxygenase. Third, 13C propane was consumed by a group of unclassified Gammaproteobacteria not previously linked to propane oxidation. This study identifies several bacterial lineages as participants in the oxidation of gaseous hydrocarbons in marine seeps and supports an alternate function for some pmoA-like genes.

This study also demonstrates the ability of SIP to identify previously unknown groups of methane-, ethane- and propane-oxidizing bacteria at a marine hydrocarbon seep, with distinct groups of bacteria found responsible for each process. These results have implications for our understanding of methane oxidation in marine environments. Novel groups of marine bacteria may contain monooxygenases related to those of terrestrial bacteria but with different substrate affinities, affecting our ability to detect them with common primer sets and to predict biogeochemical function based on the presence

or absence of these genes. The multitude of hydrocarbon compounds present in seep environments could support a range of hydrocarbon-oxidizing bacteria, and relatively little is known about which organisms consume which compounds and under what conditions. Further work, with both culturing and culture-independent techniques like SIP, is important to better understand these processes and their role in biogeochemical cycling. Importantly, these studies positioned us to conduct SIP studies in the Gulf of Mexico following the Deepwater Horizon incident, to follow up on the interaction of methanotorphy with other microbial processes such as ethanotrophy or propanotrophy.

REFERENCES

Bange, H. W., U. H. Bartell, S. Rapsomanikis, and M. O. Andreae. 1994. Methane in the Baltic and North Seas and a reassessment of the marine emissions of methane. Global Biogeochemical Cycles 8: 465-480.

Bodelier, P.L.E., Bar Gillisen, M.-J., Hordijk, K., Sinninghe Damste, J.S., Rijpstra, W.I.C., Geenevasen, J.A.J., Dunfield, P.F., 2009. A reanalysis of phospholipid fatty acids as ecological biomarkers for methanotrophic bacteria. ISME J 3, 606-617.

Bograd, S. J., F. B. Schwing, C. G. Castro, and D. A. Timothy. 2002. Bottom water renewal in the Santa Barbara Basin. Journal of Geophysical Research 107: 3216-3224, doi:10.1029/2001JC001291

Boon, P.I., Virtue, P., Nichols, P.D., 1996. Microbial consortia in wetland sediments: A biomarker analysis of the effects of hydrological regime, vegetation and season on benthic microbes. Marine and Freshwater Research 47, 27-41.

Bourne, D.G., Holmes, A.J., Iversen, N., Murrell, J.C., 2000. Fluorescent oligonucleotide rDNA probes for specific detection of methane oxidising bacteria. FEMS Microbiology Ecology 31, 29-38.

Bowman, J.P., Skerratt, J.H., Nichols, P.D., Sly, L.I., 1991. Phospholipid fatty-acid and lipopolysaccharide fatty-acid signature lipids in methane-utilizing bacteria. FEMS Microbiology Ecology 85, 15-22.

Brewer, P. G., C. Paull, E. T. Peltzer, W. Ussler III, G. Rehder, and G. Friederich. 2002. Measurements of the fate of gas hydrates during transit through the ocean water column. Geophysical Research Letters 29: 2081-2084, doi:10.1029/2002GL014727

Brooks, J.M., D.F. Reid, and B.B. Bernard. 1981. Methane in the upper water column of the northwestern Gulf of Mexico. Journal of Geophysical Research-Oceans 86: 11029-11040, doi:10.1029/JC086IC11p11029

Burke, R.A., D.F. Reid, J.M. Brooks, and D.M. Lavoie. 1983. Upper water column methane geochemistry in the eastern tropical North Pacific. Limnology And Oceanography 28: 19-32.

Carini, S., Bano, N., LeCleir, G., Joye, S.B., 2005. Aerobic methane oxidation and methanotroph community composition during seasonal stratification in Mono Lake, California (USA). Environmental Microbiology 7, 1127-1138.

Conrad, R., and W. Seiler. 1988. Methane and hydrogen in seawater (Atlantic Ocean). Deep Sea Research 35: 1903-1917, doi:10.1016/0198-0149(88)90116-1

Crisp, P.T., Brenner, S., Venkatesan, M.I., Ruth, E., Kaplan, I.R., 1979. Organic chemical characterization of sediment-trap particulates from San Nicolas, Santa Barbara,

Santa Monica and San Pedro Basins, California. Geochim. Cosmochim. Acta 43, 1791-1801.
Cynar, F.J., and A.A. Yayanos. 1992. The distribution of methane in the upper waters of the Southern California Bight. Journal of Geophysical Research-Oceans 97: 11269-11285, doi:10.1029/92JC00865
de Angelis, M.A., Lilley, M.D., Baross, J.A., 1993. Methane oxidation in deep-sea hydrothermal plumes of the endeavour segment of the Juan de Fuca Ridge. Deep Sea Research Part I: Oceanographic Research Papers 40, 1169-1186.
deAngelis, M.A., M.D. Lilley, E.J. Olson, and J.A. Baross. 1993. Methane oxidation in deep-sea hydrothermal plumes of the Endeavor Segment of the Juan de Fuca Ridge. Deep Sea Research 40: 1169-1186, doi:10.1016/0967-0637(93)90132-M
Ding, H., Valentine, D.L., 2008. Methanotrophic bacteria occupy benthic microbial mats in shallow marine hydrocarbon seeps, Coal Oil Point, California. Journal of Geophysical Research-Biogeosciences 113.
Dumont, M.G., Murrell, J.C., 2005. Stable isotope probing - linking microbial identity to function. Nature Reviews Microbiology 3, 499-504.
Emery, K. O. 1960. Water, p. 97-138. In The Sea Off Southern California, A Modern Habitat of Petroleum. John Wiley and Sons.
Fung, I., J. John, J. Lerner, E. Matthews, M. Prather, L. P. Steele, and P. J. Fraser. 1991. Three-dimensional model synthesis of the global methane cycle. Journal of Geophysical Research-Atmospheres 96: 13033-13065, doi:10.1029/91JD01247
Fuse, H., Ohta, M., Takimura, O., Murakami, K., Inoue, H., Yamaoka, Y., Oclarit, J.M., Omori, T., 1998. Oxidation of trichloroethylene and dimethyl sulfide by a marine Methylomicrobium strain containing soluble methane monooxygenase. Bioscience Biotechnology and Biochemistry 62, 1925-1931.
Griffiths, R. P., B. A. Caldwell, J. D. Cline, W. A. Broich, and R. Y. Morita. 1982. Field observations of methane concentrations and oxidation rates in the southeastern Bering Sea. Applied and Environmental Microbiology 44: 435-446.
Guckert, J.B., Ringelberg, D.B., White, D.C., Hanson, R.S., Bratina, B.J., 1991. Membrane fatty-acids as phenotypic markers in the polyphasic taxonomy of methylotrophs within the proteobacteria. J. Gen. Microbiol. 137, 2631-2641.
Guezennec, J., Fiala-Medioni, A., 1996. Bacterial abundance and diversity in the Barbados Trench determined by phospholipid analysis. FEMS Microbiology Ecology 19, 83-93.
Hanson, R.S., Hanson, T.E., 1996. Methanotrophic bacteria. Microbiological Reviews 60, 439-+.
Heeschen, K. U., R. S. Keir, G. Rehder, O. Klatt, and E. Suess. 2004. Methane dynamics in the Weddell Sea determined via stable isotope ratios and CFC-11. Global Biogeochemical Cycles 18: GB2012, doi:10.1029/2003GB002151
Hein, J. R., W. R. Normark, B. R. McIntyre, T. D. Lorenson, and C. L. Powell II. 2006. Methanogenic calcite, 13C-depleted bivalve shells, and gas hydrate from a mud volcano offshore Southern California. Geology 34: 109-112, doi:10.1130/G22098.1
Heintz, M.B., Mau, S., Valentine, D.L., 2012. Physical control on methanotrophic potential in waters of the Santa Monica Basin, Southern California. Limnology and Oceanography 57, 420-432.

Hickey, B.M. 1991. Variability in two deep coastal basins (Santa Monica and San Pedro) off Southern California. Journal of Geophysical Research 96: 16689-16708, doi:10.1029/91JC01375

Hickey, B.M. 1992. Circulation over the Santa Monica - San Pedro Basin and Shelf. Progress in Oceanography 30: 37-115, doi:10.1016/0079-6611(92)90009-O

Hickey, B.M. 1998. Coastal oceanography of western North America from the tip of Baja California to Vancouver Island (coastal segment (8,E), p. 345-393. In A. R. Robinson and K. H. Brink [eds.], The Sea, vol.11. John Wiley & Sons.

Hinrichs, K.U., Hayes, J.M., Sylva, S.P., Brewer, P.G., DeLong, E.F., 1999. Methane-consuming archaebacteria in marine sediments. Nature 398, 802-805.

Hinrichs, K.U., Hmelo, L.R., Sylva, S.P., 2003. Molecular fossil record of elevated methane levels in late pleistocene coastal waters. Science 299, 1214-1217.

Holmes, A.J., Owens, N.P.J., Murrell, J.C., 1996. Molecular analysis of enrichment cultures of marine methane oxidising bacteria. Journal of Experimental Marine Biology and Ecology 203, 27-38.

Holmes, A.J., Roslev, P., McDonald, I.R., Iversen, N., Henriksen, K., Murrell, J.C., 1999. Characterization of methanotrophic bacterial populations in soils showing atmospheric methane uptake. Appl. Environ. Microbiol. 65, 3312-3318.

Hutchens, E., Radajewski, S., Dumont, M.G., McDonald, I.R., Murrell, J.C., 2004. Analysis of methanotrophic bacteria in Movile Cave by stable isotope probing. Environmental Microbiology 6, 111-120.

Jackson, G. A. 1986. Physical oceanography of the Southern California Bight, p. 13-52. In R. W. Eppley [ed.], Plankton Dynamics of the Southern California Bight. Springer-Verlag.

Jones, A.A., Sessions, A.L., Campbell, B.J., Li, C., Valentine, D.L., 2008. D/H ratios of fatty acids from marine particulate organic matter in the California Borderland Basins. Organic Geochemistry 39, 485-500.

Judd, A.G., 2003. The global importance and context of methane escape from the seabed. Geo-Marine Letters 23, 147-154.

Karl, D.M., L. Beversdorf, K.M. Björkman, M.J. Church, A. Martinez, and E.F. DeLong. 2008. Aerobic production of methane in the sea. Nature Geoscience 1: 473-478, doi:10.1038/ngeo234

Kelley, C. 2003. Methane oxidation potential in the water column of two diverse coastal marine sites. Biogeochemistry 65: 105-120, doi:10.1023/A:1026014008478

Kennett, J.P., Cannariato, K.G., Hendy, I.L., Behl, R.J., 2000. Carbon isotopic evidence for methane hydrate instability during quaternary interstadials. Science 288, 128-133.

Kessler, J.D., Reeburgh, W.S., Valentine, D.L., Kinnaman, F.S., Peltzer, E.T., Brewer, P.G., Southon, J., Tyler, S.C., 2008. A survey of methane isotope abundance (C-14, C-13, H-2) from five nearshore marine basins that reveals unusual radiocarbon levels in subsurface waters. Journal of Geophysical Research-Oceans 113.

Kessler, J.D., Valentine, D.L., Redmond, M.C., Du, M., Chan, E.W., Mendes, S.D., Quiroz, E.W., Villanueva, C.J., Shusta, S.S., Werra, L.M., Yvon-Lewis, S.A., Weber, T.C., 2011. A Persistent Oxygen Anomaly Reveals the Fate of Spilled Methane in the Deep Gulf of Mexico. Science 331, 312-315.

Klemme, H.D., 1987. The geology of future petroleum resources, in: Forster, N.A.B., E. A. (Ed.), Treatise on Petroleum Geology Reprint series 2. American Association of Petroleum Geologists, pp. 387 - 407.

Knief, C., Lipski, A., Dunfield, P.F., 2003. Diversity and Activity of Methanotrophic Bacteria in Different Upland Soils. Appl. Environ. Microbiol. 69, 6703-6714.

Knittel, K., A. Boetius. 2009. Anaerobic oxidation of methane: Progress with an unknown process. Annual Review of Microbiology 63: 311-334, doi:10.1146/annurev.micro.61.080706.093130

Kvenvolden, K.A., 2002. Methane hydrate in the global organic carbon cycle. Terr. Nova 14, 302-306.

Lamontagne, R.A., J.W. Swinnerton, V.J. Linnenbom, and W.D. Smith. 1973. Methane concentrations in various marine environments. Journal of Geophysical Research-Oceans 78: 5317-5324, doi:10.1029/JC078I024p05317

Lelieveld, J., Crutzen, P.J., Bruhl, C., 1993. Climate effects of atmospheric methane. Chemosphere 26, 739-768.

Lidstrom, M.E., 1988. Isolation and characterization of marine methanotrophs. Antonie Van Leeuwenhoek Journal of Microbiology 54, 189-199.

Losekann, T., Knittel, K., Nadalig, T., Fuchs, B., Niemann, H., Boetius, A., Amann, R., 2007. Diversity and abundance of aerobic and anaerobic methane oxidizers at the Haakon Mosby mud volcano, Barents Sea. Applied and Environmental Microbiology 73, 3348-3362.

Lynn, R. J., and J. J. Simpson. 1987. The California Current system - the seasonal variability of its physical characteristics. Journal of Geophysical Research-Oceans 92: 12947-12966, doi:10.1029/JC092iC12p12947

Martens, C.S., Albert, D.B., Alperin, M.J., 1998. Biogeochemical processes controlling methane in gassy coastal sediments--Part 1. A model coupling organic matter flux to gas production, oxidation and transport. Cont. Shelf Res. 18, 1741-1770.

Mau, S., D.L. Valentine, J.F. Clark, J. Reed, R. Camilli, and L. Washburn. 2007. Dissolved methane distributions and air-sea flux in the plume of a massive seep field, Coal Oil Point, California. Geophysical Research Letters 34: L22603, doi:10.1029/2007GL031344

McClatchie, S., R. Goericke, A. Koslow, F. B. Schwing, S. J. Bograd, R. Charter, W. Watson, N. Lo, K. Hill, J. Gottschalk, M. L'Heureux, Y. Xue, W. T. Peterson, R. Emmett, C. Collins, G. Gaxiola-Castro, R. Duranzo, M. Kahru, B.G. Mitchell, K.D. Hyrenbach, W. J. Sydeman, R. W. Bradley, P. Warzybok, and E. Bjorkstedt. 2008. CalCOFI Report, vol. 49. The state of the California Current, 2007-2008: La Niña conditions and their effects on the ecosystem.

Mosin, O.V., Skladnev, D.A., Egorova, T.A., Shvets, V.I., 1996. Mass spectrometric evaluation of the incorporation of H-2 and C-13 into amino acids of bacteria. Bioorganicheskaya Khimiya 22, 856-869.

Neufeld, J.D., Boden, R., Moussard, H., Schafer, H., Murrell, J.C., 2008a. Substrate-Specific Clades of Active Marine Methylotrophs Associated with a Phytoplankton Bloom in a Temperate Coastal Environment. Applied and Environmental Microbiology 74, 7321-7328.

Neufeld, J.D., Chen, Y., Dumont, M.G., Murrell, J.C., 2008b. Marine methylotrophs revealed by stable-isotope probing, multiple displacement amplification and metagenomics. Environmental Microbiology 10, 1526-1535.

Nichols, P.D., Henson, J.M., Antworth, C.P., Parsons, J., Wilson, J.T., White, D.C., 1987. Detection of a microbial consortium, including type-II methanotrophs, by use of phospholipid fatty-acids in an aerobic halogenated hydrocarbon-degrading soil column enriched with natural-gas. Environmental Toxicology and Chemistry 6, 89-97.

Nichols, P.D., Smith, G.A., Antworth, C.P., Hanson, R.S., White, D.C., 1985. Phospholipid and lipopolysaccharide normal and hydroxy fatty-acids as potential signatures for methane-oxidizing bacteria. FEMS Microbiology Ecology 31, 327-335.

Normark, W.R., D. Piper, and R. Hiscott. 1998. Sea level controls on the textural characteristics and depositional architecture of the Hueneme and associated submarine fan systems, Santa Monica Basin, California. Sedimentology 45: 53-70, doi:10.1046/j.1365-3091.1998.00139.x

Pack, M. A., M. B. Heintz, W. S. Reeburgh, S. E. Trumbore, D. L. Valentine, X. Xu, E. R. M. Druffel. 2011. A method for measuring methane oxidation rates using low-levels of 14C-labeled methane and accelerator mass spectrometry. Limnology and Oceanography: Methods 9: 245-260.

Paull, C.K., Normark, W.R., Ussler, W., Caress, D.W., Keaten, R., 2008. Association among active seafloor deformation, mound formation, and gas hydrate growth and accumulation within the seafloor of the Santa Monica Basin, offshore California. Mar. Geol. 250, 258-275.

Redmond, M.C., Valentine, D.L., 2011. Natural gas and temperature structured a microbial community response to the Deepwater Horizon oil spill. Proceedings of the National Academy of Sciences.

Redmond, M.C., Valentine, D.L., Sessions, A.L., 2010. Novel methane, ethane, and propane oxidizing bacteria at marine hydrocarbon seeps identified by stable isotope probing. Applied and Environmental Microbiology, (Submitted).

Reeburgh, W. S., B. B. Ward, S. C. Whalen, K. A. Sandbeck, K. A. Kilpatrick, L. J. Kerkhof. 1991. Black Sea methane geochemistry. Deep Sea Research 38: S1189-S1210.

Reeburgh, W. S., S. C. Whalen, and M. J. Alperin. 1993. The role of methylotrophy in the global methane budget, p. 1-14. In J. C. Murrell and D. P. Kelly [eds.], Microbial Growth on C-1 Compounds. Intercept.

Reeburgh, W.S., 2007. Oceanic methane biogeochemistry. Chemical Reviews 107, 486-513.

Rehder, G., I. Leifer, P. G. Brewer, G. Friederich, and E. T. Peltzer. 2009. Controls on methane bubble dissolution inside and outside the hydrate stability field from open ocean field experiments and numerical modeling. Marine Chemistry 114: 19-30, doi:10.1016/j.marchem.2009.03.004

Rehder, G., Keir, R.S., Suess, E., Rhein, M., 1999. Methane in the northern Atlantic controlled by microbial oxidation and atmospheric history. Geophys. Res. Lett. 26, 587-590.

Rehder, G., P.W. Brewer, E.T. Peltzer, and G. Friederich. 2002. Enhanced lifetime of methane bubble streams within the deep ocean. Geophysical Research Letters 29, doi:10.1029/2001GL013966

Rehder, G., R.S. Keir, E. Suess, and T. Pohlmann. 1998. The multiple sources and patterns of methane in North Sea waters. Aquatic Geochemistry 4: 403-427, doi:10.1023/A:1009644600833

Rhee, T. S., A. J. Kettle, and M. O. Andreae. 2009. Methane and nitrous oxide emissions from the ocean: A reassessment using basin-wide observations in the Atlantic. Journal of Geophysical Research-Atmospheres 114: D12304, doi:10.1029/2008JD011662

Ryan, W. B. F., S. M. Carbotte, J. O. Coplan, S. O'Hara, A. Melkonian, R. Arko, R. A. Weissel, V. Ferrini, A. Goodwillie, F. Nitsche, J. Bonczkowski, and R. Zemsky. 2009. Global Multi-Resolution Topography synthesis. Geochemistry Geophysics Geosystems 10: Q03014, doi:10.1029/2008GC002332

Sansone, F. J., A. W. Graham, and W. M. Berelson. 2004. Methane along the western Mexican margin. Limnology and Oceanography 49: 2242-2255.

Sauer, P.E., Eglinton, T.I., Hayes, J.M., Schimmelmann, A., Sessions, A.L., 2001. Compound-specific D/H ratios of lipid biomarkers from sediments as a proxy for environmental and climatic conditions. Geochim. Cosmochim. Acta 65, 213-222.

Schimmelmann, A., Sessions, A.L., Mastalerz, M., 2006. Hydrogen isotopic (D/H) composition of organic matter during diagenesis and thermal maturation. Annu. Rev. Earth Planet. Sci. 34, 501-533.

Schubert, C.J., Coolen, M.J.L., Neretin, L.N., Schippers, A., Abbas, B., Durisch-Kaiser, E., Wehrli, B., Hopmans, E.C., Damste, J.S.S., Wakeham, S., Kuypers, M.M.M., 2006. Aerobic and anaerobic methanotrophs in the Black Sea water column. Environmental Microbiology 8, 1844-1856.

Scranton, M. I., and J. W. Farrington. 1977. Methane production in the waters off Walvis Bay. Journal Of Geophysical Research-Oceans 82: 4947-4953, doi:10.1029/JC082i031p04947

Sessions, A.L., 2006. Seasonal changes in D/H fractionation accompanying lipid biosynthesis in Spartina alternflora. Geochim. Cosmochim. Acta 70, 2153-2162.

Sessions, A.L., Burgoyne, T.W., Hayes, J.M., 2001. Correction of H-3(+) contributions in hydrogen isotope ratio monitoring mass spectrometry. Analytical Chemistry 73, 192-199.

Sessions, A.L., Hayes, J.M., 2005. Calculation of hydrogen isotopic fractionations in biogeochemical systems. Geochim. Cosmochim. Acta 69, 593-597.

Sessions, A.L., Jahnke, L.L., Schimmelmann, A., Hayes, J.M., 2002. Hydrogen isotope fractionation in lipids of the methane-oxidizing bacterium Methylococcus capsulatus. Geochim. Cosmochim. Acta 66, 3955-3969.

Sieburth, J.M., Johnson, P.W., Eberhardt, M.A., Sieracki, M.E., Lidstrom, M., Laux, D., 1987. The first methane-oxidizing bacterium from the upper mixing layer of the deep ocean - Methylomonas pelagica sp nov. Current Microbiology 14, 285-293.

Sloan, E.D., S. Subramanian, P.N. Matthews, J.P. Lederhos, and A.A. Khokhar. 1998. Quantifying hydrate formation and kinetic inhibition. Industrial & Engineering Chemistry Research 37: 3124-3132, doi: 10.1021/ie970902h

Sommer, S., O. Pfannkuche, P. Linke, R. Luff, J. Greinert, M. Drews, S. Gubsch, M. Pieper, M. Poser, and T. Viergutz. 2006. Efficiency of the benthic filter: Biological control of the emission of dissolved methane from sediments containing shallow gas hydrates at Hydrate Ridge. Global Biogeochemical Cycles 20: GB2019, doi:10.1029/2004GB002389

Sverdrup, H. U., and R. H. Fleming. 1941. The Waters off the Coast of Southern California, March to July, 1937, p. 261-378. In Bulletin of the Scripps Institute of Oceanography Technical Series. pp. 261-378, University of California Press, Berkeley.

Tavormina, P.L., Orphan, V.J., Kalyuzhnaya, M.G., Jetten, M.S.M., Klotz, M.G., 2011. A novel family of functional operons encoding methane/ammonia monooxygenase-related proteins in gammaproteobacterial methanotrophs. Environmental Microbiology Reports 3, 91-100.

Tavormina, P.L., Ussler, W., Orphan, V.J., 2008. Planktonic and sediment-associated aerobic methanotrophs in two seep systems along the North American margin. Applied and Environmental Microbiology 74, 3985-3995.

Tilbrook, B. D., and D. M. Karl. 1995. Methane sources, distributions and sinks from California coastal waters to the oligotrophic North Pacific gyre. Marine Chemistry 49: 51-64, doi: 10.1016/0304-4203(94)00058-L

Valentine, D.L., D.C. Blanton, W.S. Reeburgh, and M. Kastner. 2001. Water column methane oxidation adjacent to an area of active hydrate dissociation, Eel River Basin. Geochimica et Cosmochimica Acta 65: 2633-2640, doi:10.1016/S0016-7037(01)00625-1

Valentine, D.L., Kessler, J.D., Redmond, M.C., Mendes, S.D., Heintz, M.B., Farwell, C., Hu, L., Kinnaman, F.S., Yvon-Lewis, S., Du, M., Chan, E.W., Tigreros, F.G., Villanueva, C.J., 2010. Propane Respiration Jump-Starts Microbial Response to a Deep Oil Spill. Science 330, 208-211.

Wakeham, S.G., Amann, R., Freeman, K.H., Hopmans, E.C., Jorgensen, B.B., Putnam, I.F., Schouten, S., Damste, J.S.S., Talbot, H.M., Woebken, D., 2007. Microbial ecology of the stratified water column of the Black Sea as revealed by a comprehensive biomarker study. Organic Geochemistry 38, 2070-2097.

Ward, B. B. 1992. The subsurface methane maximum in the Southern California Bight. Continental Shelf Research 12: 735-752, doi: 10.1016/0278-4343(92)90028-I

Ward, B. B., and K. A. Kilpatrick. 1993. Methane oxidation associated with mid-depth methane maxima in the Southern California Bight. Continental Shelf Research 13: 1111-1122, doi: 10.1016/0278-4343(93)90044-X

Ward, B.B., Kilpatrick, K.A., 1993. Methane oxidation associated with mid-depth methane maxima in the southern California Bight. Cont. Shelf Res. 13, 1111-1122.

Ward, B.B., Kilpatrick, K.A., Wopat, A.E., Minnich, E.C., Lidstrom, M.E., 1989. Methane oxidation in Saanich Inlet during summer stratification. Cont. Shelf Res. 9, 65-75.

Wasmund, K., Kurtboke, D.I., Burns, K.A., Bourne, D.G., 2009. Microbial diversity in sediments associated with a shallow methane seep in the tropical Timor Sea of Australia reveals a novel aerobic methanotroph diversity. FEMS Microbiology Ecology 68, 142-151.

Wegener, G., Bausch, M., Holler, T., Thang, N.M., Prieto Mollar, X., Kellermann, M.Y., Hinrichs, K.-U., Boetius, A., 2012. Assessing sub-seafloor microbial activity by com-

bined stable isotope probing with deuterated water and 13C-bicarbonate. Environmental Microbiology 14, 1517-1527.
Wuebbles, D. J., and K. Hayhoe. 2002. Atmospheric methane and global change. Earth-Science Reviews 57: 177-210, doi: 10.1016/S0012-8252(01)00062-9
Yang, H., Huang, Y.S., 2003. Preservation of lipid hydrogen isotope ratios in Miocene lacustrine sediments and plant fossils at Clarkia, northern Idaho, USA. Organic Geochemistry 34, 413-423.
Zachos, J.C., Dickens, G.R., Zeebe, R.E., 2008. An early Cenozoic perspective on greenhouse warming and carbon-cycle dynamics. Nature 451, 279-283.
Zhang, X., K. C. Hester, W. Ussler III, P. M. Walz, E. T. Peltzer, and P. G. Brewer. 2011. In situ Raman-based measuremets of high dissolved methane concentrations in hydrate-rich ocean sediments. Geophysical Research Letters 38: L08605, doi:10.1029/2011GL047141
Zhang, X.N., Gillespie, A.L., Sessions, A.L., 2009. Large D/H variations in bacterial lipids reflect central metabolic pathways. Proceedings of the National Academy of Sciences of the United States of America 106, 12580-12586.

Table 6: Incubation protocol for waters collected from the Santa Barbara and Santa Monica Basins.

Sample ID[a]	Incubation Substrate(s)	Substrate Conc.[b]	Incubation Time
SB\$^{13}CH_4$\$CH_3D$	$^{13}CH_4 + CH_3D$	30 nM + 30 nM	5 days
SB\$^{13}CO_2$\$^{12}CH_4$	$^{13}CO_2 + {}^{12}CH_4$	60 nM + 60nM	4 days
SB\$^{13}CH_4$	$^{13}CH_4$	60 nM	5 days
SM\$^{13}CH_4$[c]	$^{13}CH_4$	60 nM	4 days
SM\$^{13}CO_2$\$^{12}CH_4$	$^{13}CO_2 + {}^{12}CH_4$	60 nM + 60nM	3 days
SM\$^{13}CH_4$\$CH_3D$	$^{13}CH_4 + CH_3D$	30 nM + 30 nM	4 days

[a]SB = Collected from Santa Barbara Basin; SM = collected from Santa Monica Basin.
[b]The total volume for each incubation was 35 L.
[c] Bag was punctured during incubation; isotopic results for this sample are not reported.

Table 7: Isotope measurements for six major fatty acid classes obtained from the five successful incubation experiments. Isotope values are presented in per mil notation relative to VPDB for ^{13}C and VSMOW for D. -- = not determined.

	C14:0		C14:1		C16:0		C16:1		C18:0		C18:1	
	$\delta^{13}C$	δD	$\delta^{13}C$	δD	$\delta^{13}C$	δD	$\delta^{13}C$	δD	$\delta^{13}C$	δD	$\delta^{13}C$	δD
SB\\$^{13}CH_4$\\$CH_3D$	-15.1	-105	-16.5	--	17.5	47.0	731	3210	-22.8	-179	44.1	-30
SB\\$^{13}CO_2$\\$^{12}CH_4$	-25.7	--	-29.6	--	-24.4	-101	-26.2	-92.1	-25	-198	-30.7	--
SB\\$^{13}CH_4$	-12.0	--	-28.9	--	58.4	-159	793	-126	-27.8	-183	13.2	-125
SM\\$^{13}CO_2$\\$^{12}CH_4$	-25.1	--	-18.9	--	-27.5	-134	-26.2	-78.3	-26.9	--	-22.8	--
SM\\$^{13}CH_4$\\$CH_3D$	-18.5	-100	--	--	-4.60	-82.0	82.3	178	-27.5	-158	-14.1	-92.9

Table 8: Water column properties of sample water taken from Santa Barbara and Santa Monica Basins.

Property	SBB	SMB
Water depth (m)	575	875
Salinity (psu)	34.3	34.4
Temperature (°C)	6.5	5.1
O_2 concentration (ml L^{-1})	0.20	0.13
Methane concentration (nM)	460	21
Methane oxidation rate (nM d^{-1})	23[1]	0.13

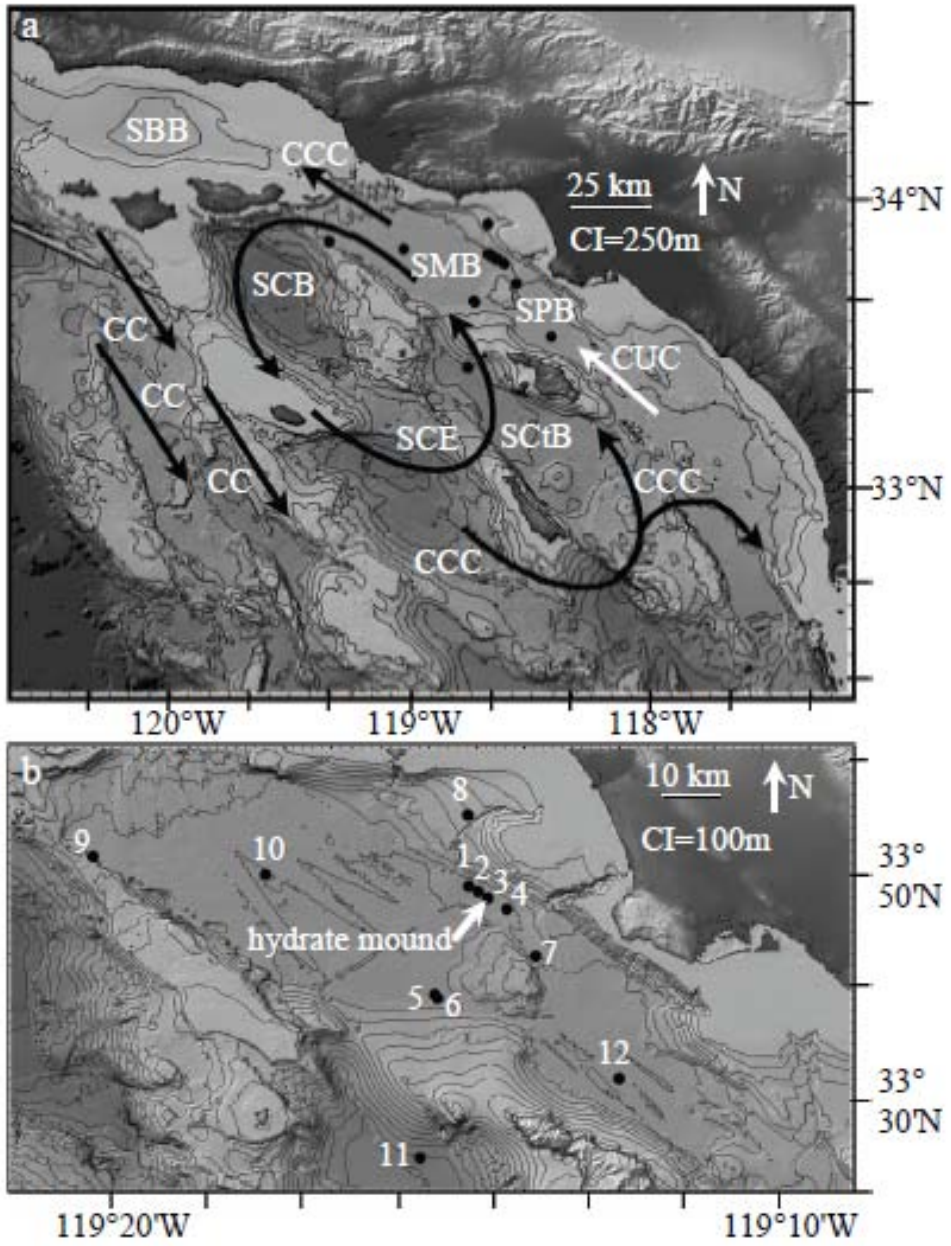

Figure 9- (a) Southern California Bight and Borderland Basins; Santa Barbara (SBB), Santa Monica (SMB), Santa Cruz (SCB), Santa Catalina (SCtB), San Pedro (SPB). Generalized circulation patterns of the California Current system are shown (Hickey 1998). Black arrows show currents in the upper water column; California Current (CC), Southern California Eddy (SCE), California Countercurrent (CCC). White arrow shows lower water column flow of California Undercurrent (CUC) through the basin. Sampling stations from both expeditions are shown as small black dots. (b) Sampling stations in the SMB (1-10). Sta. 11 is located in the SCtB and Sta. 12 in the SPB. CI = contour interval. Maps generated with GeoMapApp (Ryan et al. 2009).

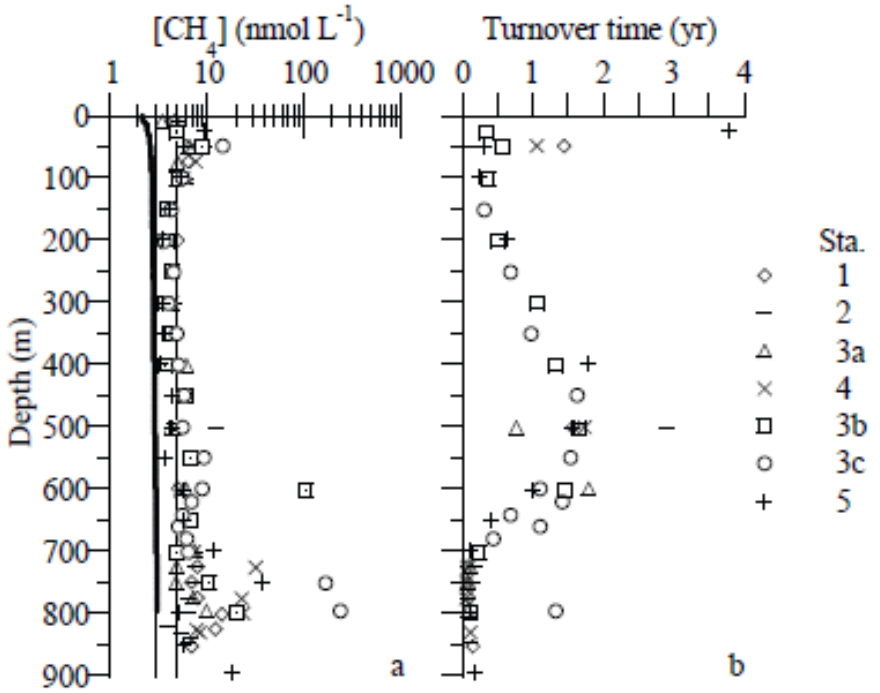

Figure 10 – Results from all hydrocasts conducted in the SMB in July 2007 (a) methane concentration - thin lines mark the 3-5 nmol L^{-1} basin-background methane concentration range. The methane concentration expected at atmospheric equilibrium at observed temperature and salinity is shown as a heavy solid line. Concentrations observed through the mid-water column on casts 3b and 3c are shown in the inset. (b) methane turnover time.

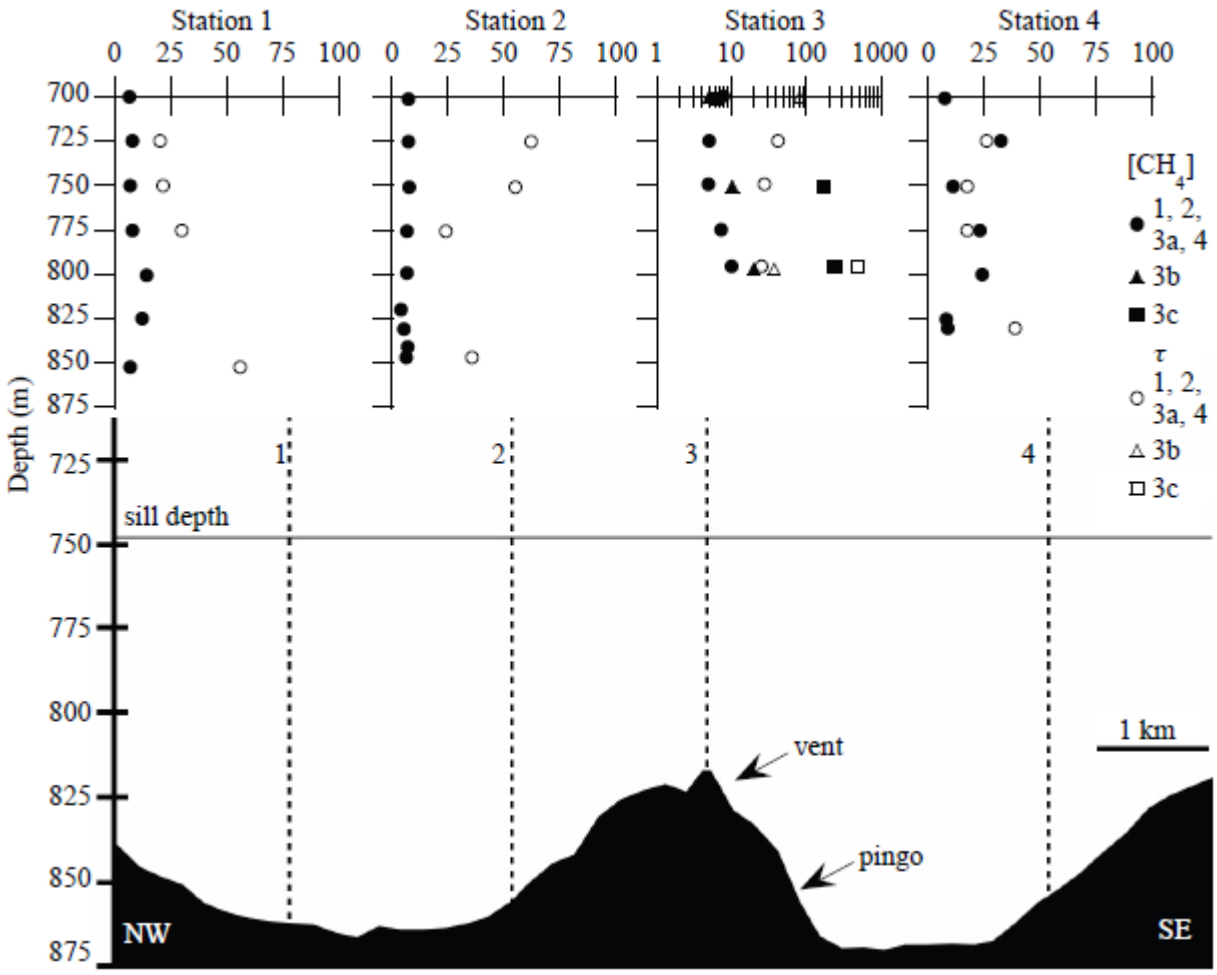

Figure 11 - Depth profiles of methane concentrations (nmol L^{-1}) and turnover times (days) below 700 m at pingo transect Sta. 1-4. Pingo profile generated with GeoMapApp (Ryan et al. 2009).

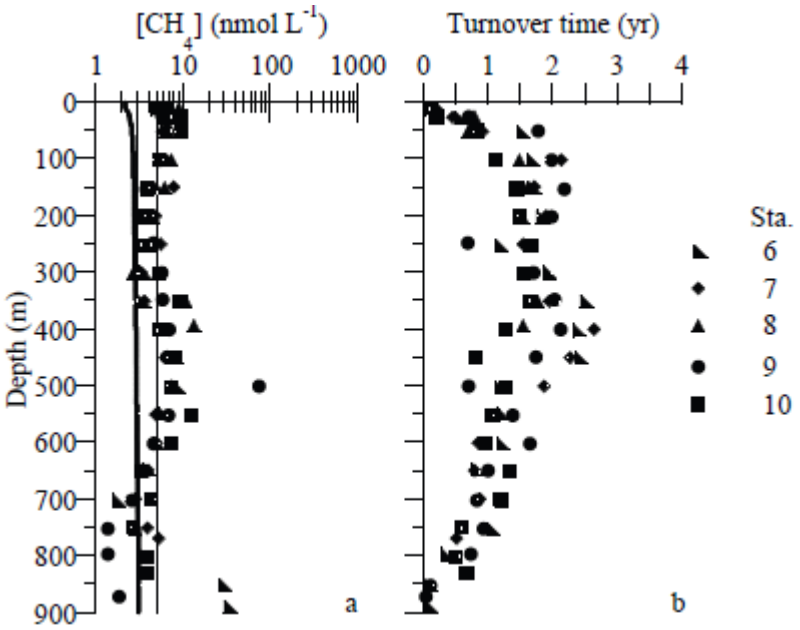

Figure 12 – Results from hydrocasts conducted in the SMB in September 2009 (a) methane concentrations, thin lines mark the 3-5 nmol L^{-1} basin-background methane concentration range. The methane concentration expected at atmospheric equilibrium at observed temperature and salinity is shown as a heavy solid line. (b) methane turnover time.

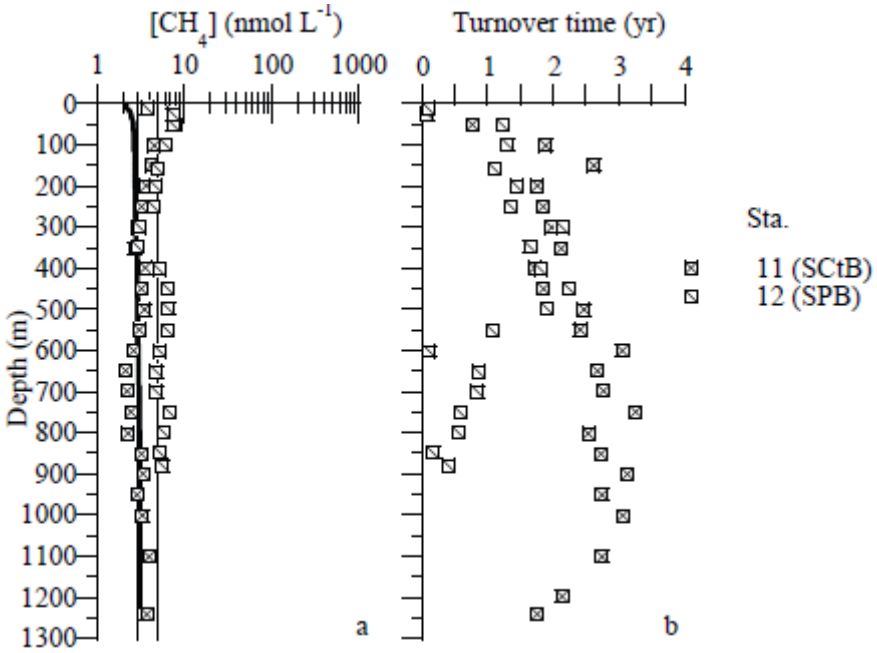

Figure 13 – Results from hydrocasts conducted in the SCtB (11) and SPB (12) in September 2009 (a) methane concentration, thin lines mark the 3-5 nmol L^{-1} basin background methane concentration range. The methane concentration expected at atmospheric equilibrium at observed temperature and salinity is shown as a heavy solid line. (b) methane turnover time.

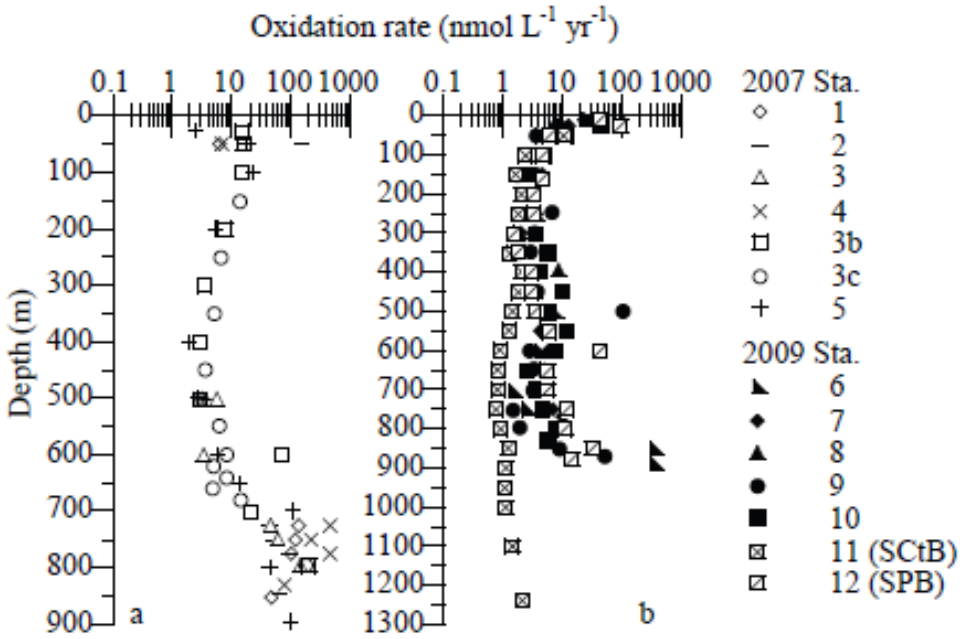

Figure 14 - Methane oxidation rates nmol L^{-1} d^{-1} (a) in the SMB in July 2007 (b) in the SMB (6-10), SCtB (11) and SPB (12) in September 2009.

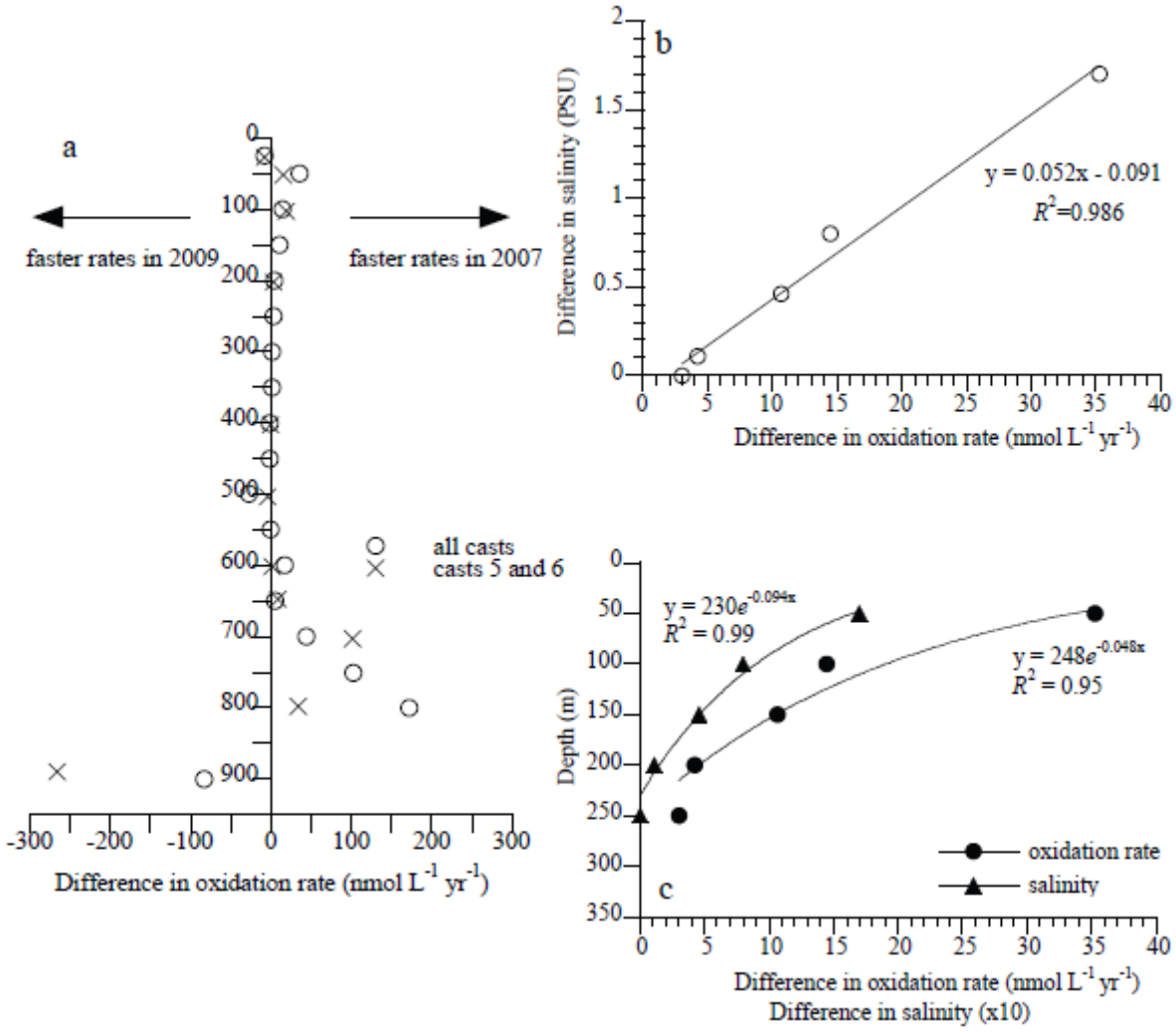

Figure 15 - (a) Difference in oxidation rates between 2007 and 2009. Circles show the difference between the averages of all rates at each depth. Xs indicate difference between casts at the same location, 5 (2007) and 6 (2009). (b) Linear relationship between difference in salinity and difference in oxidation rate between 2007 and 2009 between 50-250 m. (c) Both salinity and oxidation rate show a logarithmic decrease with depth between 50-250 m.

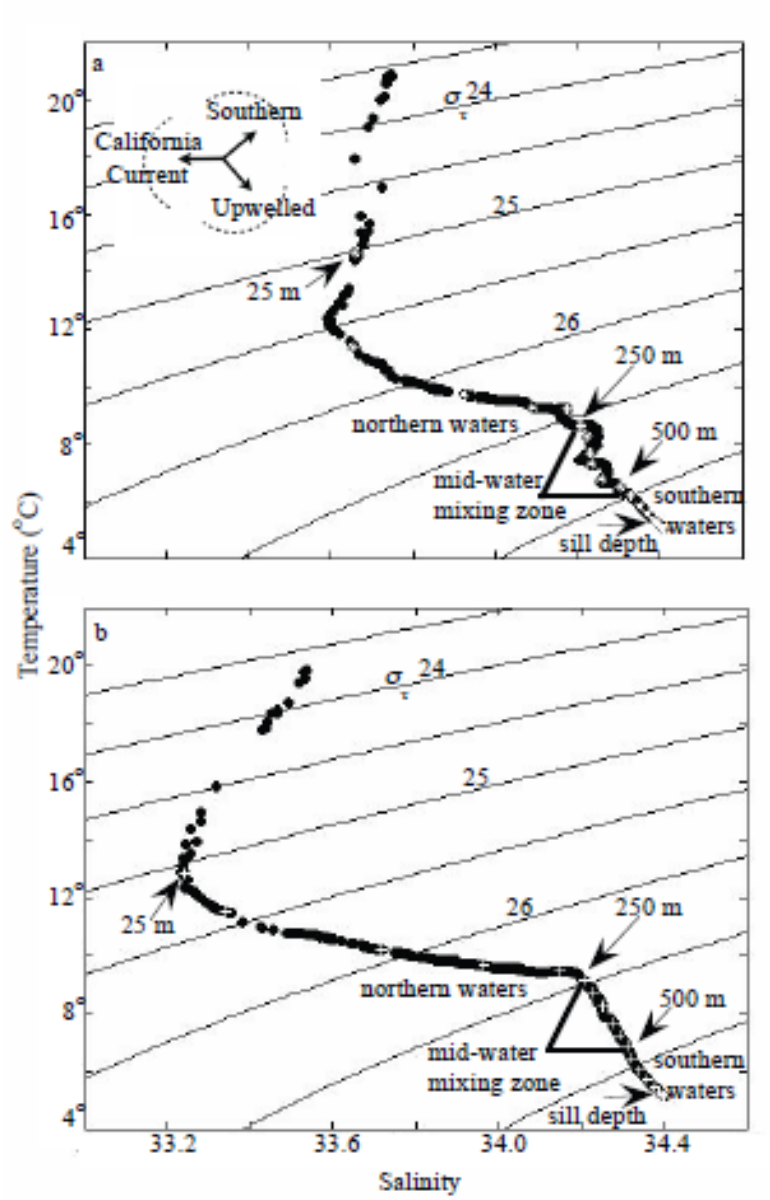

Figure 16 – Annotated temperature – salinity diagrams for (a) cast 5 in 2007, and (b) cast 6 in 2009. Markers are at 25 m, 50 m, and then every 50 m to the bottom of each cast.

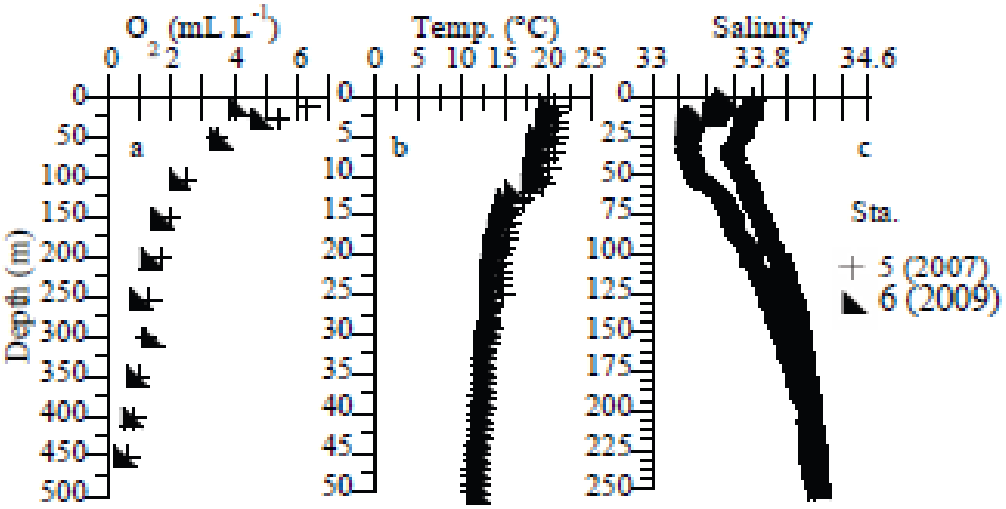

Figure 17 - Comparison between casts 5 (2007) and 6 (2009) (a) oxygen depth profiles show small divergence between casts at 100-300 m (b) upper water temperature (Temp.) profiles show the thermocline at 11-12°C in both years, (c) salinity profiles show divergence between casts above about 200 m.

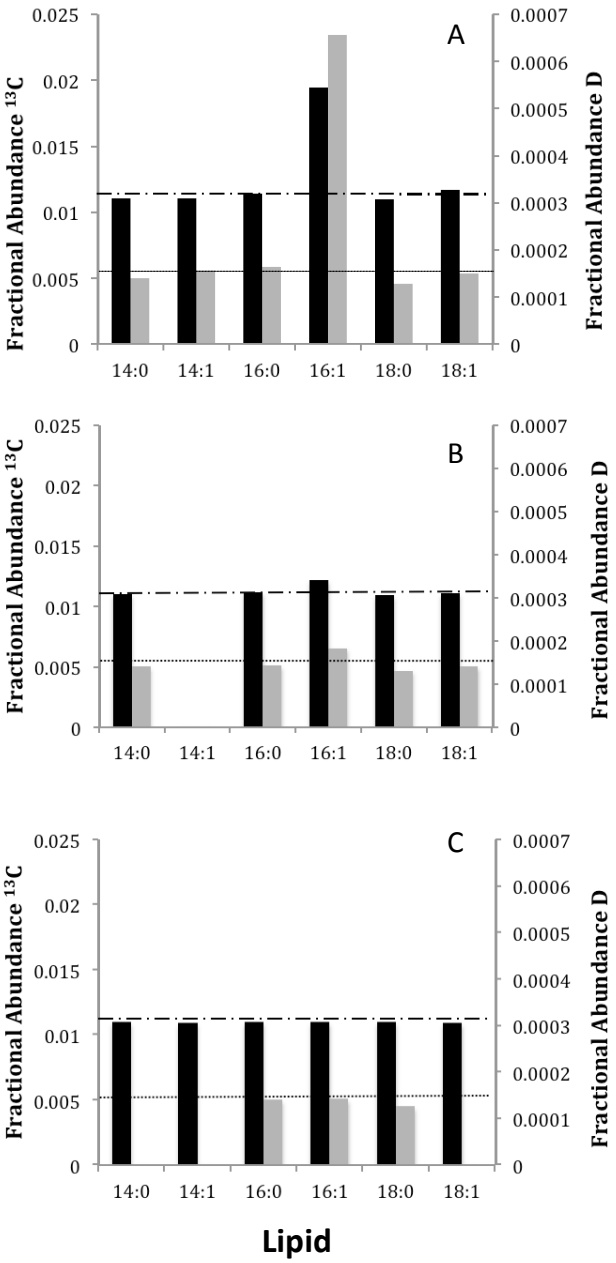

Figure 18**:** Fractional abundance of ^{13}C and D isotopes presented as percent composition of the six major lipid classes investigated for: A) SB/$^{13}CH_4$/CH_3D incubation, B) SM/$^{13}CH_4$/CH_3D incubation, and C) SB/$^{13}CO_2$/$^{12}CH_4$ incubation. The Y-axis at left shows ^{13}C fractional abundance, corresponding to the black bars, and the Y-axis at right shows the D fractional abundance, corresponding to the gray bars. The dashed-dotted line represents the value of $F^{13}C_{PDB}$ with the corresponding value given on the left axis, and the dotted line below represents the value of FD_{SMOW}, with the corresponding value on the right axis.

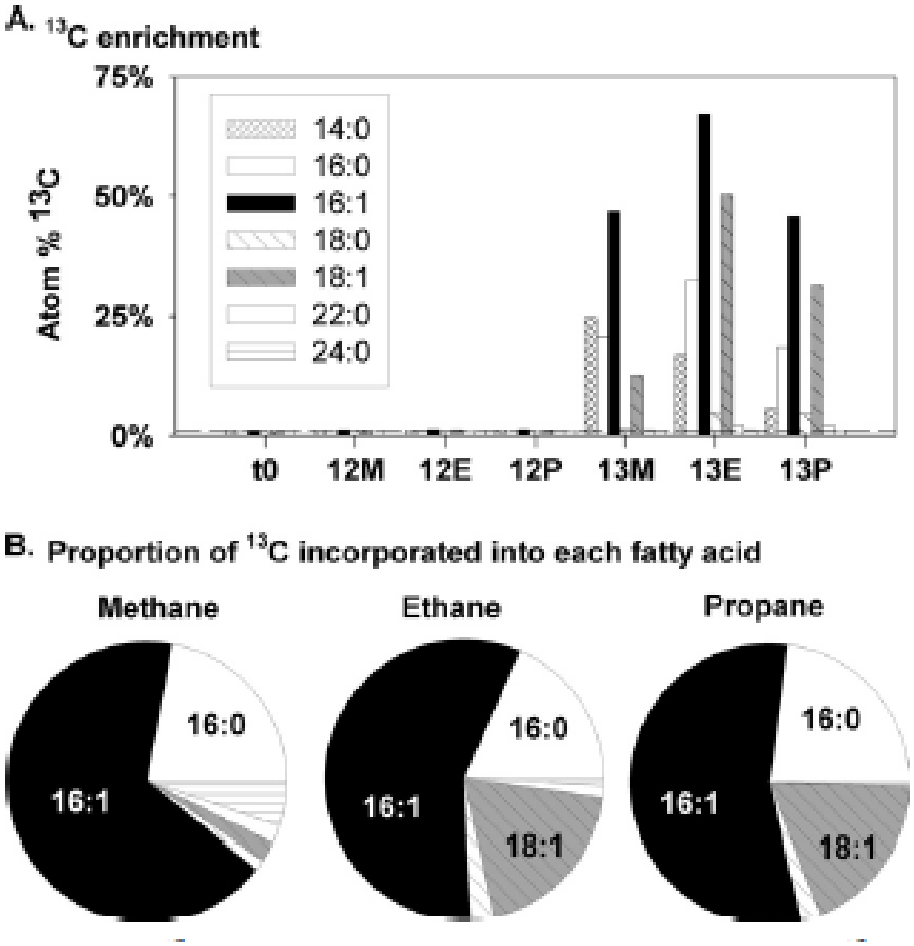

Figure 19. (A) 13C enrichment of phospholipid fatty acids of 13Cmeth-ane (M), ethane (E),and propane (P) incubations and 12C controls in initial sediment (t0) and at final time points. The 16:1 and 18:1 isomers were not differentiated. The dashed line indicates natural abundance levels of 13C. (B) Proportion of 13C incorporated into each fatty acid.

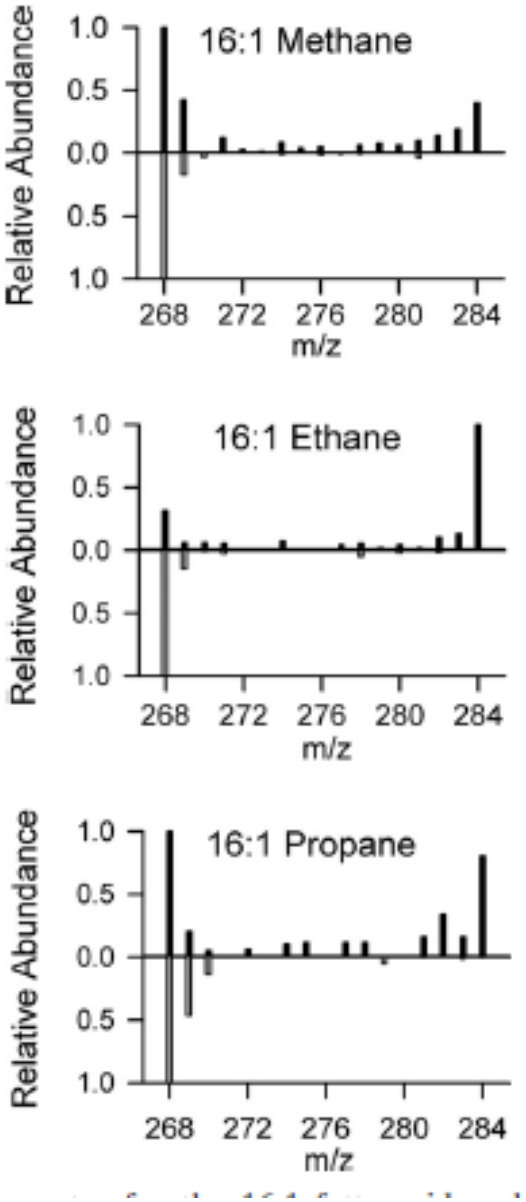

Figure 20. Mass spectra for the 16:1 fatty acid molecular ion peak, showing the extent of 13C labeling at the final time point of the methane, ethane, and propane incubations. The m/z values for the spectra span the full range from no 13C incorporation (m/z = 268) to full 13C labeling (m/z = 268 + 16 = 284). The spectra oriented upward correspond to incubations with 13C labeling, whereas the inverted spectra correspond to control incubations with substrate lacking 13C labeling. Each spectrum is normalized to the height of its tallest peak.

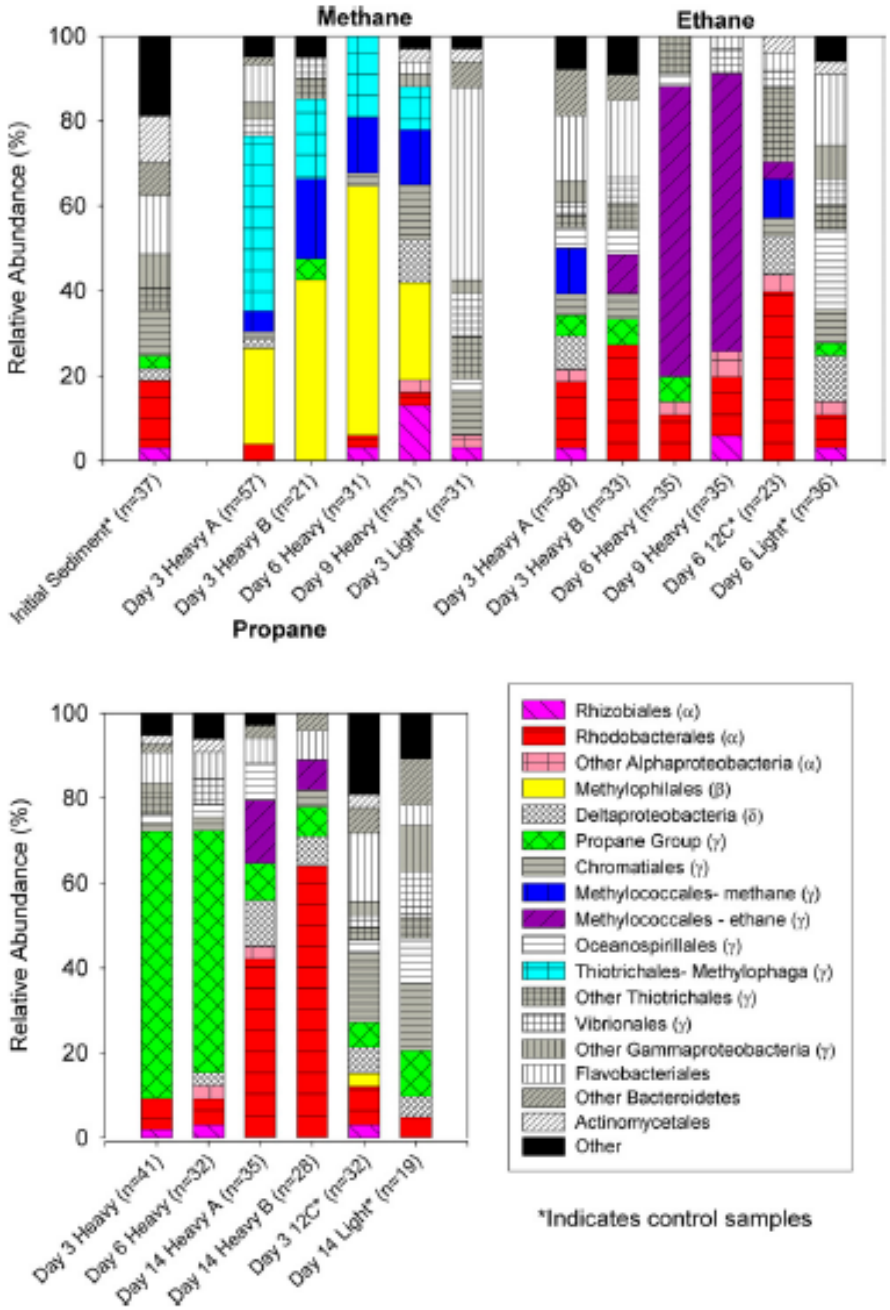

Figure 21. Relative abundances of 16S rRNA sequences in clone libraries from heavy DNA (fraction 4 or 6 [noted as Heavy A or Heavy B] or both) from the three time points of the 13C methane, ethane, and propane incubations, selected controls (light DNA from the 13C incubations and heavy DNA from the 12C controls), and the initial sediment. Sequences were grouped using the RDP Classifier tool; “other” combines sequences that, classified at the order level, represented less than 5% of the clones in any individual clone library. Representative sequences from each of the groups indicated in methane, ethane, or propane oxidation are included in the phylogenetic tree in Fig. 22.

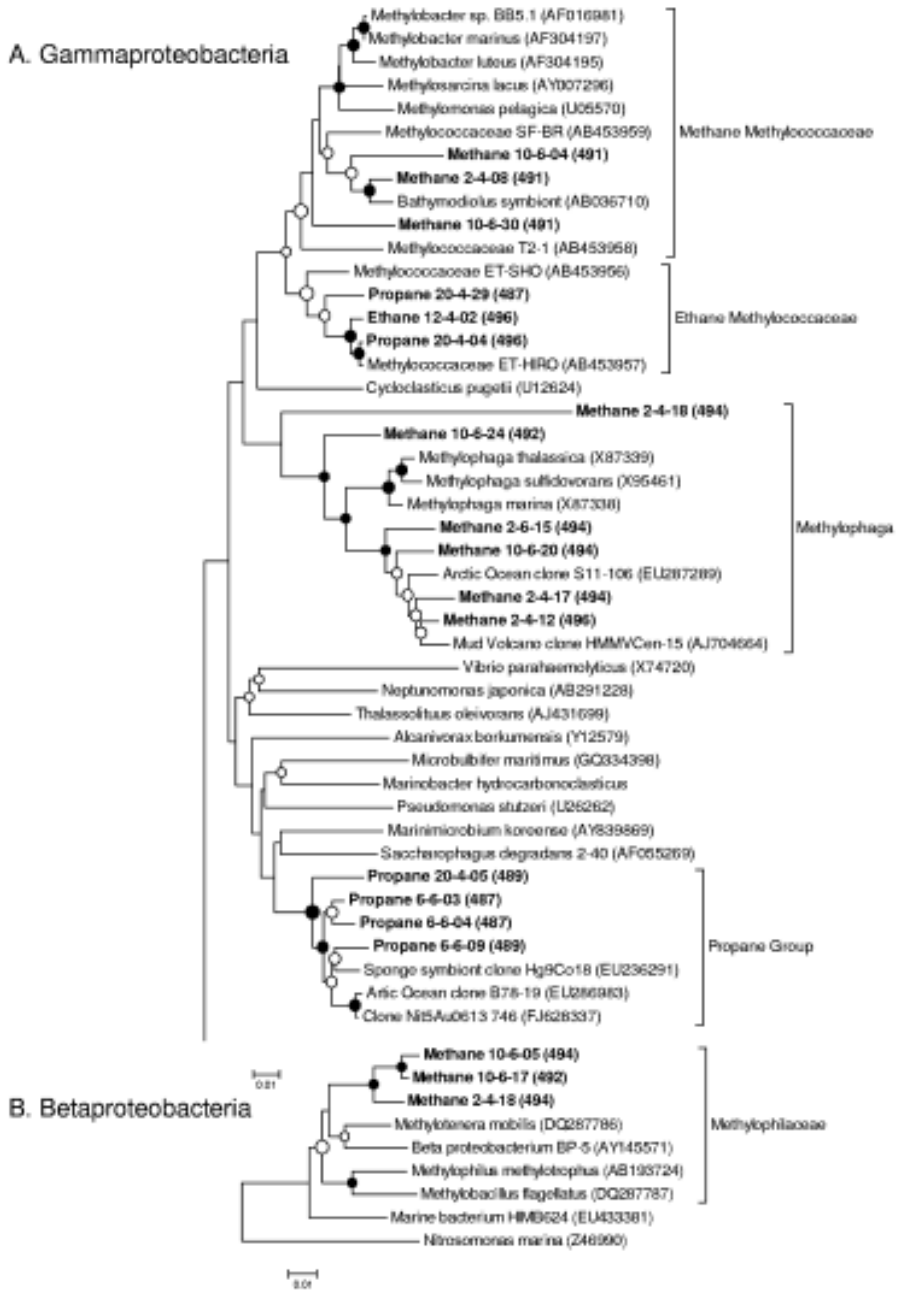

Figure 22. Neighbor-joining phylogenetic trees of the 16S rRNA gene sequences from groups involved in methane, ethane, or propane oxidation, based on their abundance in both the heavy DNA clone libraries and the heavy T-RFLP fractions, relative to light DNA and 12C controls. (A) Gammaproteobacteria; (B) Betaproteobacteria. Sequences from this study are shown in bold, with predicted MspI T-RF lengths in parentheses. Reference sequences from GenBank are shown with accession numbers in parentheses. Filled circles indicate bootstrap values above 90% and open circles bootstrap values above 50% (2,000 replicates).

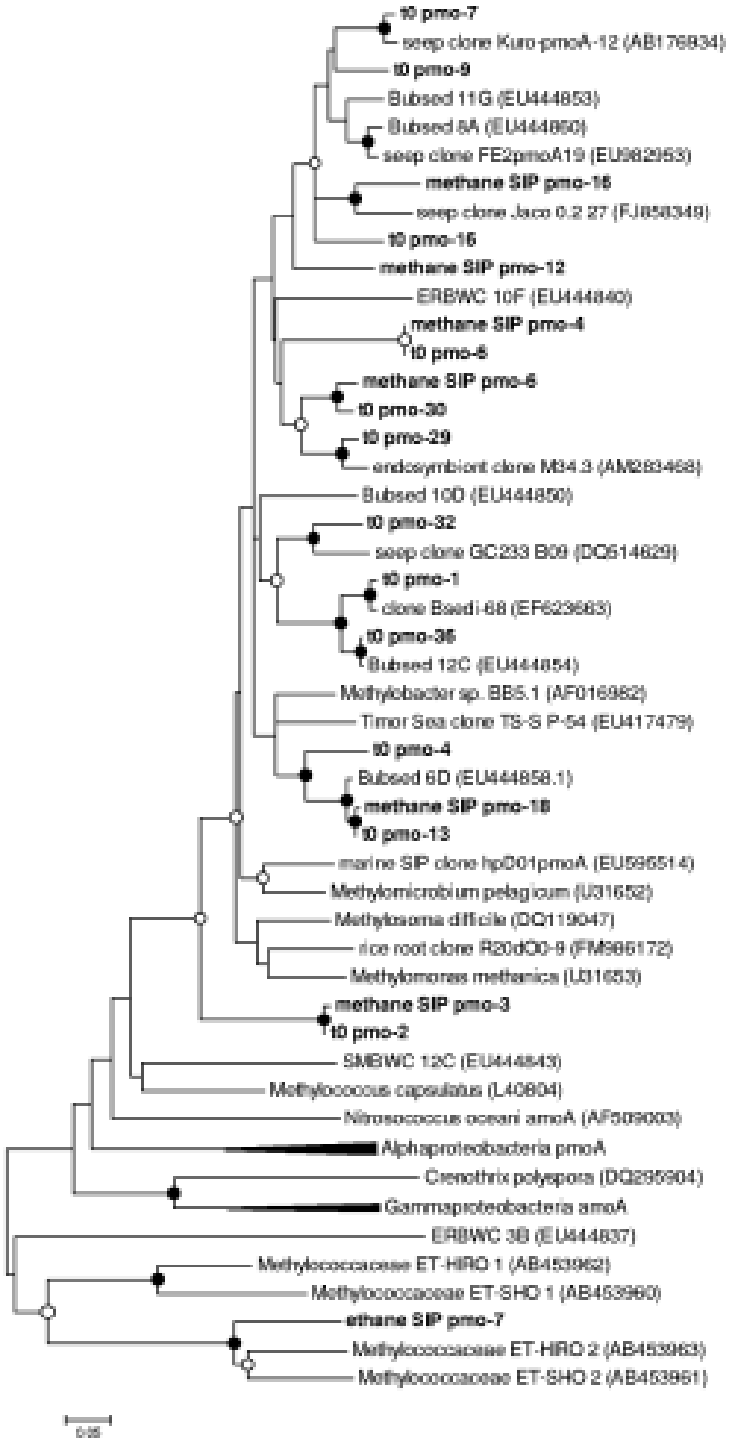

Figure 23. Neighbor-joining phylogenetic tree of pmoA gene sequences from seep sediment (t0) and methane and ethane heavy DNA sequences, plus reference sequences from GenBank (accession numbers in parentheses). Only the divergent sequences from the ethane SIP sample are shown; others were identical to those in the t0 and methane SIP samples. Filled circles indicate bootstrap values above 90% and open circles bootstrap values above 50% (2,000 replicates). The alphaproteobacterial pmoA and gammaproteobacterial amoA sequences are condensed for clarity.

Chapter 3. Pelagic Methanotrophy: Studies from the Gulf of Mexico

Preface: The original scope of this award did not include research in the Gulf of Mexico. However, in April 2010 the sinking of the Deepwater Horizon and the ensuing discharge of methane and other hydrocarbons provided a 'forbidden experiment' that serves as analog to the massive release of methane expected from decomposing gas hydrate under some ocean warming scenarios. As a result, supplementation was provided to this award to investigate the efficacy of the methanotrophic biofilter during this event, related to Tasks 4, 5, 8, 10 and 11. These efforts led to several publications in the peer review literature, with additional publications in preparation, as follows:

Valentine DL (2010) Measure methane to quantify the oil spill. **Nature** 465: 421-421.

Valentine DL, Kessler JD, Redmond MC, Mendes SD, Heintz MB, et al. (2010) Propane Respiration Jump-Starts Microbial Response to a Deep Oil Spill. **Science** 330: 208-211.

Valentine, DL. (2010) An opportunity to assess the behavior of methane released in the deep ocean. **Fire in the Ice** 10 (2)5.

*Kessler JD, *Valentine DL, Redmond MC, Du MR, Chan EW, et al. (2011) A Persistent Oxygen Anomaly Reveals the Fate of Spilled Methane in the Deep Gulf of Mexico. **Science** 331: 312-315. *Kessler and Valentine are co-first authors

Redmond MC, Valentine DL (2011) Natural gas and temperature structured a microbial community response to the Deepwater Horizon oil spill. **Proceedings of the National Academy of Sciences of the United States of America**. Doi:10.1073/pnas.1108756108

Ryerson T, Camilli R, Kessler J, Kujawinski EB, Reddy CM, et al. (2012) Chemical composition measurements quantify Deepwater Horizon hydrocarbon emissions and distribution in the marine environment. **Proceedings of the National Academy of Sciences**, USA. doi/10.1073/pnas.1110564109

Valentine DL, Mezić I, Maćešić S, Črnjarić-Žic N, Ivić S, et al. (2012) Dynamic auto-inoculation and the microbial ecology of a deep water hydrocarbon irruption. **Proceedings of the National Academy of Sciences of the United States of America**. doi/10.1073/pnas.1108820109

Redmond MC, PA Tavormina, VJ Orphan and DL Valentine (in preparation) Dynamics of Hydrocarbon Monooxygenase Genes in the Deep Ocean Following the Deepwater Horizon Spill.

Summary: The Deepwater Horizon mobile offshore drilling unit exploded and then sank in April, 2010. This event led to a rupture of the well head and petroleum discharged from the Macondo well for nearly three months. The single most abundant hydrocarbon emitted was methane, followed by other hydrate-associated gases: ethane and propane. The hydrocarbon gases and some fraction of the oil became trapped in the deep water where they became available for consumption by marine bacteria including methanotrophs. We investigated the dynamics methane consumption and methanotrophic populations in the resulting deepwater blooms. We found a succession of metabolisms in which higher hydrocarbons including ethane and propane drove a majority of total respiration at the early stages of the bloom, followed later by methanotrophs. Methanotrophs were found to bloom with a greater lag than other hydrocarbon degraders,

and they appeared to bloom concurrently with methylotrophs, presumably due to cross feeding on methanol. A coupled physical oceanographic-chemical-microbial model was developed to describe the observed variations in respiration rates, which revealed the regional scale of the methanotrophic response in the months that followed the event. All methane anomalies were found to be consumed within ~2 months of the last emissions, providing one end member of the timeframe for consumption of a massive methane discharge to the deep ocean.

INTRODUCTION

The oil spill at Mississippi Canyon block 252 following the sinking of the Deepwater Horizon was unprecedented because it occurred at 1.5 km water depth. The slow buoyant migration of petroleum from this depth allows time for dissolution of volatile hydrocarbons (Yapa, L.K. et al. 2008; Dasanayaka and Yapa 2009; Camilli, Reddy et al. 2010), including the natural gases methane (CH_4 or C1), ethane (C_2H_6 or C2), and propane (C_3H_8 or C3), that would readily escape to the atmosphere if released in shallow water. These gases may co-occur with oil in the water (Camilli, Reddy et al. 2010) or possibly fractionate from oil during ascent (Chen and Yapa 2004). Based on the cumulative discharge estimates reported by the US government through Aug 1, 2010 (USGS 2010) and a gas-to-oil ratio of 3000 cubic feet per barrel (at atmospheric pressure), we calculate that 1.5×10^{10} moles of natural gas was emitted to the deep water over the course of the spill in addition to the oil. We investigated the deep plumes of oil and gas over a four month period to better understand the microbial processes that affected oil and gas, with an emphasis on the methanotrophic biofilter.

RESULTS AND DISCUSSION

Experimental studies of gas metabolism and microbial community dynamics

The Deepwater Horizon spill was the first to cause the concurrent release of oil and natural gas at great depth and the formation of deep-water oil plumes. We first investigated the distribution, fate, and impacts of these hydrocarbons at 31 stations located 1–12.5 km from the active spill site (Fig 24A) during the PLUMES (Persistent and Localized Underwater Methane Emission Study) expedition of the RV *Cape Hatteras*, June 11–21, 2010.

In the vicinity of the spill, propane, ethane, and methane were most abundant at depths greater than 799 m and formed plume structures (Fig 24C) with dissolved concentrations as high as 8 μM, 16 μM, and 180 μM for the three gases, respectively. These gases were orders of magnitude less concentrated at shallower depths (Fig 24C), confirming suggestions (Valentine 2010), results from a non-calibrated spectrometric survey (Camilli, Reddy et al. 2010), and models ((Yapa, L.K. et al. 2008; Dasanayaka and Yapa 2009) and references there in) that the vast majority of the emanated gas dissolves or is otherwise partitioned (e.g., as gas hydrate) at depth, and remains there. We classify sites with >500 nM methane at >799 m depth as deep hydrocarbon plumes. The 500-nM threshold, roughly 20–50-fold greater than background levels of methane in the Gulf of Mexico (Brooks 1975), is above the methane levels typically found around natural seeps (Valentine, Blanton et al. 2001; Grant and Whiticar 2002; Mau, Sahling et al. 2006; Mau, Valentine et al. 2007; Reeburgh 2007). We observed deep hydrocarbon plumes at 29 of the 31 stations where methane measure-

ments were made, and we collected 73 distinct plume samples from different depth horizons at these stations. One persistent plume at 1000-1200m depth located to the southwest of the spill site (Fig 24C) was identified previously ((JAG) 2010; Camilli, Reddy et al. 2010; Schrope 2010). We also identified separate plumes at similar depths to the north and to the east, as well as a distinctive shallower plume at 800-1000 m depth also located to the east. The reason for having plumes in opposing directions presumably relates to complex current patterns in the area.

Vertical casts revealed varying levels of oxygen depletion within the hydrocarbon plumes, as measured in situ with an oxygen sensor and confirmed onboard ship through Winkler titrations (Winkler 1888) of the sampled water (Fig 24B). Apparent oxygen anomalies were calculated by subtracting the Winkler-derived values from an interpolated background profile; we take these anomalies as proxies for the extent of respiration. The greatest oxygen anomaly observed from a titrated sample was 37.7 μM, with greater anomalies observed at other locations by the sensor.

The ratio of methane to ethane and propane varied substantially throughout the deep plumes. However, at the locations with highest hydrocarbon concentrations, the lower end-member values converged at 10.85 for C1/C2 (Fig 25A) and 19.8 for C1/C3 (Fig 25B); we take these values to represent the ratio of methane to ethane and propane, respectively, at the plume origin. Numerous locations display higher ratios, which we interpret as preferential loss of propane and ethane relative to methane, a pattern reported previously for biodegradation in hydrocarbon seeps (Kinnaman, Valentine et al. 2007). Variation in the C2/C3 ratio (Fig 25C) further suggests preferential loss of propane compared to ethane, also an established biodegradation pattern (Kinnaman, Valentine et al. 2007).

Because bacterial propane and ethane consumption occur with characteristic kinetic isotope effects (Kinnaman, Valentine et al. 2007), we measured the carbon isotopic composition of both gases in deep plume waters to assess the extent of their biodegradation. Samples with C1/C3 greater than 19.8 displayed a relative ^{13}C-enrichment in propane. Comparison of the ^{13}C-propane enrichment to the fractional loss of propane (Fig 25D), determined from the C1/C3 ratio, indicates that biodegradation occurs with an isotopic enrichment factor (ε) of -6.3. Determination of ε by this method is valid since ε is relatively small (< 20) (Gelwicks, Risatti et al. 1989; Gelwicks, Risatti et al. 1994). A similar analysis for ethane based on C1/C2 ratios provides evidence for biodegradation occurring with ε of -11.8. Both values are similar to the minimum respective values of -5.9 and -11.2 determined from a previous mesocosm study (Kinnaman, Valentine et al. 2007). These isotopic results demonstrate significant levels of propane and ethane biodegradation at many locations in the deep plumes, and the concordance of these measurements confirms the utility of gas ratios as a quantitative measure of in-plume biodegradation.

In order to assess the importance of ethane and propane as respiratory substrates their loss patterns were compared with the observed oxygen anomalies. Propane and ethane anomalies were calculated from their ratios to methane in reference to their source ratios and the ambient methane concentration, and these anomalies were normalized to oxygen equivalents assuming the stoichiometry of complete respiration. Regression of the observed oxygen anomaly against the propane anomaly (Fig 26A) yields a line of slope 1.71 and indicates that 58% of the oxygen anomaly can be linked

to propane. A similar analysis for propane plus ethane indicates that 70% of the oxygen anomaly can be linked to respiration of these two gases (Fig 26A). This result suggests that ethane and propane are the dominant respiratory substrates in the early development of deep-water hydrocarbon plumes. However, this relationship is expected to break down as plumes mature because propane and ethane are observed to be quantitatively removed well before methane (Fig 25) and are presumed to be removed before less soluble n-alkanes greater than five carbons in length. Once ethane and propane have been consumed, respiration rates are expected to drop; such a drop, when combined with mixing, could account for the weak respiration signal (< 0.8 μM d^{-1}) reported for the more distal SW plume horizon by other investigators (Camilli, Reddy et al. 2010). The residual oxygen anomaly not accounted for by propane and ethane respiration (~30%) presumably derives from other hydrocarbons. Butane is expected to contribute significantly to this oxygen drawdown, as it is often similar in concentration to propane in thermogenic hydrocarbon gases, is relatively soluble, and is also readily biodegraded (Kinnaman, Valentine et al. 2007; Mastalerz, de Lange et al. 2009).

The bacterial capacity for propane and ethane biodegradation was investigated by adding ^{13}C-labelled substrate into freshly collected plume waters and monitoring label conversion to $^{13}C\text{-}CO_2$. Time series measurements conducted for one plume location (Fig 25E and F) reveal an initial stage where product accumulates at a constant rate (Fig 25F), followed by a marked increase after 24 hours (Fig 25E). We interpret the initial rate as the maximum potential rate of biodegradation by the basal population, with saturation of the population's enzymatic capacity leading to zeroth-order kinetic behavior. The later increase then indicates a growth or biosynthetic response by the microbial community to the elevated substrate level. This interpretation is supported by the observation that zeroth-order kinetic behavior occurs at high levels of added label, while higher-order kinetic behavior results from addition of smaller quantities of labeled substrate. Samples treated with mercuric chloride showed no appreciable production of $^{13}C\text{-}CO_2$, further confirming the biological nature of ethane and propane oxidation.

Variations in consumption of propane and methane by the developing microbial community were assessed for different oxygen anomalies using ^{13}C and ^{3}H tracers, respectively. In all cases fresh duplicate plume samples were incubated in the dark near in-situ temperature with tracer for 24 h. In methane measurements, $^{3}H\text{-}CH_4$ tracer levels were <2% of ambient methane, allowing for a direct calculation of methane oxidation (Valentine, Blanton et al. 2001). In propane measurements, the lower sensitivity for stable isotope analyses necessitated addition of large quantities of tracer, increasing total propane concentration substantially over ambient levels. We consider only those propane tracer experiments (n=14) in which the addition was >4 times the ambient level, and consider the resulting rates from 24-h incubations to represent the maximum propane-oxidizing potential for the basal population. Propane-oxidizing potentials were greater at locations with higher propane anomalies (Fig 27B), suggesting a priming effect wherein environmental exposure to propane induces increased propane-respiration capacity. In comparison, methane oxidation rates were generally low in the plume horizon, with a median value of just 10 nM d^{-1} (n=25), 1-2 orders of magnitude too low to account for the oxygen anomalies. One plume location displayed an anomalously high methane oxidation rate of 820 nM d^{-1}, with cumulative methane consumption weakly supported by this location having the most ^{13}C-enriched methane ($\delta^{13}C\text{-}CH_4$ of -58.5 ±

0.8‰; n=3) compared to all other locations sampled (δ^{13}C-CH_4 = -61.3 ± 2.2‰; n= 17). A paucity of ethane and propane at this location suggests extensive biodegradation, and comparison of methane oxidation rates to C1/C2 for all rate measurements reveals a positive exponential correlation (Fig 27A). We interpret this relationship to reflect a slower substrate response and growth of methanotrophs relative to ethane degraders in the plume, though direct inhibition cannot be excluded. Based on this result we suggest that the development of methanotrophic communities in deep hydrocarbon plumes is delayed with respect to that of ethane- and propane-consuming communities.

To identify potential propane- and ethane-consuming bacteria active in the deep plumes, we collected and sequenced bacterial DNA from five locations containing distinctive propane and ethane anomalies. A cloning-based survey of the 16S rRNA gene was dominated by several sequences related to known hydrocarbon degraders—*Cycloclasticus* (Dyksterhouse, Gray et al. 1995; Geiselbrecht, Hedlund et al. 1998; Chung and King 2001; Maruyama, Ishiwata et al. 2003), *Colwellia (Brakstad, Nonstad et al. 2008)*, and members of the *Oceanospirillaceae (Hedlund, Geiselbrecht et al. 1999)*—indicating a low diversity bloom of hydrocarbon-oxidizing bacteria in the deep plumes. The plume closest to the wellhead had the highest levels of hydrocarbons and the least evidence for biodegradation, and yielded the lowest proportion of putative hydrocarbon degraders (52 %) relative to typical mesopelagic bacteria. We take this location to represent an early developmental stage in the bloom of hydrocarbon oxidizing bacteria. The remaining four locations were each dominated by two or three clades of putative hydrocarbon degraders (Fig 26B), suggesting low bacterial diversity in the fresh plume. The low diversity is consistent with previous findings (Hazen, Holman et al. 2010), though different organisms appear dominant in these plumes. The three locations for which the propane anomaly accounted for ≥50% of respiration were dominated almost exclusively by *Cycloclasticus* and *Colwellia*, whereas one location with a lower hydrocarbon anomaly (42% of the oxygen anomaly) also contained other putative oil degraders related to the *Oceanospirillaceae*, similar to previously-observed sequences (Hazen, Holman et al. 2010). Based on these results we suggest that the observed relatives of *Cycloclasticus* and or *Colwellia* are blooming as a result of their capacity to consume propane, ethane, and potentially butane, though not at the exclusion of other bacteria or metabolisms. While *Cycloclasticus* is known for its ability to degrade aromatic compounds, sequences observed here are 90% similar to putative ethane oxidizers identified by stable isotope probing (Redmond, Valentine et al. 2010), indicating the capability in this evolutionary lineage.

While there are many potential impacts of the deep hydrocarbon plumes in the Gulf of Mexico, we demonstrate a link between consumption of propane and ethane, oxygen utilization, and bacterial blooms. We suggest that propane, ethane, and possibly butane, provide a majority of the respiratory substrate feeding an initial bacterial bloom, with possible synergistic effects on the degradation of higher hydrocarbons, and a lag in the development of methanotrophic communities. The extent to which various hydrocarbon substrates may feed respiration is dependent on their concentration and bioavailability, and can now be estimated from available data. We estimate that methane, ethane and propane released from the Deepwater Horizon leak will exert a biological oxygen demand in the deep plume horizon of 8.3×10^{11} g O_2 for methane respiration, 1.3×10^{11} g O_2 for ethane, and 1.0×10^{11} g O_2 for propane. In comparison, as-

suming that half of all chemical dispersion occurred subsurface, we calculate that the oil dispersed into the deep subsurface will exert a maximum biological oxygen demand of 4.4×10^{11} g O_2, based on recent US government estimates (USGS 2010) of both natural and chemical dispersion. Based on these calculations we predict the persistence of oxygen anomalies in the deep plume horizon summing to ~1.5×10^{12} g of O_2, with an accompanying transition in dominant respiratory substrates from propane and ethane to oil to methane.

Based on chemical and isotopic distributions and on tracer studies conducted onsite, we demonstrated that propane and ethane were primary drivers of microbial respiration during the active spill, accounting for up to 70% of the observed oxygen depletion in fresh plumes. We suggested that propane and ethane trapped in the deep water fed low-diversity bacterial blooms and rapid respiration, potentially priming the population of oil-degrading bacteria. This propane- and ethane-dependent bloom phase was succeeded by slower respiration of methane and presumably oil in aging plumes.

In order to track the fate of methane we returned to the Gulf of Mexico in September and October, 2010, for a series of expeditions aboard the *NOAA Ship Pisces*. A survey of over 100 stations in the northern Gulf of Mexico revealed an extensive subsurface plume from the Deepwater Horizon – as identified by oxygen anomalies, the presence of chemical dispersant, and fluorescence indicative of aromatic hydrocarbons (Figure 28). However, methane was absent from the plume, suggestive of consumption by methanotrophic bacteria. An assessment of the microbial community indicated the community contained a high proportion of methanotrophic and methylotrophic bacteria (Figure 29). To determine if the results were reasonable based on chemical and biological considerations, and simple model was developed to interpolate the time course change in methanotrophic rate and population (Figure 30). The rates and population needed by the model to explain results were within reason, based on observations from hydrothermal plumes and the basin studies discussed in Chapter 2.

Taken together, the tracking of a hydrocarbon intrusion layer throughout the northern Gulf of Mexico, the paucity of CH_4 in the affected waters a month or more after the hydrocarbon emissions had ceased, the magnitude of the DO anomaly relative to emitted hydrocarbons (Table 9), and the prevalence of a methanotrophic microbial community (Fig. 29) suggest that CH_4 emitted from the Deepwater Horizon event was quantitatively consumed by August 2010. Given the slow rates of methanotrophy observed near the wellhead in June 2010 we suggest a bloom of methanotrophic bacteria occurred in these waters sometime between the end of June and the beginning of August 2010, and that it likely occurred after affected waters had flowed away from the wellhead. This assertion is supported by previous observations that rates of methanotrophy increased as C_2H_6 was depleted in the hydrocarbon intrusions.

Modelling of methanotrophic potential

The irruption of gas and oil into the Gulf of Mexico during the Deepwater Horizon event fed a deep-sea bacterial bloom that consumed hydrocarbons in the affected waters, formed a regional oxygen anomaly, and altered the microbiology of the region. To better understand these processes, we develop a coupled physical-metabolic model to assess the impact of mixing processes on these deep ocean bacterial communities and their capacity for hydrocarbon and oxygen utilization (Figure 31). We find that observed

biodegradation patterns are well described by exponential growth of bacteria from seed populations present at low abundance, and that current oscillation and mixing processes played a critical role in distributing hydrocarbons and associated bacterial blooms within the NE Gulf of Mexico (Figure 32). Mixing processes also accelerated hydrocarbon degradation through an autoinoculation effect, wherein water masses in which the hydrocarbon irruption had caused blooms later returned to the spill site with hydrocarbon-degrading bacteria persisting at elevated abundance (Figure 33). Interestingly, while the initial irruption of hydrocarbons fed successive blooms of different bacterial types, subsequent irruptions promoted consistency in the structure of the bacterial community (Figure 32). These results highlight an impact of mixing and circulation processes on biodegradation activity of bacteria during the Deepwater Horizon event, and suggest an important role for mixing processes in the microbial ecology of deep ocean environments.

REFERENCES

Brakstad, O. G., I. Nonstad, et al. (2008). "Responses of microbial communities in Arctic sea ice after contamination by crude petroleum oil." Microbial Ecology **55**(3): 540-552.

Brooks, J. M. (1975). Sources, sinks, concentrations and sub-lethal effects of light aliphatic and aromatic hydrocarbons in the Gulf of Mexico. Oceanography. College Station, Texas A&M. **Ph.D.**

Camilli, R., C. M. Reddy, et al. (2010). "Tracking Hydrocarbon Plume Transport and Biodegradation at Deepwater Horizon." Science.

Chen, F. and P. D. Yapa (2004). "Modeling gas separation from a bent deepwater oil and gas jet/plume." Journal of Marine Systems **45**: 189-203.

Chung, W. K. and G. M. King (2001). "Isolation, characterization, and polyaromatic hydrocarbon degradation potential of aerobic bacteria from marine macrofaunal burrow sediments and description of Lutibacterium anuloederans gen. nov., sp. nov., and Cycloclasticus spirillensus sp. nov." Appl Environ Microbiol **67**(12): 5585-5592.

Dasanayaka, L. K. and P. D. Yapa (2009). "Role of plume dynamics phase in a deepwater oil and gas release model." J. Hydroenviron. Res. **2**: 243.

Dyksterhouse, S. E., J. P. Gray, et al. (1995). "Cycloclasticus pugetii gen. nov., sp. nov., an aromatic hydrocarbon-degrading bacterium from marine sediments." Int J Syst Bacteriol **45**(1): 116-123.

Geiselbrecht, A. D., B. P. Hedlund, et al. (1998). "Isolation of marine polycyclic aromatic hydrocarbon (PAH)-degrading Cycloclasticus strains from the Gulf of Mexico and comparison of their PAH degradation ability with that of puget sound Cycloclasticus strains." Appl Environ Microbiol **64**(12): 4703-4710.

Gelwicks, J. T., J. B. Risatti, et al. (1989). "Carbon Isotope Effects Associated with Autotrophic Acetogenesis." Organic Geochemistry **14**(4): 441-446.

Gelwicks, J. T., J. B. Risatti, et al. (1994). "Carbon-Isotope Effects Associated with Aceticlastic Methanogenesis." Applied and Environmental Microbiology **60**(2): 467-472.

Grant, N. J. and M. J. Whiticar (2002). "Stable carbon isotopic evidence for methane oxidation in plumes above Hydrate Ridge, Cascadia Oregon Margin." Global Biogeochemical Cycles **16**(4): -.

Hazen, T. C., H.-Y. N. Holman, et al. (2010). "Deep-Sea Oil Plume Enriches Indigenous Oil-Degrading Bacteria." Science.

Hedlund, B. P., A. D. Geiselbrecht, et al. (1999). "Polycyclic aromatic hydrocarbon degradation by a new marine bacterium, Neptunomonas naphthovorans gen. nov., sp. nov." Appl Environ Microbiol **65**(1): 251-259.

JAG (2010). Inter-Agency Joint Analysis Group Review of Preliminary Data to Examine Subsurface Oil In the Vicinity of MC252#1 May 19 to June 19, 2010.

Kinnaman, F. S., D. L. Valentine, et al. (2007). "Carbon and hydrogen isotope fractionation associated with the aerobic microbial oxidation of methane, ethane, propane and butane." Geochimica Et Cosmochimica Acta **71**(2): 271-283.

Maruyama, A., H. Ishiwata, et al. (2003). "Dynamics of microbial populations and strong selection for Cycloclasticus pugetii following the Nakhodka oil spill." Microb Ecol **46**(4): 442-453.

Mastalerz, V., G. J. de Lange, et al. (2009). "Differential aerobic and anaerobic oxidation of hydrocarbon gases discharged at mud volcanoes in the Nile deep-sea fan." Geochimica Et Cosmochimica Acta **73**(13): 3849-3863.

Mau, S., H. Sahling, et al. (2006). "Estimates of methane output from mud extrusions at the erosive convergent margin off Costa Rica." Marine Geology **225**(1-4): 129-144.

Mau, S., D. L. Valentine, et al. (2007). "Dissolved methane distributions and air-sea flux in the plume of a massive seep field, Coal Oil Point, California." Geophysical Research Letters **34**(22): -.

Redmond, M. C., D. L. Valentine, et al. (2010). "Novel Methane, Ethane, and Propane Oxidizing Bacteria at Marine Hydrocarbon Seeps Identified by Stable Isotope Probing." Appl Environ Microbiol.

Reeburgh, W. S. (2007). "Oceanic methane biogeochemistry." Chemical Reviews **107**(2): 486-513.

Schrope, M. (2010). "Oil cruise finds deep-sea plume." Nature **465**: 274-275.

USGS (2010). Deepwater Horizon MC252 Gulf Incident Oil Budget: Government Estimates - Through August 01 (Day 104).

Valentine, D. (2010). "Measure methane to quantify the oil spill." Nature **465**(7297): 421.

Valentine, D. L., D. C. Blanton, et al. (2001). "Water column methane oxidation adjacent to an area of active hydrate dissociation, Eel River Basin." Geochimica Et Cosmochimica Acta **65**(16): 2633-2640.

Winkler, L. W. (1888). "Die Bestinmmung des im Wasser Saurstoffes." Ber. Dtsch. Chem. Ges. **21**: 2843-2855.

Yapa, P. D., D. L.K., et al. (2008). "Modeling the Impact of an Accidental Release of Methane Gas in Deepwater." Oceans **1-4**: 109-118.

Table 9. Hydrocarbon emission estimates and oxygen removal potentials

Hydrocarbon	Quantity Emitted (moles)	Stoichiometric Ratio O_2:Hydrocarbon	O_2 Removing Potential (moles)	Dissolved O_2 Removed (moles)
CH_4	$0.91 – 1.25\times10^{10}$	2:1	$1.83 – 2.50\times10^{10}$	
C_2H_6	$0.85 – 1.16\times10^{9}$	3.5:1	$2.96 – 4.05\times10^{9}$	
C_3H_8	$4.60 – 6.28\times10^{8}$	5:1	$2.30 – 3.14\times10^{9}$	
Oil[a] as $(-CH_2-)$	$0.93 – 1.00\times10^{10}$	1.5:1	$1.40 – 1.50\times10^{10}$	
		Total	$3.76 – 4.72\times10^{10}$	$3.00 – 3.90\times10^{10}$

[a] = only oil in the deepwater intrusion layers

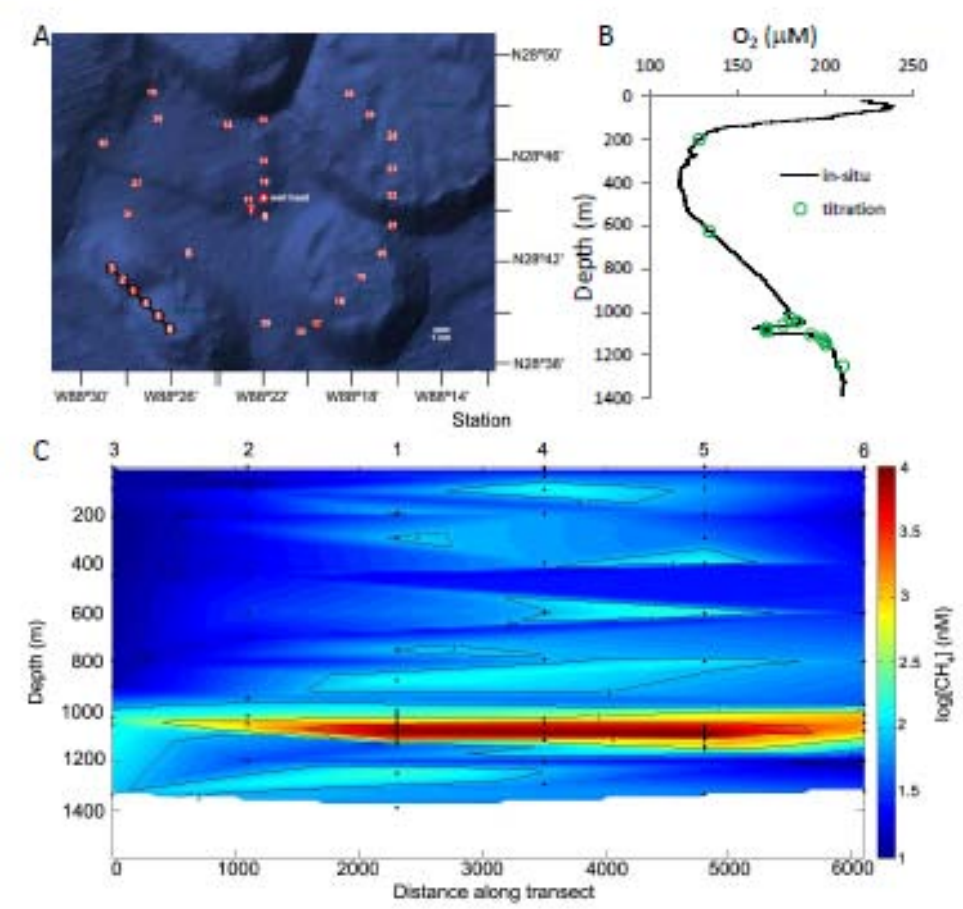

Figure 24. (A) Locations of the sampling stations relative to the well head, overlaid on a Google Earth image of the site. (B) Depth distribution for oxygen from station H-1 displaying the in-situ sensor data (solid line) and data from Winkler titrations (green circles). (C) Contour plot of methane concentration along a transect from H3 to H6. Note the log scale.

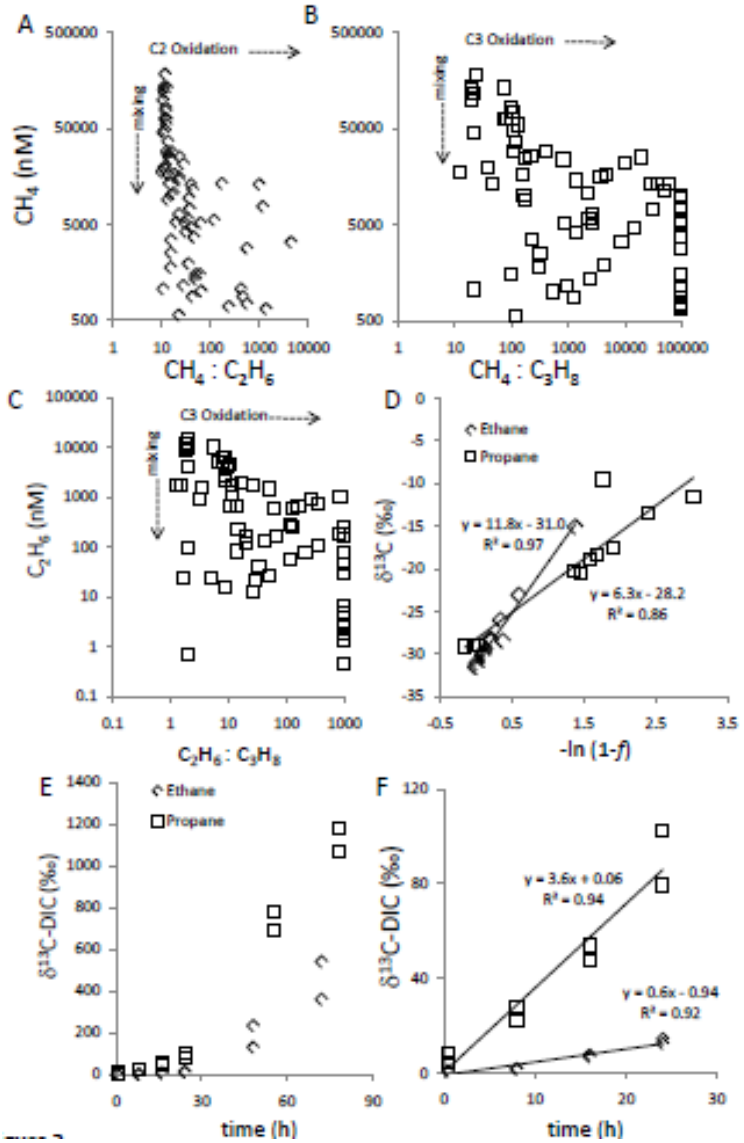

Figure 25. (A) Variation in C1/C2 relative to methane concentration for all deep plume samples (CH_4 > 500 nM). (B) Variation in C1/C3 relative to methane for all plume samples. All samples with C1/C3 > 10,000 are displayed with a value of 10,000. (C) Variation in C2/C3 relative to ethane. All samples with C2/C3 > 1000 are displayed with a value of 1,000. (D) Comparison of the fractional loss of propane or ethane versus $\delta^{13}C$ (n = 12 for propane; n = 16 for ethane). The slopes of the linear regressions provide isotopic enrichment factors (Gelwicks, Risatti et al. 1989; Gelwicks, Risatti et al. 1994) assuming a closed isotopic system. (E) Time course change in $\delta^{13}C$ of dissolved inorganic carbon after treatment of fresh 160 mL replicate samples with 100μL of ^{13}C propane or ethane and incubation in the dark near in-situ temperature. Samples treated with mercuric chloride displayed no appreciable increase in $\delta^{13}C$-DIC. (F) Blow up of panel E highlighting the first 24 hours.

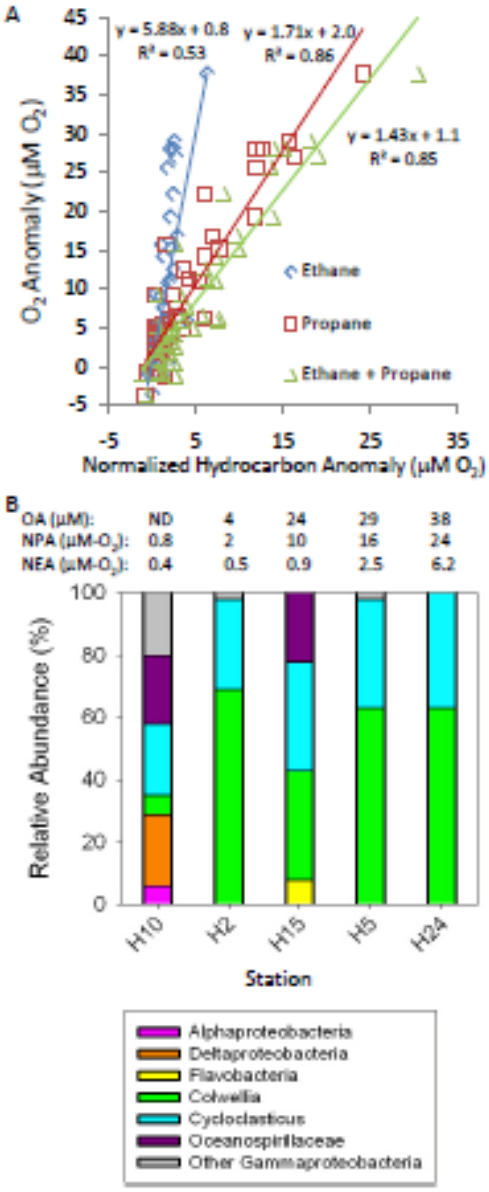

Figure 26. (A) Comparison of the oxygen anomaly derived from Winkler titrations with normalized hydrocarbon anomalies derived from variation in C2/C1 and C3/C1. Results of linear regression are provided (n= 36 for each regression). (B) Results from DNA surveys for bacterial 16SrRNA genes at five plume locations representing different levels of biodegradation. The numbers of clones sequenced for each location are as follows: H10, 31; H2, 42; H15, 26; H5, 48; H24, 48. OA is the oxygen anomaly; NPA is the normalized propane anomaly, NEA is the normalized ethane anomaly, and ND is not detected.

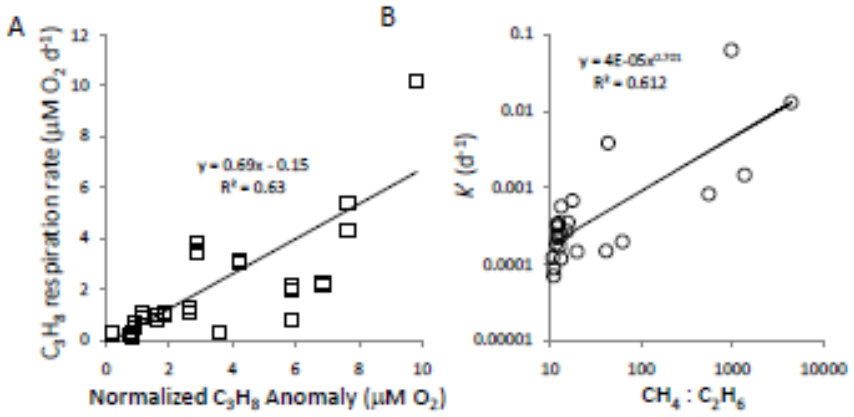

Figure 27. (A) Comparison of potential propane oxidation rates measured by ^{13}C tracer conversion, with propane anomalies determined from the C1/C3 ratios in the source water. All treatments were conducted in duplicate (both shown; n=28) with fresh 160 mL samples incubated for 24 hours near in-situ temperature in the dark. (B) Comparison of the effective pseudo first order rate constant for methane oxidation versus the extent of ethane loss relative to methane (C1/C2).

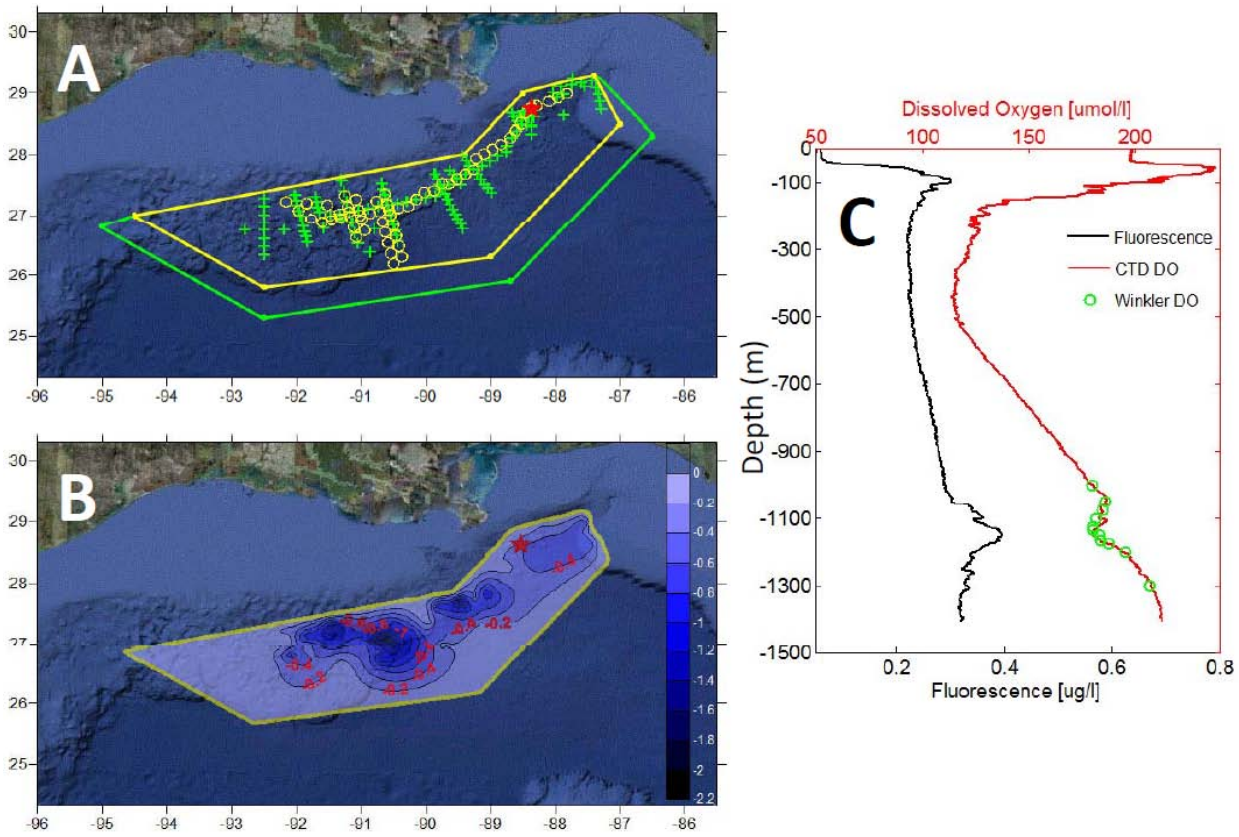

Figure 28. (A) Sampling stations overlaid on a Google Earth image highlighting the area of the intrusion. Blue plus, red diamond, and white triangle symbols indicate sampling stations for the 18 August – 2 September, 7 – 17 September, and 22 September – 4 October 2010, expeditions respectively. The yellow and green boundaries indicate the extent of the contouring bounds as determined from the extent of the DO and fluorescence anomalies and bathymetric restrictions. (B) Contour plot within the yellow boundary of the vertically integrated DO anomaly at each station using data from the 18 August – 2 September 2010 expedition. Units are moles DO m^{-2}. (C) Profiles of DO (SBE-43, Sea-Bird Electronics Inc.; red line calibrated with Winkler titrations) and fluorescence (UV AquaTracka (Emission = 360nm), Cheslea Technologies Group; black line). The green circles represent Winkler titration samples. Station PC198 (26.7098ºN, 90.6286ºW).

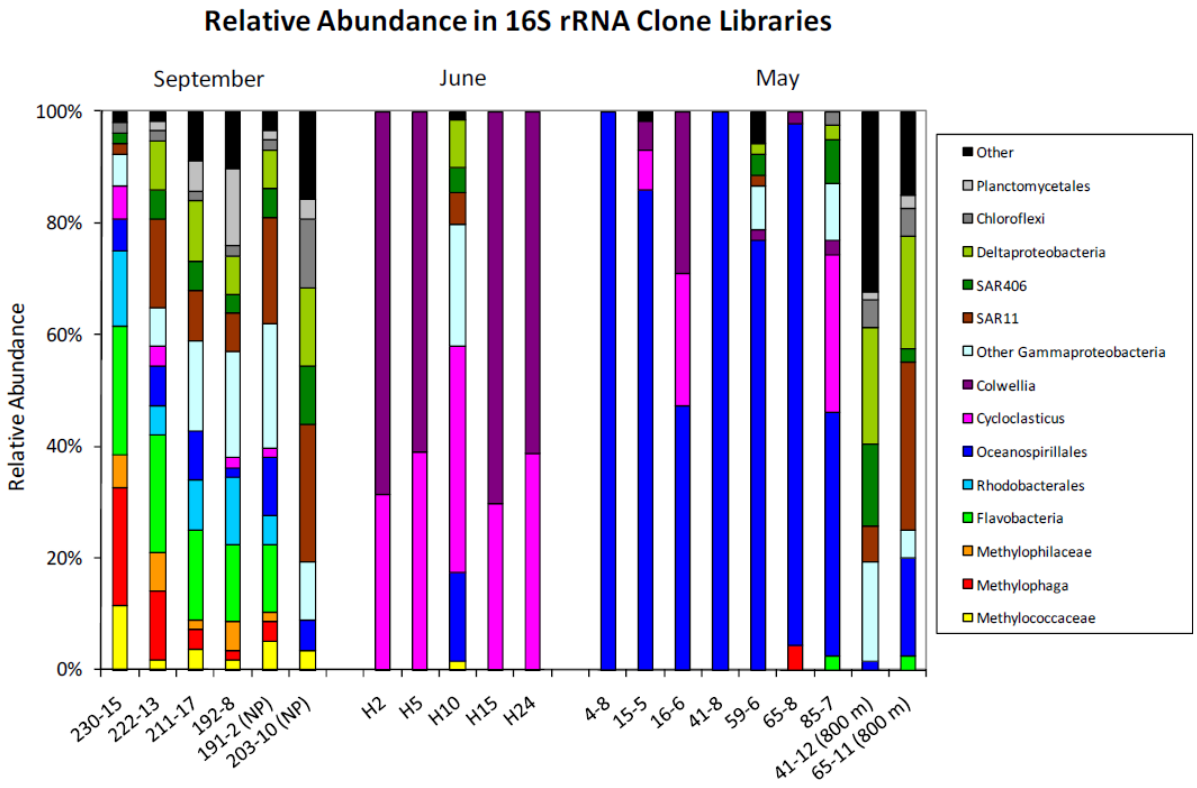

Figure 29. Results from DNA surveys for bacterial 16S rRNA genes representing changes in community structure associated with oxidation of CH_4 in samples collected from 7-17 September 2010. Stations are shown from left to right in order of decreasing reductions in DO. Stations 192, 222, 230, and 211, had DO and fluorescence anomalies (integrated oxygen reductions of 1.1, 0.7, 0.5, and 0.1 mol/m^2, respectively), while stations 191, 242 and 203 did not (integrated oxygen reductions <0.00001 mol/m^2). Methylotrophs (*Methylococcaceae*, *Methylophaga*, and *Methylophilaceae*) are indicated by shading. The "Other" category includes groups observed at <5% in all samples, predominately *Acidobacteria, Actinobacteria*, and *Verrucomibrobia*. *n* = 56 – 79 per station for a total of 492.

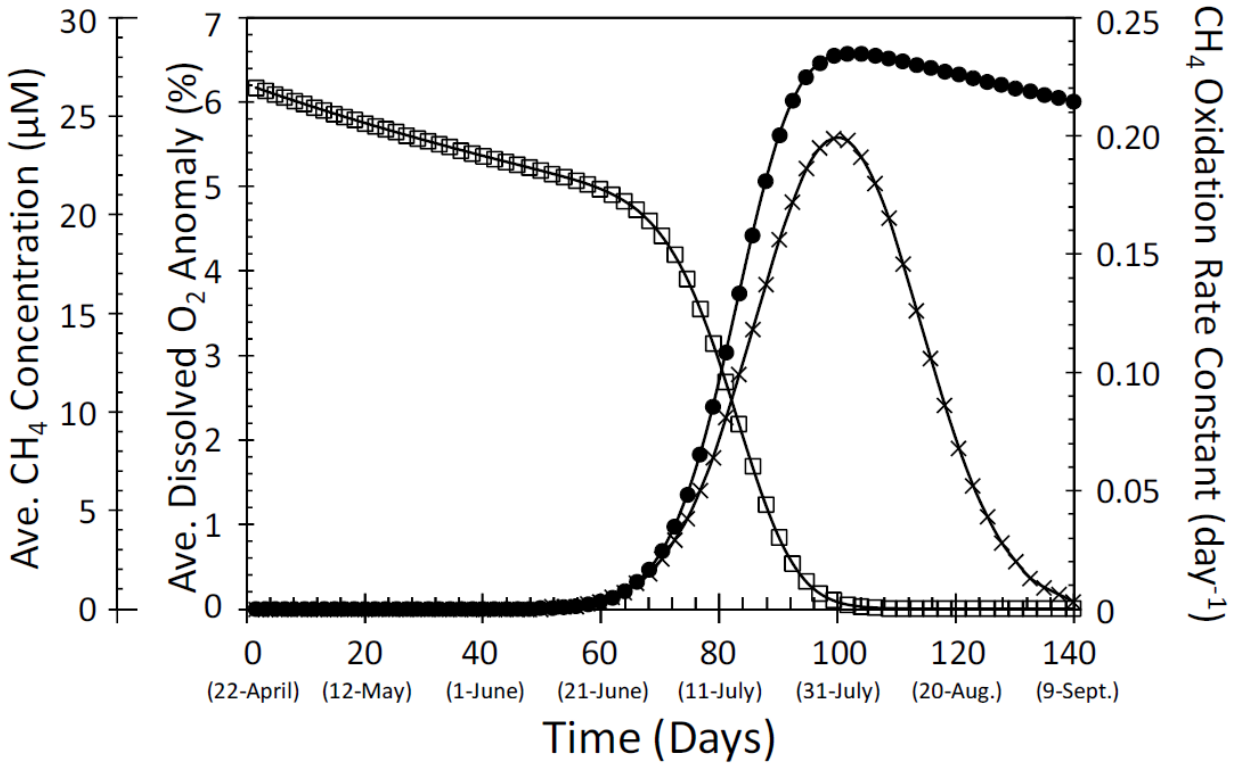

Figure 30. Model results from a one-dimensional time-dependent model of (●) average DO anomaly from CH_4 respiration (μM reduction in the intrusion layer), (□) average CH_4 concentration (μM), and (×) first-order CH_4 oxidation rate constants ($days^{-1}$) in the intrusion layers. Labels (A) – (D) on the figure represent measured values. (A) Avg CH_4 Concentration = 25 μM (range = 0.57 – 183 μM; *n* = 73), 11-20 June; (B) Avg CH_4 concentration = 1.43 ± 2.00 nM (*n* = 671), Avg CH_4 oxidation rate constant = 0.0015 $days^{-1}$ (range = 0.0005 – 0.0038 day^{-1}, *n* = 10), 7-17 September; (C) Avg CH_4 oxidation rate constant = 0.001 day^{-1} (range = 0 – 0.0127 day^{-1}, *n* = 22 minus one outlier), 11-20 June; (D_M) Max Dissolved O_2 Anomaly = 36.7 μM, (D_A) Avg Dissolved O_2 Anomaly = 5.6 ± 5.8 μM (*n* = 202), 18 August – 4 October, 2010.

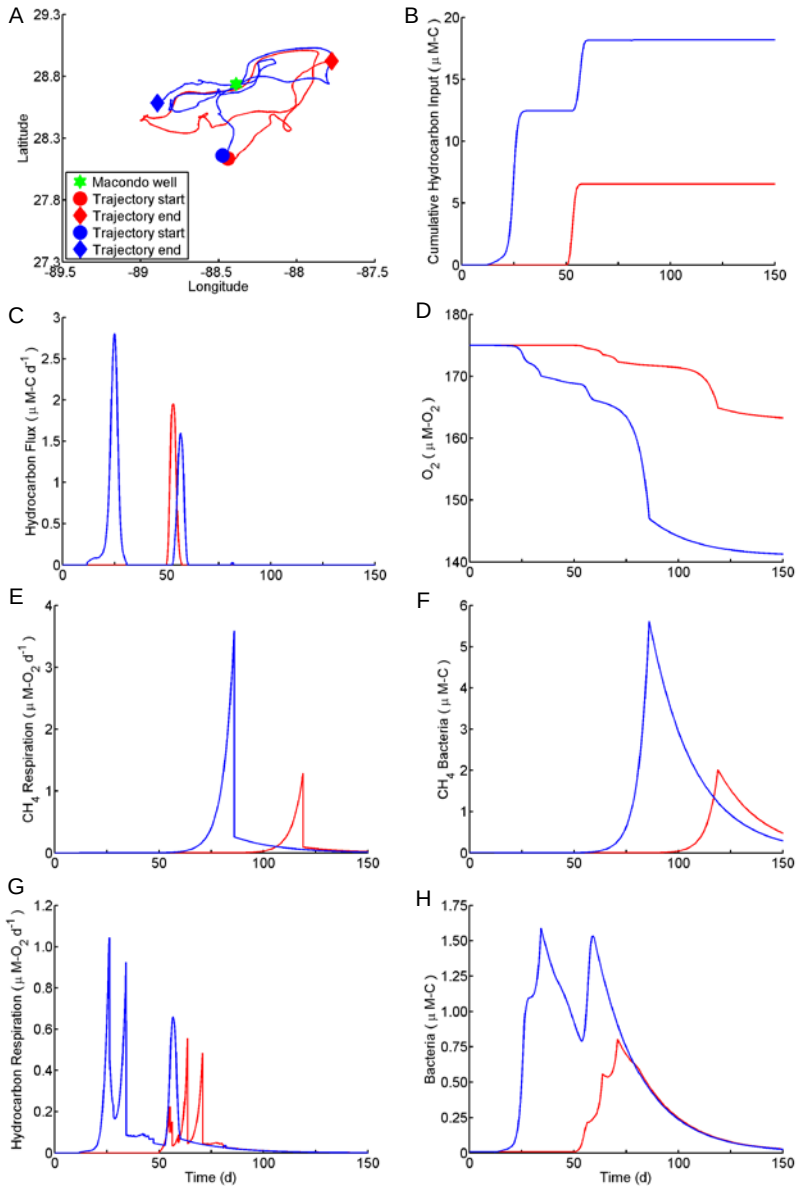

Figure 31. An analysis of the autoinoculation effect through comparison of two water parcels with single (red) and double (blue) exposure histories. A) Trajectories of two water parcels for 150 days starting April 23, 2010. B) The time-course of cumulative hydrocarbon input to the parcels. C) The time course of hydrocarbon flux into the two parcels. D) Time course of dissolved oxygen concentration in the parcels, attributed to hydrocarbon respiration. E) Time course of respiration rate linked to methane consumption in the two parcels, F) Time course of bacterial growth for organisms consuming methane (Met and Met'). G) Time course of respiration rate linked to consumption of 25 non-methane hydrocarbons in the two parcels, H) Time course of bacterial growth for organisms consuming 25 non-methane hydrocarbons (Excludes Met and Met'). Units for bacterial abundance are shorthand for μmol-C L^{-1}.

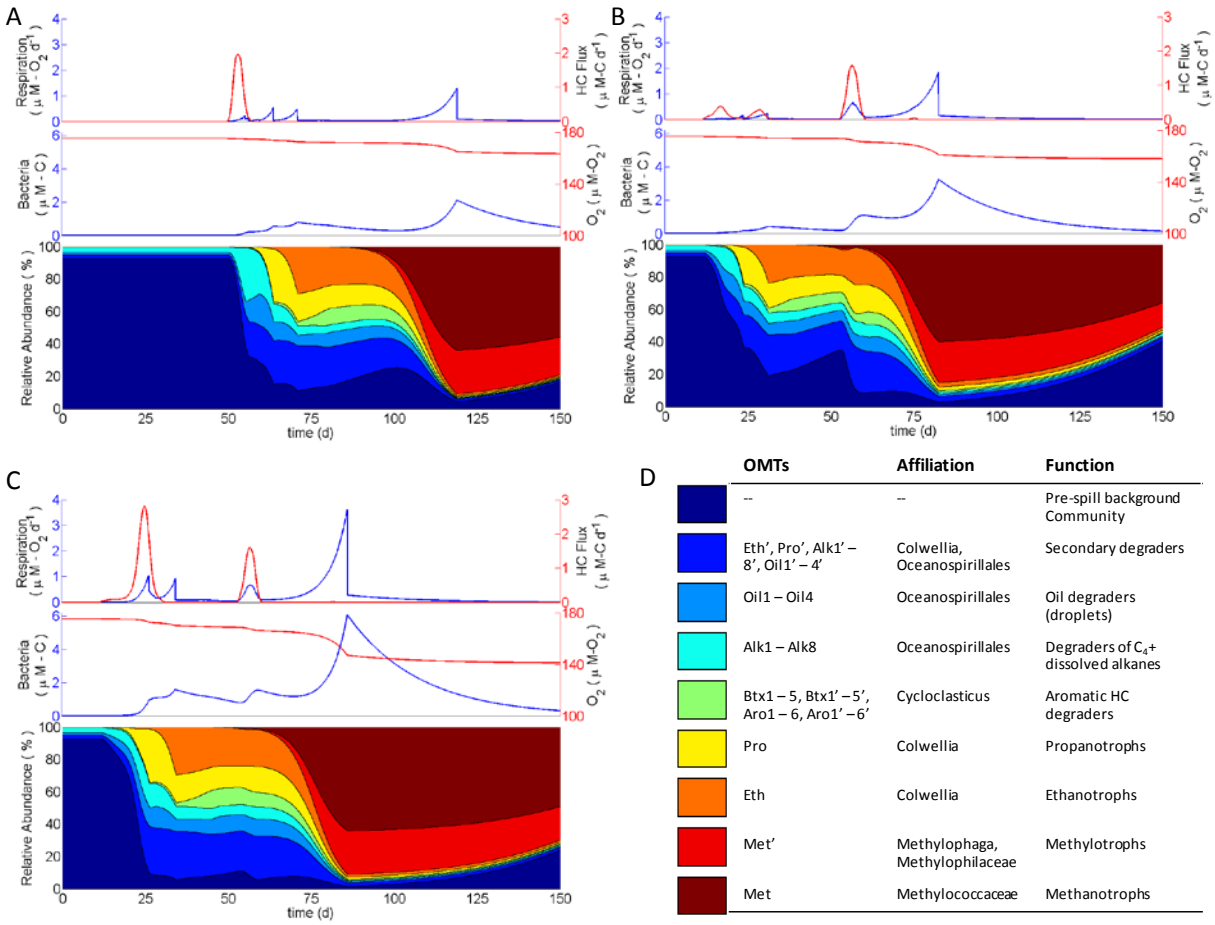

Figure 32. Comparison of microbial community dynamics in water parcels with different exposure histories, all starting April 23, 2010. A) Time-course change in hydrocarbon flux (red) and respiration rate (blue) shown at top, dissolved oxygen concentration (red) and bacterial abundance (blue) shown at middle, and the relative composition of the microbial community shown at bottom, for a parcel experiencing a single exposure. B) Time-course changes as described for panel A, for a parcel experiencing a triple exposure. C) Time-course changes as described in panel A, for a parcel experiencing a double exposure. D) Tabulated legend identifying the OMTs, their putative phylogenetic affiliation, and their ecosystem function.

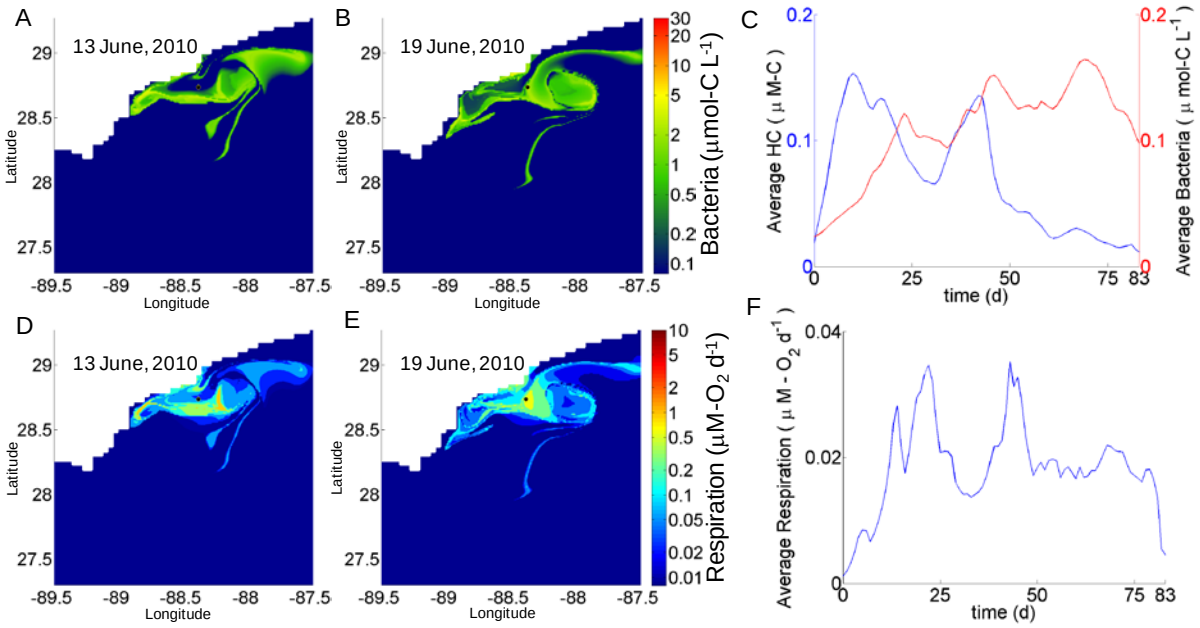

Figure 33. Impact of recirculation on hydrocarbon abundance, bacterial population, and metabolism. A and B) Spatial distribution of bacterial abundance prior to (A) and during (B) the early stages of an autoinoculation event. C) Time course change in average abundance for bacteria consuming non-methane hydrocarbons, and the average summed concentration of these chemicals integrated over the computational domain. D and E) Spatial distribution of hydrocarbon respiration rate prior to (D) and during (E) the early stages of the same autoinoculation event. F) Time course change in the average respiration rate for bacteria consuming non-methane hydrocarbons, integrated over the computational domain. Because the size of the computation domain is 2^{o} lat × 2^{o} lon, a small number of parcels exit the domain near the end of the simulation.

CONCLUDING REMARKS:

The focus of the current research program was to provide a greater understanding of the role methanotrophy plays in preventing methane release from gas hydrate to the environment. The results from this research contribute significantly to achieving this goal. Through the combination of oxidation rate measurements, stable isotope probing of active metabolism and molecular microbiological analyses of methanotrophic genes we were able to demonstrate the importance of type I methanotrophic bacteria as consumer of methane released into deep ocean waters of the Pacific Ocean and the Gulf of Mexico. Similarly, we used these same techniques to show that similar bacteria also inhabit filamentous microbial mats that exist in areas where methane seeps at the sea floor, and can actively metabolize dissolved methane that reaches the mat.

These efforts contribute substantially to our understanding of methane's fate when released from hydrates, but raises a new set of questions as to the environmental and biological controls on methanotrophy. Issues of future concern are considered below within the context of the conclusions from the present study.

1) Our studies in the Santa Barbara Basin, Santa Monica Basin and the Gulf of Mexico demonstrate that marine methanotrophs are dynamic in their ability to respond to methane inputs, even under suboxic conditions. In our studies to date we have encountered two fundamental limitations for aerobic methanotrophs: their substrates, methane and oxygen. However, there may be distinct limitations faced by methanotrophs in other settings, such as nutrient limitation that prevents growth. Nutrients that inhibit methanotrophs are likely to include nitrogen, phosphorus, iron and possibly copper. Addressing the issue of nutrient limitation will be important for our ability to predict efficacy of the aerobic methanotrophic biofilter for a given geographic setting.
2) Our studies in Pacific hydrocarbon seeps and in the Gulf of Mexico have identified marine methanotrophs active in these systems as relatives of *Methylococcaceae*, though not at the exclusion of other lineages. A greater understanding of these bacteria would be useful in understanding the dynamics of the methanotrophic biofilter. Several directions are likely to be useful including both environmental and laboratory studies. Isolation and cultivation approaches would provide great insight to metabolic capabilities and patterns. Environmental studies might provide ecological and biogeochemical insights as to how these bacteria acclimate to the dynamic methane hydrate environment. Importantly, we retained samples that might allow for genome sequencing of single cells from environmental samples collected in the methane plume arising from the Deepwater Horizon incident. These samples were preserved for cell sorting and single cell genome amplification. Thus far we have sorted and amplified from one other sample, from which we amplified the genomes of over 100 isolated cells. From a second sample we anticipate being able to amplify and sequence the genomes of several ecotypes of marine methanotrophs.
3) Our research on microbial mats has shown clearly that marine methanotrophs occupy mats when methane is present. We know the identity of bacteria involved, but our knowledge of their efficacy in-situ is incomplete. It is clear from our labora-

tory studies that mats metabolize methane at a relatively slow rate compared to the ebullition in a major seep field – suggesting they are ineffective filters in this environment. What is not clear though is their efficacy in environments where the upward flux of methane is diffusive or advective – but where concentrations are insufficient to force gas to exsolve and bypass the benthic biofilter.

4) Our studies focused on three geographical areas: the Pacific margin of North America, the Eastern Tropical North Pacific and the Gulf of Mexico (as well as one lacustrine study in the Alaskan Arctic). What remains unresolved is the extent to which our observations can be applied to other waters such as the Atlantic and Arctic Oceans. Some of our observations should readily translate, but the Arctic Ocean in particular has other characteristics such as sea ice and a fresh water cap that may modulate methanotrophic activity.
5) Our present results demonstrate that hydrocarbon gases besides methane (i.e., ethane, propane and butane) are also readily consumed by marine bacteria when released to the ocean. Because gas hydrate accommodates these gases in addition to methane, it is important to study the dynamics of these gases to understand their impacts on the methanotrophic biofilter and their impacts on the environment. Factors that remain unknown include: the nature and extent of competition between methanotrophs and bacterial consumers of ethane, propane and butane; the potential for inhibition of methanotrophs by these gases or the bacteria that consume them; indirect impacts of these gases on the microbial community such as by altering predation patterns; and the selectivity of methanotrophs for methane versus an analog like ethane.
6) Our results show a clear bloom of marine methanotrophs upon the addition of methane to various waters, and our results further indicate that methane's carbon is rapidly transferred from methanotrophs to secondary consumers including methylotrophs. Methylotrophs presumably cross-feed on methanol excreted by methanotrophs, but the importance and details of this interaction remain undefined. In order to understand the ecology of methane oxidation in the ocean (which would improve our predictive capability for the methanotrophic biofilter) these critical trophic relationships need to be defined and studies conducted to determine the sensitivity of methanotrophy to the interaction between primary consumers, secondary consumers, and predators.
7) Our collaborative results from ice-covered lakes in the Arctic indicate a high methanotrophic potential, even under suboxic/anoxic conditions that accompany ice cover. Iron concentrations appear to be elevated in this system and results suggest a linkage between methanotrophy and reduction of iron (III), presumably to iron (II). The anaerobic oxidation of methane with iron (III) as oxidant has been suggested in marine sediment and in other saline systems, with evidence remaining equivocal. The extent and nature of interactions between methane and iron is important for understanding the fate of methane from thawing permafrost that accumulates in Arctic lakes under conditions of ice cover.
8) Our results from gas hydrate sites offshore California suggest that biogenic methane venting from the sea floor within the gas hydrate stability field dissolves into the ocean water near the top of the stability field, consistent with previous studies. This contrasts to the Gulf of Mexico where thermogenic gas and gas/oil seeps ap-

pear to survive transport to shallow depths near the mixed layer. Such variability in the depth of dissolution is likely to have impacts on the efficacy of the methanotrophic biofilter as methane is more likely to escape from the mixed layer depth than from the top of the gas hydrate stability field. The biological response at these different depths may also be distinct and serves as an important target for future investigations.

Acknowledgment: "This material is based upon work supported by the Department of Energy under Award Number DE- NT0005667."

National Energy Technology Laboratory

626 Cochrans Mill Road
P.O. Box 10940
Pittsburgh, PA 15236-0940

3610 Collins Ferry Road
P.O. Box 880
Morgantown, WV 26507-0880

One West Third Street, Suite 1400
Tulsa, OK 74103-3519

1450 Queen Avenue SW
Albany, OR 97321-2198

2175 University Ave. South
Suite 201
Fairbanks, AK 99709

Visit the NETL website at:
www.netl.doe.gov

Customer Service:
1-800-553-7681